Technische Universität München

Fakultät für Mathematik

Optimal Control of Intrinsically Compliant Robots

Diplomarbeit

von

Christopher Schindlbeck

Themensteller:	Prof. Dr. Oliver Junge (TUM)
Betreuer:	Dr. Sami Haddadin (DLR)
Abgabetermin:	14. September 2012

Meinem Vater gewidmet

Eidesstattliche Erklärung

Ich versichere, dass ich die von mir an der Technischen Universität München eingereichte Diplomarbeit zum Thema

"Optimal Control of Intrinsically Compliant Robots"

ohne Hilfe Dritter und ohne Benutzung anderer als der angegebenen Quellen und Hilfsmittel angefertigt und die den benutzten Quellen wörtlich oder inhaltlich entnommenen Stellen als solche kenntlich gemacht habe. Diese Arbeit hat in gleicher oder ähnlicher Form noch keiner Prüfungsbehörde vorgelegen.

München, den 14. September 2012

Christopher Schindlbeck

Abstract

The vast majority of robots in industrial environments is designed and modeled as stiff multi-body systems. Striving for position accuracy and repeatability, any elasticity is regarded as parasitic effects that poses a source of unwanted oscillatory behavior. The compliance is typically realized via impedance control requiring force/torque sensors in each joint, so-called active compliance. Although robots are often praised to outperform humans, this is only true to a very small extent. In general, mammals are capable of outstanding performances with respect to a large variety of different tasks and have been optimized for them over large periods of time through evolutionary processes. Presumably, the feature to store and release energy enables humans to be superior to robots in terms of highly dynamic motions with high peak velocity outputs. Over the recent years, the concept of intrinsically compliant robots has drawn significant attention in the robotics community. The basic idea is to transfer the biological features inherent in the musculoskeletal system to robotics by introducing elastic transmission elements on joint level. These passively compliant systems are not only expected to be more robust against external shock impacts, but also to come closer to human capabilities in terms of robustness and performance. So-called variable stiffness actuators can not only adjust positioning, but also the joint stiffness in order to emulate mammalian muscle (pre-)tension. Although several mechanical systems are being developed right now, only limited work on controlling these novel devices on a fundamental theoretical basis has been considered. This thesis aims to investigate robotic systems with elastic transmission elements between the motor and link under the objective of maximizing the velocity of the final link. In particular, the exploitation of joint elasticity as a temporary energy storage mechanism is to be inverstigated. Since the constraint on the maximum allowable spring deflection is vital to the systems health and any violation would lead to a permanent damage of the system, this constraint plays an important role throughout the thesis. Moreover, the benefits of elastic/variable stiffness robots versus their rigid counterparts are examined. The aforementioned aspects are investigated using mass spring systems to retrieve (as much as possible) analytical solutions and for the nonlinear counterparts, numerical methods are employed in order to unveil similarities or show the limitations of simplified models.

Contents

Chapter 1

Introduction

Over the recent years, a paradigm shift has taken place in the field of anthropomorphic robotics, which marks a transition from rigid robots to robots with elastic transmission elements. Until recently, robots have been designed to be mechanically as rigid as possible to meet the demands of tasks, predominantly from the industrial sector. There, typical applications involve welding parts in an assembly line or accurate pick and place operations. The high stiffness of the mechanical structure is beneficial for such tasks, where precision and short execution times are important. Any elasticity in the structure is considered detrimental to the performance, since it may cause oscillatory behavior, or degrade position accuracy. Also, describing rigid dynamics is simpler and therefore avoids complex control architectures.

Furthermore, since these industrial robotic systems were constructed without any regard to potential human-robot interaction, they need to be fenced off for safety reasons. However, in order to make such direct interaction feasible, corresponding features need to be designed into the robots. For safety reasons, the mechanical architecture of a robot should also be constructed to be as intrinsically safe as possible instead of solely relying on active control. Nowadays, compliance in mechanically rigid robots is achieved by impedance control using the information of force-torque sensors in the corresponding joints. For shock impacts, however, the control loop cannot react sufficiently fast to avoid damage in the system. This makes these type of robotic systems prone to external force impacts, which may harm them significantly.

Another aspect of rigid robots is that the stiff coupling between motor and link will not allow the link velocity to exceed the motor velocity considerably. In the strive for performance in terms of speed, one seeks to find mechanisms without this restriction. Nature may serve as leading archetype for the design. Biomechanical investigations have come to the consensus that muscles interact in sophisticated patterns to optimize certain motion sequences [86]. For example, increasing the tension is realized by simultaneously contracting the muscles in the associated muscle pair [103]. Moreover, observations show that energy is stored and released in the muscles while running [92]. For tasks with high peak velocity outputs, such as throwing, a sequenced actuation of muscles occurs to transfer the energy internally from the proximal to the distal parts of the arm [5, 44, 87]. This leads to the consideration of a bio-inspired robot design.

So-called intrinsically compliant robots are in the focus of current robotics research [3, 61,

94, 105, 108] in order to address the issues mentioned before. The basic idea is to introduce elastic elements on joint level and therefore realizing passive compliance that can also be combined with active compliance schemes. The long-term objective is not necessarily to mimic the human characteristics as exact as possible, but to be inspired by characteristics of the mammalian musculoskeletal system and find new ways to improve robot design and control.

In summary, the overall expected benefits of passively elastic systems are

- Efficiency from an energetic perspective
- Robustness to external forces or (shock) impacts due to intrinsic elasticity/passive compliance
- Task-specific adaptability and force accuracy
- Safety aspects and compliance in human-robot interaction

The latest research focuses on a particular noteworthy subset of intrinsically compliant actuators which comprises joint mechanisms that are capable of adjusting their stiffness via additional motors (so-called variable stiffness actuators). Roughly speaking, a distinction can be made between antagonistic joint designs, following a close imitation of the mammalian muscle structure and quasi-antagonistic joint designs that reduce the mechanical complexity, while trying to retain the advantages of variable stiffness actuation. Although an increase of actuators may gain a potential advantage performance-wise and increase the controllability of a robot, it also poses a challenge to handle the highly nonlinear and complex dynamics that inevitably come along with it.

Related work and state of the art

This new and uprising branch in robotics is still in its infancy and no unified joint concept has been clearly found yet. A large variety of different concept methodologies has been proposed over the years, ranging from pneumatic [29, 98, 104] to chemical [27] or (mostly) spring-based actuators [39, 75, 94, 107, 109].

In the recent past, some research has already been addressed towards the aforementioned potential benefits. Optimal control approaches exploiting the natural dynamics for highly dynamic tasks, such as explosive movements, were considered in [18, 42, 52, 73]. Complex limit cycle movements for a biped walking robot with antagonistic driven joints in the lower limbs have been achieved in [109, 110]. The robustness of a robotic system with intrinsically compliant joint mechanisms is shown in [50], leaving the system intact after it has been smashed with a baseball bat. Safety analysis regarding human-robot interaction based on different metrics, while simultaneously trying to meet the competing requirements for safety and performance, can be found in [17, 51, 98, 112].

A prototype of a fully articulated intrinsically compliant robot has recently been developed at the *Institute of Robotics and Mechatronics* of the *Deutsches Zentrum für Luft- und Raumfahrt e.V.* (DLR). The so-called *Hand Arm System* (HASy) [50] has anthropomorphic kinematics that closely match its biological counterpart, the human arm. Furthermore, it incorporates various variable stiffness actuation principles. Per joint, the system is equipped with a spring

element as well as two motors. While one of the motors controls the link position, the other is able to alter the joint stiffness. This is done by a mechanism that displaces nonlinearly shaped cam disks, which directly influence the joint stiffness as well as its progressive characteristics.

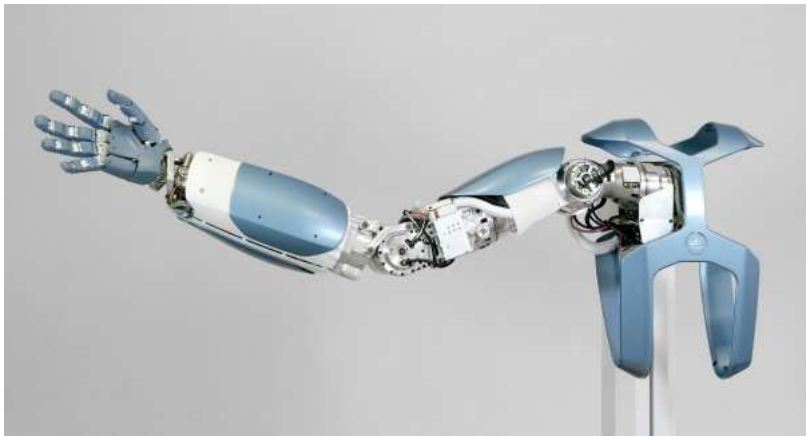

Figure 1.1: The DLR Hand Arm System

Contributions of the thesis

Despite the large variety of different concepts, only few basic properties for these novel devices are well understood from a theoretical point of view. This thesis aims at pursuing such efforts to further understand how elastic multi-limbed structures can be exploited by suitable energy shifts in the system. Throughout this thesis, the goal will in particular to be how to maximize the velocity of the last mass/link in a serial robotic structure. The overall goal of the analysis is to obtain basic insight into these elastic systems.

To retrieve analytical results for unveiling the inherent characteristics of these systems, a simplified model, consisting of concatenated masses interconnected by linear springs is used and thoroughly analyzed. The absence of gravitational or parasitic effects such as friction or damping facilitates these initial analytical considerations. Additionally, the system is varied in terms of the number of masses and springs, or the property to directly adjust the stiffness via an external control, i.e. treat bounded joint stiffness as an additional input.

For highly nonlinear systems, such as the double pendulum, where it is known that a closed-form solution does not exists, numerical analysis is applied. Therefore, a full set of constraints is taken into account to obtain reasonable results that stand real-world requirements. This includes spring deflection constraints, bounded motor velocities and motor/link positions.

As opposed to earlier works, where a simplified motor model (a velocity input, explained later on) was assumed and analyzed analytically [82] as well as numerically [59], here a force/torque input will be considered, which represents the physical reality more accurately. As a direct consequence, the motor dynamics are described by twice the number of generalized coordinates as opposed to the simplified case, which results in demanding calculations, both analytically and numerically.

Structure of the thesis

The thesis is organized as follows:

- Chapter 2 gives a short introduction to robot mechanics and dynamics from a multibody perspective. The difference between rigid, elastic, and intrinsically compliant robots is elaborated and the basic idea for the derivation of the dynamics is demonstrated.
- Chapter 3 introduces the theory of optimal control, which provides the main mathematical framework in this thesis. To grasp the background of the necessary conditions for a local minima in optimal control, the theory of calculus of variations is briefly described. Since (almost) all optimal control problems considered in this thesis belong to the class of singular optimal control problems, this particular type is described in more detail. Finally, numerical treatment of optimal control problems is delineated with a particular spotlight on pseudospectral methods. These will serve as method of choice throughout the numerical analysis in this thesis.
- Chapter 4 investigates properties of different mass spring systems where the goal is to maximize the velocity of the final mass. A force input serves as control acting on the first mass. As mentioned earlier, the systems are varied in terms of the number of masses or the property to additionally adjust the stiffness of the corresponding springs via external controls. Moreover, for the case of constant stiffness with two masses, a deflection constraint is analyzed.
- Chapter 5 discusses the single and double elastic pendulum as examples for (fully) nonlinear dynamics. For the elastic single pendulum, a deflection constraint is imposed to show similarities to the mass spring system with two masses and deflection constraint in the previous chapter. Furthermore, the effects of constant or variable stiffness are examined in the elastic double pendulum with respect to maximizing its end-effector velocity.
- Chapter 6 finalizes the thesis with concluding remarks about the key results and an outlook about future work.

Chapter 2

Robot Mechanics

2.1 Introduction to Multibody Systems

A multibody system can be defined as a finite number of rigid and flexible (deformable) bodies with distributed masses. These bodies are interconnected by elements that are assumed to be massless, such as springs, dampers, joints and actuators [28]. The joints are constraint elements that decrease the mobility of the system. A great number of structural and mechanical systems are modeled as a multibody system, e.g. vehicles and heavy machinery, aircraft and space structures, gearboxes and robotic systems.

In this thesis, only rigid multibody system are considered. For a thorough description of flexible multibody systems, please refer to [45, 95].

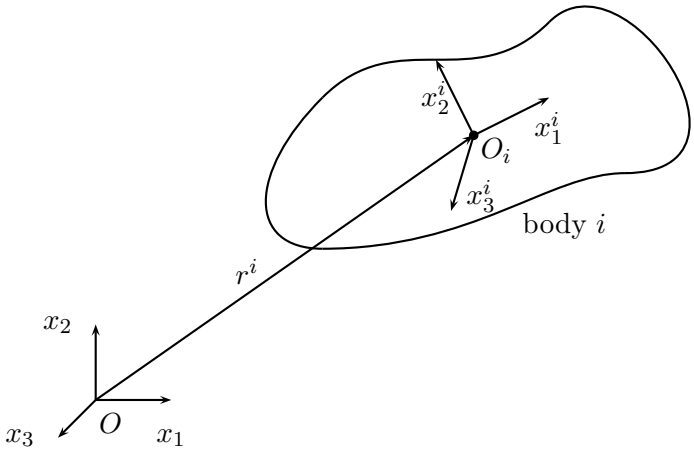

Figure 2.1: As opposed to flexible multibody systems, the particles of the body i are fixed w.r.t. the corresponding body coordinate frame O_i.

A rigid body in three dimensional space has six *degrees of freedom* (DoF). Three independent coordinates are needed to describe the body translation and three independent coordinates are

necessary for the description of the orientation $\tilde{q}_i = [r_1^i, r_2^i, r_3^i, \vartheta_1^i, \vartheta_2^i, \vartheta_3^i]$ w.r.t. a distinguished reference frame O_i, see Figure 2.1.

The user is free to choose a representation, e.g. for the rotation, such as *Euler* parameter, *Euler* angles or *Rodrigues* parameter. However, some representations may be redundant, i.e. the rotation is described by more than three parameter that are interrelated. This is particularly useful for the avoidance of singularities that are inherent in a three parameter representation [95].

A multibody system consisting of n_b rigid bodies may therefore have $6 \cdot n_b$ DoF. Nevertheless, due to the aforementioned constraint elements the bodies may not be able to move independently. This is mathematically described by algebraic constraints that are imposed on the system. A distinction is made between

- *holonomic* constraints
$$C(\tilde{q}_1, ..., \tilde{q}_n) = 0, \tag{2.1}$$
- *nonholonomic* constraints
$$C(\tilde{q}_1, ..., \tilde{q}_n, \dot{\tilde{q}}_1, ..., \dot{\tilde{q}}_n) = 0 \tag{2.2}$$
that are imposed on the motion and that are not integrable, i.e. the constraints cannot be written as time derivatives of some function of the coordinates [111],
- *rheonomic* constraints that depend on the time explicitly $C(\tilde{q}, t) = 0$ and
- *scleronomic* constraints that do not depend on the time explicitly $C(\tilde{q}) = 0$.

Examples for nonholonomic systems are e.g. a car without the consideration of sliding in the (horizontal) plane or the *Foucault* pendulum. The integrability of the nonholonomic constraints needs to be tested if they are not indeed holonomic constraints only disguised as nonholonomic constraints. These constraints occur more sporadically and are more difficult to treat.

The DoF of a multibody system in a three dimensional *Cartesian* space are defined as

$$n := 6 \cdot n_b - n_c, \tag{2.3}$$

where n_c is the number of (linearly independent) constraint equations with $n_c \leq n$. (2.3) is known as *Kutzbach* criterion [97]. The dynamics of a multibody system together with the constraints can be written in the subsequent, so-called *descriptor form* [20]

$$\tilde{M}(\tilde{q})\ddot{\tilde{q}} + \tilde{Q}(\tilde{q}, \dot{\tilde{q}}) + \tilde{C}_{\tilde{q}}(\tilde{q})^T \cdot \lambda = 0 \tag{2.4a}$$
$$\tilde{C}(\tilde{q}) = 0, \tag{2.4b}$$

where $\tilde{M} \in \mathbb{R}^{n_{\tilde{q}} \times n_{\tilde{q}}}$ is the mass matrix, $\tilde{Q} \in \mathbb{R}^{n_{\tilde{q}}}$ a vector comprising weight- and external forces (actuators, friction etc.) and $\tilde{C}_{\tilde{q}} := \frac{\partial \tilde{C}}{\partial \tilde{q}} \in \mathbb{R}^{n_c \times n_{\tilde{q}}}$ the constraint *Jacobian* matrix which is adjoined by *Lagrangian* parameter $\lambda \in \mathbb{R}^{n_c}$. (2.4) is a *differential-algebraic equation* (DAE) where the algebraic equation (2.4b) forces the solution of the ordinary differential equation (ODE) (2.4a) to lie on a (sub-)manifold. In multibody systems the manifold is spanned by

mechanical linking elements or geometric restrictions. By bringing (2.4a) into a first-order ODE with $x = \left[\tilde{q}, \dot{\tilde{q}}\right]$, the DAE is transformed into so-called semi-explicit form

$$\begin{aligned} \dot{x} &= f(x(t), t) \\ 0 &= g(x(t), t) \end{aligned} \tag{2.5}$$

as opposed to an (fully) implicit DAE

$$F_{\text{imp}}(\dot{\tilde{q}}(t), \tilde{q}(t), t) = 0. \tag{2.6}$$

If the *Jacobian* $F_{\text{imp},\dot{\tilde{q}}}$ is regular, then the function (2.6) can be solved locally w.r.t. $\dot{\tilde{q}}$ and an explicit ODE is obtained. Otherwise the system decomposes into an ODE and additional algebraic equations. Two types of indices are mentioned in the literature of DAEs, the differentiation index and the perturbation index (the latter is not relevant for this thesis). The differentiation index of a DAE is defined as the minimal number of differentiations such that the equations allow to extract an explicit ODE system, using only algebraic manipulations.

Because of the constraints, the coordinates $\tilde{q}$ are not fully independent from each other and therefore redundant. A minimal set of coordinates that fully describes the system are so-called *generalized coordinates*[1] $q \in \mathbb{R}^n$ with $n := 6n_b - n_c$. Expressing the dynamics with these coordinates yields the minimal form for holonomic multibody systems [16, 95].

$$M(q)\ddot{q} = h(q, \dot{q}, t). \tag{2.7}$$

The descriptor form (2.4) and the minimal form (2.7) have both their advantages and disadvantages [78, 96]

- The descriptor form is readily formalized and the modeling is more intuitive. Therefore, it is easier to understand because the kinetic and kinematic information is readily available. The drawback is that for an increasing number of bodies the dimension increases dramatically compared to the minimal form. Typically, constrained mechanical systems yield an index-3 DAE which is difficult to handle from a numerical viewpoint. The descriptor form is preferred if one is interested in the constraining forces.
- The minimal form is often highly nonlinear and it is difficult to formalize and implement a method for the calculations. For multibody systems with closed kinematic chains it is often very difficult to even find a minimal set of coordinates, whereas for tree-structured multibody systems it is always possible to find a global set of generalized coordinates [93]. However, since it is an ODE without algebraic constraints, it is advantageous for (closed-loop) control and simulation purposes.

Henceforth, the aim will be to obtain a minimal form for the systems.

2.2 Principles for the Derivation of the Dynamics

The dynamics (also: equations of motion) can be derived by a multitude of different approaches, to name a few

[1] Also: *minimal coordinates*

- *D'Alembert principle*
  Virtual[2] displacements δr^i for each position coordinate introduce additional forces acting on the body. In order to regain the equilibrial state (virtual) work is necessary. The *D'Alembert principle of virtual work* states that the work done by external forces corresponding to any set of virtual displacements is zero [101]:

$$\delta W = \sum_i (F^i - m^i a^i)\delta r^i = 0 \tag{2.8}$$

  From the *D'Alembert* principle the *Lagrange equations of the second kind*[3] can be derived [97] as

$$\frac{d}{dt}\left(\frac{\partial T}{\partial \dot{q}}\right) - \frac{\partial T}{\partial q} + \frac{\partial U}{\partial q} = \tau, \tag{2.9}$$

  where $\tau \in \mathbb{R}^n$ is the *generalized force* with τ_i acting on the generalized coordinate q_i [76]. T and U denote the kinetic and potential energy of the system explained in more detail subsequently.

- *Hamilton principle*
  This is an elegant approach that derives the dynamics via energetic considerations. The kinetic energy of a rigid body is composed of rotational and translational energy. For a body i with inertia tensor I_i, mass m_i, center of mass C_i, linear velocity $v = \dot{r}$ and angular velocity ω_i it is given as

$$T_i = \frac{1}{2} m_i \dot{r}_{C_i}^T \dot{r}_{C_i} + \frac{1}{2} \omega_i^T I_i \omega_i. \tag{2.10}$$

  The total kinetic energy of a multibody system is then the summation over all bodies

$$T = \sum_{i=1}^{n_b} T_i \tag{2.11}$$

  The potential energy for the i-th body and the total multibody system is

$$U_i = -m_i g_{\text{vec}}^T r_{C_i} + U_{\text{ref},i} \qquad\qquad U = \sum_{i=1}^{n_b} U_i, \tag{2.12}$$

  where g_{vec} is the vector of gravitational force and the constant $U_{\text{ref},i}$ is a reference potential [30]. Expressing the position and velocity in terms of the generalized coordinates

$$r = r(q) \qquad\qquad \dot{r} = \frac{d}{dt} r(q) = \frac{\partial r}{\partial q}\dot{q} = \dot{r}(q, \dot{q}) \tag{2.13}$$

  induces the dependencies $T = T(q, \dot{q})$ and $U = U(q)$. Defining the scalar function or so-called *Lagrangian* as

$$\mathcal{L}(\dot{q}, q) = T(\dot{q}, q) - U(q), \tag{2.14}$$

[2] Virtual is meant in the sense of fictitious/thought.
[3] The first kind in terms of *Cartesian* coordinates is not of interest in this thesis.

Hamilton's Principle of Least Action [9] then states that a system between two times t_0 and t_f tries to minimize the integral (or "action")

$$\int_{t_0}^{t_f} \mathcal{L}(q, \dot{q}) dt. \tag{2.15}$$

With the theory of *Calculus of Variations* (CoV) introduced later on, the *Euler-Lagrange* equations can be derived

$$\frac{d}{dt}\frac{\partial \mathcal{L}}{\partial \dot{q}} - \frac{\partial \mathcal{L}}{\partial q} = 0. \tag{2.16}$$

In terms of the kinetic and potential energy this can be reformulated as

$$\frac{d}{dt}\left(\frac{\partial T}{\partial \dot{q}}\right) - \frac{\partial T}{\partial q} + \frac{\partial U}{\partial q} = 0. \tag{2.17}$$

(2.17) is in accordance with the *Lagrange* equations of the second kind (2.9) derived from the principle of *D'Alembert* without the consideration of generalized forces, i.e. for conservative systems.

This approach is sufficient for holonomic systems and yields a concise derivation for low-dimensional problems. For practical purposes, however, this approach is not the most efficient due to extensive computing time. The subsequent algorithm is more suited for real-time implementations [65].

- *Newton-Euler algorithm*
  This is a recursive algorithm based on the linear and angular momentum principles of *Newton* and *Euler*. It is amenable to computer-aided calculations and therefore suited for the automatic generation of the equations of motion for high-dimensional systems with a computer algebra system.

- *Projection equation*
  Although this approach is cumbersome for low-dimensional systems, the inherent modular architecture proves beneficial for larger systems with many identical structured subsystems. Furthermore, a seamless integration of nonholonomic and flexible body systems is possible [19].

Pendulum example

Figure 2.2 depicts a mathematical pendulum suspended at $\tilde{q} = [0, 0]$ with link length $l > 0$, mass m and gravitational constant g (friction will not be considered). The *Cartesian* coordinates $\tilde{q} := [x, y]$ denote the position of the mass at the end of the pendulum. The descriptor form results from the consideration of forces acting on the mass in the *Cartesian* space:

$$\begin{gathered} \begin{bmatrix} m & 0 \\ 0 & m \end{bmatrix} \begin{pmatrix} \ddot{x} \\ \ddot{y} \end{pmatrix} + \begin{pmatrix} 0 \\ mg \end{pmatrix} + \begin{pmatrix} 2x \\ 2y \end{pmatrix} \lambda = \tilde{M}\ddot{\tilde{q}} + \tilde{Q} + \tilde{C}_{\tilde{q}}^T \lambda = 0 \\ x^2 + y^2 - l^2 = \tilde{C}(\tilde{q}) = 0 \end{gathered} \tag{2.18}$$

The link is assumed to be rigid and therefore the mass can only move on a circle around the origin of the reference frame $\tilde{q} = [x, y]$ with radius l. This is described by the holonomic

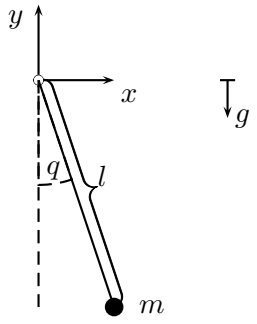

Figure 2.2: Single unforced mathematical pendulum

constraint $\tilde{C}(\tilde{q}) = 0$, which needs to be differentiated three times in order for the derivative of λ to appear explicitly

$$\frac{d}{dt}\tilde{C}(\tilde{q}) = 2x\dot{x} + 2y\dot{y} \tag{2.19a}$$

$$\frac{d^2}{dt^2}\tilde{C}(\tilde{q}) = \dot{x}^2 + \dot{y}^2 - yg \tag{2.19b}$$

$$\frac{d^3}{dt^3}\tilde{C}(\tilde{q}) = \frac{2\lambda}{m}x\dot{x} + \frac{2\lambda}{m}y\dot{y} + \dot{y}g + \frac{l^2}{m}\dot{\lambda} \tag{2.19c}$$

With $\hat{x} := [x, y, \dot{x}, \dot{y}]$ and (2.19c), the descriptor form (2.18) can be brought into the form of an ODE and therefore (2.18) is an index-3 DAE.

For the derivation of the minimal form via the *Hamilton* principle the energetic quantities are needed. The mass is assumed to be concentrated and not distributed ($\Rightarrow I \equiv 0$). The center of mass is located at

$$r_{C_1} = \begin{pmatrix} l\sin(q) \\ -l\cos(q) \end{pmatrix} \tag{2.20}$$

so that the kinetic energy results in

$$T(q, \dot{q}) = \sum_{i=1}^{1} T_i = \frac{1}{2}m\dot{r}_{C_1}^T\dot{r}_{C_1} + \frac{1}{2}\omega^T\underbrace{I}_{=0}\omega = \frac{1}{2}m\left(\dot{q}^2l^2\cos^2(q) + \dot{q}^2l^2\sin^2(q)\right) = \frac{1}{2}m\dot{q}^2l^2. \tag{2.21}$$

The potential energy due to (2.12) is given as

$$U(q) = -m\begin{pmatrix} 0 \\ -g \end{pmatrix}^T\begin{pmatrix} l\sin(q) \\ -l\cos(q) \end{pmatrix} = -mgl\cos(q). \tag{2.22}$$

With the *Euler-Lagrange* equation (2.17)

$$\frac{d}{dt}\left(\frac{\partial T}{\partial \dot{q}}\right) - \frac{\partial T}{\partial q} + \frac{\partial U}{\partial q} = ml^2\ddot{q} + mgl\sin(q) \stackrel{!}{=} 0 \tag{2.23}$$

the dynamics in minimal form $M\ddot{q} + h(q) = 0$ (cf. (2.7)) follow immediately as

$$m\ddot{q} + \frac{gm}{l}\sin(q) = 0. \tag{2.24}$$

2.3 Preliminaries of Rigid Robots

The word robot originates from the czech term "robota", which roughly translates as forced labor. While the average person understands a robot as a fully articulated, anthropomorphic and sophisticated mechanical being as known from science fiction literature, the definition of a robot among engineers is ambiguous and not unified. In [46] a definition is given as follows:

> *A robot is a machine capable of performing tasks with some level of autonomy and flexibility, in some type of environment. To achieve this capability, a robot integrates one or several sensory-motor functions together with communication and information processing capabilities.*

The incorporation of low-level and high-level features makes robotics an interdisciplinary interweaved science. High-level features, such as perceiving and reacting to external stimuli from the environment on an abstract level (planning and reasoning), are not topic of this thesis. Here, it will be sufficient to understand a robot as an actuated system that can be modeled as nonconservative multibody system whose control is of primary interest.

The robotics community differentiates between *serial* and *parallel robots*, where the differentiation is based on the underlying kinematic structure. Consecutive coordinate systems that can be articulated against each other yield a kinematic chain. The topology of robotic systems can be subdivided into chain-like, tree-structured and closed-looped structures [65], where the last two lead to the class of parallel robots.

A serial robot (or: *manipulator*) is modeled as an alternating chain of links (rigid bodies of Chapter 2.1) and joints. The joints may be either revolute or prismatic joints. Some others include cylindrical, planar, screw or spherical [30], but occur more rarely. In this thesis only serial robots with revolute joints are considered.

Locating the position of the last coordinate frame in the *Cartesian* space (also: *end-effector*) by a given set of joint angles is known as *forward kinematics*. *Inverse kinematics* is the problem of finding the joint angles that would lead to a pre-specified *Cartesian* position of the end-effector. For the calculation of the energies in in the previous chapter it was necessary to locate the position of the center of masses in the bodies. A standardized convention widely used in the robotic community is the *Denavit-Hartenberg* notation [30, 106]. However, the kinematics in this thesis will be simple enough so that this convention is not necessary.

Dynamics of rigid robots

While kinematics only treats the motion of the system without regarding the forces which cause it, dynamics also includes the study of forces. Since robots are modeled as multibody systems, the dynamics take the form of (2.7), written in the typical form for robotics [76]:

$$M(q)\ddot{q} + c(q,\dot{q}) + g(q) = \tau_F + \tau_m = \tau \tag{2.25}$$

The mass matrix $M(q) \in \mathbb{R}^{n\times n}$ is symmetric and positive definite, therefore always invertible and $M^{-1}(q)$ exists [25, 76, 99]. $c(q,\dot{q}) \in \mathbb{R}^n$ is the vector of centripetal/*Coriolis* force terms

and $g(q) \in \mathbb{R}^n$ the gravitational vector. Nonconservative forces $\tau \in \mathbb{R}^n$ typically appear on the right-hand side. This includes external forces, such as the motor torques τ_m and dissipative effects, such as friction τ_F. The kinetic energy can be conveniently expressed as

$$T = \frac{1}{2}\dot{q}^T M(q)\dot{q}. \tag{2.26}$$

2.4 Flexible Joint Robot Dynamics

The assumption that robotic systems consist only of rigid links and actuators is an idealized assumption. For slow movements or when no (force) interaction with the environment occurs, this might be close to the real system, but it is obvious that in general this is a simplification. There is always mechanical flexibility inherent in the robotic structure, e.g. induced by transmission elements, such as gears or by a lightweight architecture of the links. This leads to deflections between the motor and link positions. These small uncertainties are not considered in the model (2.25) and the error propagates throughout the serial structure of the robot. This typically results in undesired effects that lead to deviations of the end-effector from the calculated results or more generally to a degradation of the expected performance. One of the most frequent application of robotics in the industry is the welding of parts in an assembling line. As a direct consequence, the welding line is not tracked with the desired accuracy.

To cope with these problems, a new dynamic model is necessary. Flexible link models would lead to the already mentioned flexible multibody systems, which are difficult to calculate (in real-time). Furthermore, the high-fidelity control of these devices is a rather unsolved problem. Here, the joint is remodeled so that uncertainties are emulated by a small spring with high stiffness constant. Joint and motor can take different positions now so that the system needs twice the number of generalized coordinates of the rigid body robot to be fully described

$$\Theta = \begin{pmatrix} q \\ \theta \end{pmatrix} \in \mathbb{R}^{2n}, \tag{2.27}$$

where $\theta \in \mathbb{R}^n$ denotes the motor-side and $q \in \mathbb{R}^n$ the link-side positions. The deflection $\varphi = \theta - q$ between link and motor is assumed to be small. Due to this fact, it is sufficient here for the transmitted joint torque to assume a linear dependence on the deflection

$$\tau_J = K(\theta - q), \tag{2.28}$$

where $K = diag\{k_1, ..., k_n\}$ is a positive definite stiffness matrix. Moreover, for the derivation of the dynamics, [99] postulates the following assumptions

A1) *Joint deflections are small, so that flexibility effects are limited to the domain of linear elasticity.*

A2) *The actuators' rotors are modeled as uniform bodies having their center of mass on the rotation axis.*

A3) *Each motor is located on the robot arm in a position preceding the driven link.*

These assumptions are reasonable and most real-world robots fulfill them. For the derivation of the dynamics for the new model via the *Lagrangian* approach (2.14), the energetic quantities are needed. In addition to the kinetic energy of the link $\mathcal{T}_{link}$, the kinetic energy of the motor $\mathcal{T}_{motor}$ needs to be considered now as well, so that the total kinetic energy of the flexible joint robot is $\mathcal{T} = \mathcal{T}_{link} + \mathcal{T}_{motor}$. The kinetic energy of the link remains unchanged compared to the kinetic energy of the rigid body robot (2.26)

$$\mathcal{T}_{link}(q, \dot{q}) = \frac{1}{2}\dot{q}^T M_L(q)\dot{q}, \tag{2.29}$$

with $M_L(q)$ being the link mass matrix (former $M(q)$). The kinetic energy of the motor is only contributed by the kinetic energy of the rotor so that it can be calculated from

$$\mathcal{T}_{motor} = \mathcal{T}_{rotor} = \sum_{i=1}^{n} \mathcal{T}_{rotor,i} = \sum_{i=1}^{n} \frac{1}{2} m_{r_i} v_{r_i}^T v_{r_i} + \frac{1}{2}\omega_{r_i}^T I_{r_i} \omega_{r_i}, \tag{2.30}$$

where m_{r_i}, $v_{r_i}(q, \dot{q})$ and $\omega_{r_i}(\dot{\theta})$ denote the mass, linear velocity and angular velocity of the i-th rotor body. The corresponding inertia tensor $I_i = diag\{I_{xxr_i}, I_{yyr_i}, I_{zzr_i}\}$ is of diagonal form due to assumptions. The third assumption guarantees the form of

$$\mathcal{T}_{rotor} = \frac{1}{2}\dot{q}^T \left[M_R(q) + S(q)B^{-1}S^T(q)\right]\dot{q} + \dot{q}^T S(q)\dot{\theta} + \frac{1}{2}\dot{\theta}^T B\dot{\theta}, \tag{2.31}$$

where $M_R(q)$ is the rotor mass matrix, B the diagonal rotor inertia matrix and $S(q)$ encodes the inertial coupling between the links and motors. This can be written in a compact form in terms of the new generalized coordinates as

$$\mathcal{T} = \frac{1}{2}\dot{\Theta}^T \mathcal{M}(\Theta)\dot{\Theta} = \frac{1}{2}\begin{pmatrix}\dot{q}^T & \dot{\theta}^T\end{pmatrix}\begin{bmatrix} M(q) & S(q) \\ S^T(q) & B \end{bmatrix}\begin{pmatrix}\dot{q} \\ \dot{\theta}\end{pmatrix}, \tag{2.32}$$

with $M(q) := M_L(q) + M_R(q) + S(q)B^{-1}S^T(q)$. Similarly, the potential energy of the rigid body robot needs to be extended appropriately. For the potential energy of the flexible joint robot the gravitational energy $\mathcal{U}_{grav}$ is supplemented by elastic energy $\mathcal{U}_{elas}$ stored in the (virtual) spring

$$\mathcal{U} = \mathcal{U}_{grav}(q) + \mathcal{U}_{elas}(q, \theta) = \mathcal{U}_{grav,link}(q) + \mathcal{U}_{grav,motor}(q) + \mathcal{U}_{elas}(q, \theta), \tag{2.33}$$

with

$$\mathcal{U}_{elas}(q, \theta) = \frac{1}{2}(\theta - q)^T K(\theta - q) = \frac{1}{2}\varphi^T K \varphi. \tag{2.34}$$

The gravitational energy by the motor is the same as the one given in (2.12). The full dynamic model is then derived using the *Lagrangian* $\mathcal{L}(\Theta, \dot{\Theta}) = \mathcal{T}(\Theta, \dot{\Theta}) - \mathcal{U}(\Theta)$ as

$$\begin{bmatrix} M(q) & S(q) \\ S^T(q) & B \end{bmatrix}\begin{pmatrix}\ddot{q} \\ \ddot{\theta}\end{pmatrix} + \begin{pmatrix} c(q, \dot{q}) + c_1(q, \dot{q}, \dot{\theta}) \\ c_2(q, \dot{q}) \end{pmatrix} + \begin{pmatrix} g(q) + K(q - \theta) \\ K(\theta - q) \end{pmatrix} = \begin{pmatrix} 0 \\ \tau_m \end{pmatrix} \tag{2.35}$$

or in the compact form (2.25) written in terms of the generalized coordinates $\Theta, \boldsymbol{\tau} \in \mathbb{R}^{2n}$:

$$\mathcal{M}(\Theta)\ddot{\Theta} + c(\Theta, \dot{\Theta}) + g(\Theta) = \boldsymbol{\tau} \tag{2.36}$$

Reduced flexible joint model

For robots with high gear reductions in the joints, the inertial coupling between links and motors can be neglected. The equivalent assumption is that the angular velocity of the rotors is only due to their own spinning. This simplifies the kinetic energy of the rotor from (2.31) to $\mathcal{T}_{rotor} = \frac{1}{2}\dot{\theta}^T B\dot{\theta}$ and the coupling matrix vanishes $S \equiv 0$ [99]. The reduced model follows immediately as[4]

$$\begin{aligned} M(q)\ddot{q} + c(q,\dot{q}) + g(q) + K(q-\theta) &= 0 \\ B\ddot{\theta} + K(\theta - q) &= \tau_m. \end{aligned} \tag{2.37}$$

The first n equations belong to the link-side dynamics and the last n equations to the motor-side dynamics. It is beneficial that the dynamics appear in a decoupled manner and the motor-side dynamics are even linear. This model is sufficient for most real-world robots and successful implementations for control schemes have been implemented, see e.g. [4].

2.5 Intrinsically Compliant Robots

As mentioned earlier, the flexible joint model was necessary to cope with uncertainties that arise in the control of a mechanically rigid robot. The deflections are an undesired byproduct and the aim is to diminish these effects by appropriate vibration damping control.

This is fundamentally different for a new generation of robots currently being developed and which is in the focus of current research. As in Chapter 1 already briefly mentioned, these so-called *intrinsically compliant robots* (also: *intrinsic elastic joint robots*) are equipped with mechanisms that permit inherent impedance behaviors on a joint level. The corresponding actuators are called *variable stiffness actuators* or *variable impedance actuators* if the stiffness can be adjusted or just *intrinsically compliant joints* if the stiffness is constant throughout. The recently completed EU project *VIACTORS* [2] was solely dedicated to variable impedance actuators. Here, the deflections are a desired effect that one wishes to exploit with regards to performance, e.g. by storing and releasing potential energy.

Design proposals

A number of different submissions for joint designs with variable stiffness have been proposed over the last few years. An overview can be found in [53]. Generally, the designs can be roughly grouped into the categories of *preload variable design* and *transmission variable design*, where the former evolved from actuators with constant stiffness and the latter is human-inspired [39]. Most of them incorporate mechanical springs to alter the impedance characteristics, but there have also been experiments with other mechanism, such as electroactive polymer [27] or pneumatic [29, 104] actuators, which will not be considered here.

[4] *Coriolis* and centrifugal terms c_1 and c_2 from (2.35) arise because of the presence of the coupling matrix [99].

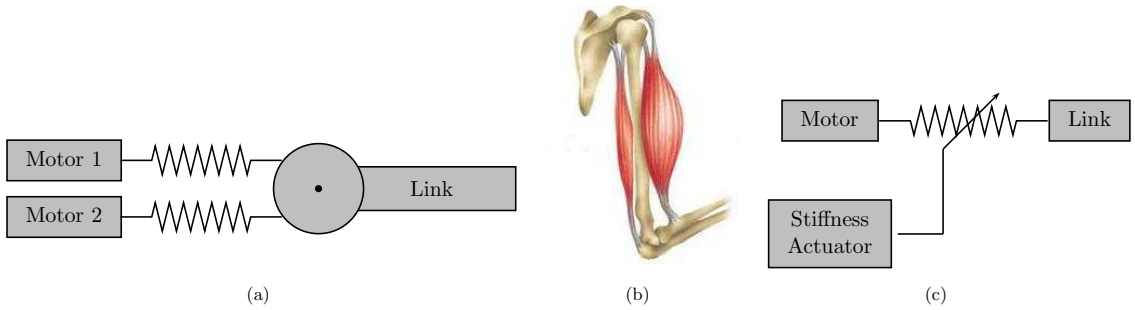

Figure 2.3: (a) Antagonistic joint design with (b) human antetype [1]; (c) Quasi-antagonistic design

The human-inspired actuators fall under the category of antagonistic and quasi-antagonistic design. The antagonistic design tries to emulate the muscle-tendon-bone structure prevalent in almost all vertebrates by two motors that are connected to the link via springs, see Figure 2.3(a). It bases on the principle that many muscle work in pairs with a so-called agonist and antagonist muscle. The analogy to robotics is that actuators correspond to muscles, tendons to springs and bones to links. Tendons (and also ligaments) are passive compliant elements in the human musculoskeletal system that are not only very stiff, but also exhibit nonlinear stiffness characteristics which enables the human to adjust its joint stiffness a-priori by simultaneous contraction (or retraction) of both the agonist and antagonist muscle [50]. A quasi-antagonistic joint only uses one motor and spring, but in addition a mechanism that can adjust the stiffness, see Figure 2.3(c).

Dynamics

As opposed to the previous chapter of flexible joint robots, the deflection here is not small, i.e. $\varphi = \theta - q \gg 0$ and intentionally used to store and release potential energy. The dynamics can be described by

$$\begin{aligned} M(q)\ddot{q} + c(q,\dot{q}) + g(q) - \tau_J &= 0 \\ B\ddot{\theta} + \tau_J &= \tau_m \\ 0 &= f_{SA}(\ddot{\sigma}, \dot{\sigma}, \sigma, \tau_{SA}). \end{aligned} \tag{2.38}$$

The first two equations describe the motor and link dynamics already known from the Chapter 2.4. These remain unchanged except that τ_J is not generated by a spring assumed to be in the domain of linear elasticity. Assumptions A2) and A3) still hold and the requirements can be met by mechanical design. The third equation describes implicitly the dynamics of a mechanism that is able to influence the transmitted torque by some output σ and is controlled by τ_{SA}. The transmitted joint torque $\tau_J = \tau_J(q, \theta, \sigma)$ then undergoes a nonlinear transformation depending on q, θ and σ. The entire system is controlled by the motor and stiffness actuator inputs $u = (u_1, u_2)^T := (\tau_m, \tau_{SA})^T$, see Figure 2.4.

For example, the variable stiffness joint "*Floating Spring Joint*" (FSJ) developed at the DLR has the capability of adjusting the impedance characteristics via cam disks [107]. The spring

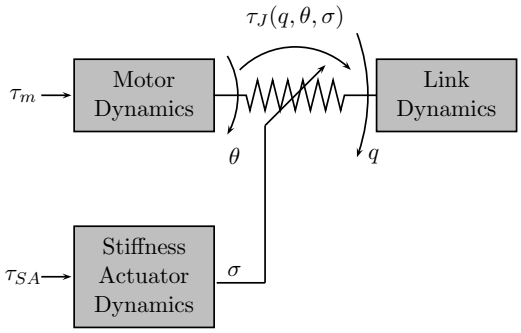

Figure 2.4: Schematic for a variable stiffness robot with quasi-antagonistic design.

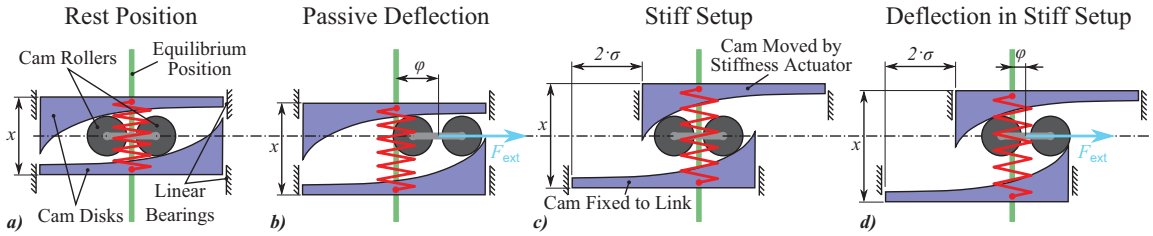

Figure 2.5: The DLR FSJ: Schematic overview (taken from [107]) for different configurations: (a),(b) show the cam disks in initial configuration and (c),(d) in displaced configuration.

is compressed from its initial state by lowering the distance σ between the two cam disks, see Figure 2.5. The dynamics of σ can for example be described by a PT2 element. For optimization purposes it is helpful to obtain an analytical expression of the first derivative that can be passed to the optimization software in order to speed up the process. The nonlinear transformation takes the form of a progressive spring characteristic induced by design of the cam disks

$$\tau_J = c_1 \left(e^{c_2((\theta-q)-\sigma)} - e^{c_2(-(\theta-q)-\sigma)} \right), \tag{2.39}$$

where c_1, c_2 are positive parameters that can be found in the course of joint identification, e.q. via least-square error approximations [59].

For theoretical considerations later on, the system needs to be simplified. Assuming the torque behaves linearly in terms of the deflection and the stiffness can be controlled directly. This results in

$$\tau_J(q,\theta,\sigma) = \sigma(\theta - q) = K(\theta - q) = u_2(\theta - q), \tag{2.40}$$

where u_2 is the control corresponding to the stiffness. The stiffness actuator dynamics are eliminated. Future work will consider elastic joint torques of more complex form, such as (2.39).

Velocity controlled variable stiffness actuator model

Another simplification can be made for the motor dynamics. The underlying assumption is that the motor dynamics are much faster than the link dynamics for intrinsically elastic robots. This is due to the fact that the motor torque is greater than the transmitted joint torque[5]. Formally, this can be shown by bringing the dynamics into so-called *singular perturbation* form. The basic idea is to decompose the system into subsystems with "fast" and "slow" dynamics. For more on singular perturbation theory see e.g. [64]. Applying a pure P-control results in [52]

$$B\ddot{\theta} + \tau_J = \tau_m \stackrel{!}{=} K_P(u - \dot{\theta}), \tag{2.41}$$

where K_P is the proportional control gain. Define $\varepsilon := K_p^{-1}$ so that (2.41) becomes

$$\varepsilon \left(B\ddot{\theta} + \tau_J \right) = u - \dot{\theta}. \tag{2.42}$$

For $\varepsilon \to 0$ the first-order dynamics

$$u = \dot{\theta} \tag{2.43}$$

are obtained. As a result, the dynamics of a velocity controlled variable stiffness robot are

$$\begin{aligned} M(q)\ddot{q} + c(q,\dot{q}) + g(q) - \tau_J &= 0 \\ \dot{\theta} &= u. \end{aligned} \tag{2.44}$$

This simplification enhances computational speed but is only truly valid if the deflection is small enough so that the link inertia takes a negligible effect on the motor dynamics.

Constraints

Every real-world system is subject to certain constraints imposed by e.g. design, electric and mechanical components or the environment. The actuators in every robotic system can only generate a certain motor torque, so the input is bounded. Furthermore, joint angles are limited so that no self-collisions occur. For intrinsically compliant robots the spring can only expand to a certain degree. This constraint on the deflection is particularly important and must not be violated at all cost because the robotic system will or might get damaged. From a mathematical point of view, this leads to inequality constraints depending on the state $C(x) \leq 0$ and control $C(u) \leq 0$ or potentially even in mixed form $C(x,u) \leq 0$.

A robotic system that incorporates all the features mentioned before, is the DLR HASy, which has been briefly mentioned in Chapter 1. It is equipped with four quasi-antagonistic FSJ joints and additional three antagonistic (BAVS) joints. In total, the arm has 7 DoF which corresponds to the degrees of freedom of the human arm [50]. The hand itself is highly complex but not of interest in this thesis.

1 DoF intrinsically compliant robot (Pendulum example continued)

Returning to the example of Chapter 2.2, the dynamics of the single pendulum can be easily extended to a 1 DoF intrinsically compliant robot. The pendulum is acted upon an external

[5]The assumption does not hold for flexible joint robots, where the range of K is at least an order of magnitude larger.

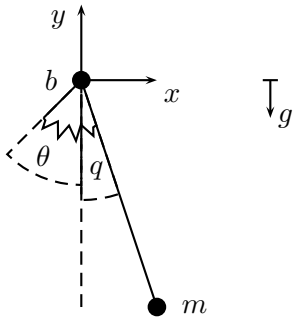

Figure 2.6: 1 DoF intrinsically compliant robot

torque τ_J transmitted through the joint, so that (2.24) becomes

$$m\ddot{q} + \frac{mg}{l}\sin(q) = \tau_J. \tag{2.45}$$

Let θ be the motor position, b the motor inertia and τ_m the torque generated by the motor, then the motor dynamics take the form of (2.38)

$$b\ddot{\theta} + \tau_J = \tau_m. \tag{2.46}$$

Together with the assumption of a linear relation between joint torque and deflection as in (2.37), where k is the stiffness constant, this yields the dynamics of the 1 DoF intrinsically compliant robot:

$$\begin{aligned} m\ddot{q} + \frac{gm}{l}\sin(q) + k(q-\theta) &= 0 \\ b\ddot{\theta} + k(\theta - q) &= \tau_m \end{aligned} \tag{2.47}$$

Chapter 3

Calculus of Variations and Optimal Control Theory

Calculus of Variations (CoV) deals with minimizing functionals subject to either integral, differential or algebraic constraints (and arbitrary combinations of those).
Among the first problems relating to CoV (and by far the most popular examples in textbooks) were

- Isoperimetric Problem:
  For example, find the plane curve of a given length encompassing the greatest area. This problem reaches far back in time and the anecdote of *Queen Dido of Carthage* (ca. 850 BC) is often told, where she was promised as much land as might lie within the boundaries of an oxhide (cut to fine strips and tied together) and the sea coast. Legend has it that *Carthage* was founded this way.

- Brachistochrone Problem:
  Find the shortest path in a vertical plane between two points such that a particle will traverse it in shortest time (where the acceleration is only due to gravity). Originally proposed by *Johann Bernoulli* (1667-1748) and published in the scientific journal *Acta Eruditorum* in 1696 and addressed to the greatest mathematicians of that time.

Leonhard Euler (1707-1783) and *Joseph-Louis Lagrange* (1736-1813) systematically tackled these problems with their variational approach and laid the fundamentals for further investigation of CoV. Since its inception, the theory has been applied to a large variety of physical and mathematical problems and many famous mathematicians contributed to the field over time, such as *Isaac Newton* (1643-1727), *Gottfried Wilhelm Leibniz* (1646-1716), *Adrien-Marie Legendre* (1752-1833) in the 18th century, significantly extended by *Carl Jacobi* (1804-1851), *Karl Theodor Weierstrass* (1815-1897), *David Hilbert* (1862-1943) in the 19th century (for an in-depth look into the history of CoV see e.g. [49]).

Optimal control theory is a subset of CoV dealing with an differential equation and additional constraints, such as algebraic equality and inequality constraints. The function in CoV is split up into state and control variables with different demands on smoothness. Optimal control problems arise in many diverse branches such as robotics [25], chemical engineering [66, 100], economics [91] and aerospace applications [14, 62, 68] to only name a few.

CoV preliminaries are given in the following to grasp the underlying nature of optimal control theory, which is then introduced along with a few of its fundamental aspects as constraints, singular optimal control problems, and the corresponding numerical treatment.

3.1 Calculus of Variations

The most basic CoV problem one can think of is to minimize

$$J_a(x(t)) = \int_{t_0}^{t_f} \phi(x(t), \dot{x}(t), t)dt \rightarrow \min! \tag{3.1}$$

subject to fixed initial and end points

$$x(t_0) = x_0, \tag{3.2a}$$
$$x(t_f) = x_f. \tag{3.2b}$$

For now, it is assumed that $x \in C^1([t_0, t_f], \mathbb{R})$ and $\phi \in C^2([t_0, t_f] \times \mathbb{R}^{2n}, \mathbb{R})$. The subsequent lemma is crucial for the derivation of the necessary conditions:
Lemma 3.1.1 (Fundamental Lemma of CoV)**.**
Let $F \in C^0([t_0, t_f], \mathbb{R})$ and $\eta \in C^1([t_0, t_f], \mathbb{R})$ with $\eta(t_0) = \eta(t_f) = 0$ then:

$$\forall \eta : \qquad \int_{t_0}^{t_f} F \cdot \eta dt = 0 \Rightarrow F \equiv 0 \tag{3.3}$$

The proof is usually carried out by contradiction and uses test functions with small compact support. It can be found in every well-assorted optimal control book, e.g. [67, 71].

First-order necessary condition

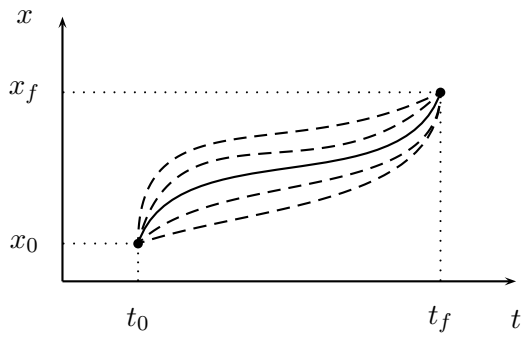

Figure 3.1: Optimal solution x^* (solid) and comparison curves (dashed) for fixed initial time and state, as well as final time and state.

Assuming the existence of an optimal solution x^*, the procedure to derive the necessary conditions is as follows:
x^* is linearly embedded in a one-dimensional family of comparison curves (see Figure 3.1)

$$x^* + \varepsilon\delta x, \tag{3.4}$$

with $\varepsilon \in \mathbb{R}$ and $\delta x \in C^1([t_0, t_f], \mathbb{R})$. For small ε the perturbed curves are close in the sense of the 1-norm and the obtained necessary conditions only hold for weak solutions (see Figure 3.2). However, if the strong solution is in C^1 it is also a weak solution [71]. If no variations at initial and endpoints are allowed then $\delta x(t_0) = \delta x(t_f) = 0$ and so these points remain fixed. Insertion of (3.4) into (3.1) leads to

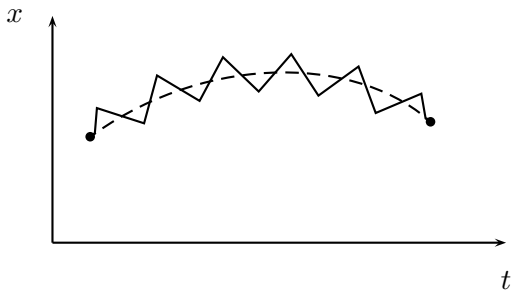

Figure 3.2: Weak (dashed) and strong (solid) solution

$$J_a(x^* + \varepsilon\delta x) = \int_{t_0}^{t_f} \phi(x^* + \varepsilon\delta x, \dot{x}^* + \varepsilon\dot{\delta x}, t)dt. \tag{3.5}$$

The *Gâteaux-Derivative* [80] can be seen as generalization of the well-known directional derivative and is defined between locally convex topological vector spaces, e.g. *Banach* spaces, as

$$\delta J_a(x^*; \delta x) = \lim_{\varepsilon \to 0} \frac{J_a(x^* + \varepsilon\delta x) - J_a(x^*)}{\varepsilon} = \frac{d}{d\varepsilon} J_a(x^* + \varepsilon\delta x)\bigg|_{\varepsilon=0}. \tag{3.6}$$

In the context of CoV, equation (3.6) is called the first variation. In (unconstrained) static optimization, an approach with the *Taylor* expansion around perturbations of the local minimum leads to the first-order necessary condition $f'(x) = 0$ ($f : \mathbb{R} \to \mathbb{R}$, f sufficiently smooth). An analogous ansatz can be made for dynamic optimization problems which yields that the first variation needs to vanish in order to obtain a first-order necessary condition for a local minimum [71]. Therefore,

$$\frac{d}{d\varepsilon} J_a(x^* + \varepsilon\delta x)\bigg|_{\varepsilon=0} \overset{!}{=} 0 \tag{3.7}$$

needs to hold. Now, the necessary condition can be derived for the problem (3.1)

$$\frac{dJ_a}{d\varepsilon}\bigg|_{\varepsilon=0} = \int_{t_0}^{t_f} \underbrace{\frac{\partial\phi}{\partial x}}_{=:\phi_x}(x^*, \dot{x}^*, t) \cdot \delta x + \underbrace{\frac{\partial\phi}{\partial\dot{x}}}_{=:\phi_{\dot{x}}}(x^*, \dot{x}^*, t) \cdot \dot{\delta x} dt \tag{3.8}$$

Integrating by parts, the unknown $\dot{\delta x}$ in the second integral term disappears

$$\left.\frac{dJ_a}{d\varepsilon}\right|_{\varepsilon=0} = \phi_{\dot{x}}\delta x\Big|_{t_0}^{t_f} + \int_{t_0}^{t_f}(\phi_x - \frac{d}{dt}\phi_{\dot{x}})\delta x dt \tag{3.9}$$

The importance of the Fundamental Lemma of CoV now becomes evident, as it finalizes the derivation by applying it to (3.9)

$$\frac{\partial}{\partial x}\phi(x^*, \dot{x}^*, t) - \frac{d}{dt}\frac{\partial}{\partial \dot{x}}\phi(x^*, \dot{x}^*, t) = 0. \tag{3.10}$$

Note that this step implicitly demands that $\phi \in C^2$ ($\frac{\partial}{\partial \dot{x}}\phi$ needs to be in C^1). For less smoothness such as $\phi \in C^1$, one has to resort to the *Lemma of DuBois-Reymond*. (3.10) is the infamous *Euler-Lagrange equation* and all of its solutions are called *extremals* [71]. The *Euler-Lagrange* equation is an explicit ODE of second order and describes together with the boundary conditions (3.2) a *two-point boundary value problem* (TPBVP). For varying initial and endpoints, the ODE (3.10) must suffice the so-called *natural boundary conditions*

$$\phi_{\dot{x}}\Big|_{t_0} = 0, \qquad \phi_{\dot{x}}\Big|_{t_f} = 0. \tag{3.11}$$

Free end state and end time

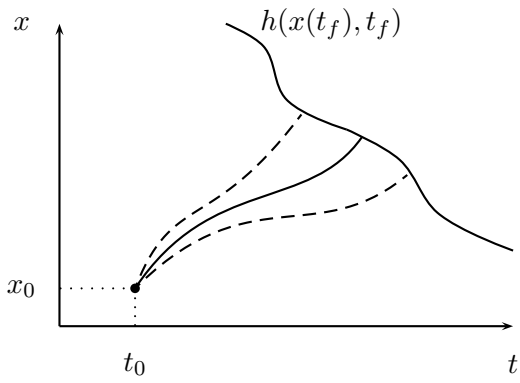

Figure 3.3: Optimal solution x^* (solid) and comparison curves (dashed)

Assume that the end condition is not given as a boundary condition in the form (3.2b) but rather implicitly as

$$h(x(t_f), t_f) = 0. \tag{3.12}$$

In order to get *admissible* variations, the problem has to be transformed into an unconstrained problem. This is achieved by adjoining (3.12) with a *Lagrange* parameter $\nu \in \mathbb{R}^{n_\nu}$ to the cost functional (3.1) so that the reformulated cost functional reads as

$$J(x(t)) := \nu \cdot h(x(t_f), t_f) + \int_{t_0}^{t_f} \phi(x(t), \dot{x}(t), t)dt. \tag{3.13}$$

In addition to variations of the function x along the trajectory, variations of the final time and final state need to be considered now as well:

$$J(\varepsilon) = \nu \cdot h(x(t_f) + \varepsilon\delta x(t_f), t_f + \varepsilon\delta t_f) + \int_{t_0}^{t_f+\varepsilon\delta t_f} \phi(x(t) + \varepsilon\delta x, \dot{x}(t) + \varepsilon\dot{\delta x}, t)dt \tag{3.14}$$

Preceding as in (3.8)-(3.9)

$$\left.\frac{dJ}{d\varepsilon}\right|_{\varepsilon=0} = \nu\cdot\frac{\partial h}{\partial x_f}\delta x_f + \nu\cdot\frac{\partial h}{\partial t_f}\delta t_f + \phi\Big|_{t_f}\delta t_f + \phi_{\dot{x}}\Big|_{t_f}(\delta x_f - \dot{x}\delta t_f)\Big|_{t_f} + \int_{t_0}^{t_f}\left[\phi_x - \frac{d}{dt}\phi_{\dot{x}}\right]\delta x dt \tag{3.15}$$

and grouping terms with the help of the relation $\delta x_f = \delta x(t_f) + \dot{x}\delta t_f$ [67, 88], the first variation for free final time and state is obtained

$$\begin{aligned}\delta J = &+ \left(\nu\cdot\frac{\partial h}{\partial x_f} + \phi_{\dot{x}}\right)\Big|_{t_f}\delta x_f \\ &+ \left(\nu\cdot\frac{\partial h}{\partial t_f} + \phi - \dot{x}\phi_{\dot{x}}\right)\Big|_{t_f}\delta t_f \\ &+ \int_{t_0}^{t_f}\left[\phi_x - \frac{d}{dt}\phi_{\dot{x}}\right]\delta x dt.\end{aligned} \tag{3.16}$$

Together with the boundary conditions at initial time and the Fundamental Lemma, the TPBVP can be formulated as

$$\phi_x - \frac{d}{dt}\phi_{\dot{x}} = 0 \tag{3.17}$$

subject to

$$\begin{aligned} t_0 &= 0, \\ x(t_0) &= x_0, \\ \nu\cdot\frac{\partial h}{\partial x_f} + \phi_{\dot{x}}\Big|_{t_f} &= 0, \\ \nu\cdot\frac{\partial h}{\partial t_f} + (\phi - \dot{x}\phi_{\dot{x}})\Big|_{t_f} &= 0, \\ h(x(t_f), t_f) &= 0, \end{aligned} \tag{3.18}$$

where $h(x(t_f), t_f) = 0$ are the so-called side conditions [22]. This can be carried out analogously for free initial time and state, albeit uncommon in engineering applications.

General first variation

To further extend the problem formulation, a finite amount of discontinuities of the solution is permitted. This means $x \in C_p^1([t_0, t_f], \mathbb{R})$, the function space of piecewise continuously differentiable functions. Without loss of generality only one jump at t_J is considered, the extension to multiple jumps is straightforward. Again, the jump condition is adjoined in the same manner as before as well as initial and terminal conditions by $g := \nu \cdot h(...)$, making the functional

$$J(x(t)) = g(t_0, t_J, t_f, x(t_0), x(t_J^-), x(t_J^+), x(t_f)) + \int_{t_0}^{t_f}\phi(x(t), \dot{x}(t), t)dt \tag{3.19}$$

The general first variation is derived as seen previously with the corresponding variations (cf. [80])

$$\begin{aligned}
\delta J = &+ \left[\frac{\partial g}{\partial t_0} - (\phi - \dot{x}\phi_{\dot{x}})\right]\Bigg|_{t_0} \delta t_0 \\
&+ \left[\frac{\partial g}{\partial t_J} + (\phi - \dot{x}\phi_{\dot{x}})^- - (\phi - \dot{x}\phi_{\dot{x}})^+\right]\Bigg|_{t_J} \delta t_J \\
&+ \left[\frac{\partial g}{\partial t_f} + (\phi - \dot{x}\phi_{\dot{x}})\right]\Bigg|_{t_f} \delta t_f \\
&+ \left[\frac{\partial g}{\partial x_0} - \phi_{\dot{x}}\right]\Bigg|_{t_0} \delta x_0 \\
&+ \left[\frac{\partial g}{\partial x_J^-} + \phi_{\dot{x}}^-\right]\Bigg|_{t_J} \delta x_J^- + \left[\frac{\partial g}{\partial x_J^+} - \phi_{\dot{x}}^+\right]\Bigg|_{t_J} \delta x_J^+ \\
&+ \left[\frac{\partial g}{\partial x_f} + \phi_{\dot{x}}\right]\Bigg|_{t_f} \delta x_f \\
&+ \int_{t_0}^{t_f} \left[\phi_x - \frac{d}{dt}\phi_{\dot{x}}\right] \delta x dt,
\end{aligned} \tag{3.20}$$

where $x(t_J^{\pm}) := \lim_{\varepsilon \to 0, \varepsilon > 0} x(t_J \pm \varepsilon)$.

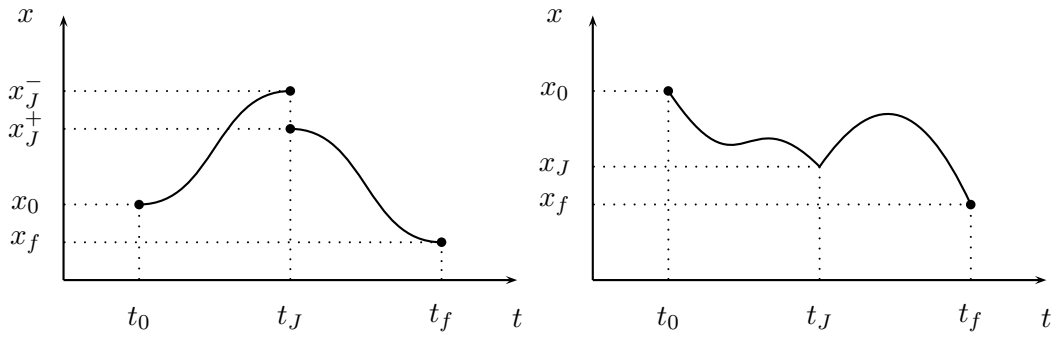

Figure 3.4: Discontinuity (left) and corner (right) at t_J

Due to interior point conditions (terms 2, 5 and 6 of (3.20)) this is not a TPBVP anymore. Now a *multi-point boundary value problem* (MPBVP) needs to be solved comprising the *Euler-Lagrange equation* and corresponding point conditions.

Corner conditions

If a continuous solution is desired, $x \in C_c^1([t_0, t_f], \mathbb{R})$, then the condition at a jump is $x_J^- - x_J^+ = 0$. Again, adjoining it with a *Lagrange* parameter ν to the term g (arguments of g dropped for readability) $\tilde{g} := g + \nu(x_J^- - x_J^+)$ leads to the following partial derivatives

$$\frac{\partial \tilde{g}}{\partial t_J} = 0, \qquad \frac{\partial \tilde{g}}{\partial x_J^+} = -\nu, \qquad \frac{\partial \tilde{g}}{\partial x_J^-} = \nu. \tag{3.21}$$

Summands 2,5 and 6 from the first variation (3.20) for varying t_J, x_J^+ and x_J^- yield

$$\left[\underbrace{\frac{\partial \tilde{g}}{\partial t_J}}_{=0} + (\phi - \dot{x}\phi_{\dot{x}})^- - (\phi - \dot{x}\phi_{\dot{x}})^+\right]\Bigg|_{t_J} = 0 \tag{3.22}$$

$$\left[\underbrace{\frac{\partial \tilde{g}}{\partial x_J^-}}_{=\nu} + \phi_{\dot{x}}^-\right]\Bigg|_{t_J} = 0 \qquad \left[\underbrace{\frac{\partial \tilde{g}}{\partial x_J^+}}_{=-\nu} - \phi_{\dot{x}}^+\right]\Bigg|_{t_J} = 0 \tag{3.23}$$

Solving (3.23) for ν together with (3.22) becomes

$$\phi_{\dot{x}}^- = \phi_{\dot{x}}^+ \tag{3.24a}$$

$$(\phi - \dot{x}\phi_{\dot{x}})^- = (\phi - \dot{x}\phi_{\dot{x}})^+ \tag{3.24b}$$

(3.24a) and (3.24b) are called first and second *Erdmann-Weierstrass* corner condition, respectively. The *Hamiltonian* (or *Hamilton* function) is defined as

$$H := \phi(x, \dot{x}, t) - \dot{x}\phi_{\dot{x}}(x, \dot{x}, t) \tag{3.25}$$

The *Beltrami identity* (a special case of *Noether's (first) theorem*) states that the *Hamiltonian* is constant if the independent variable does not appear explicitly (time-invariant case)

Proof

$$\frac{d}{dt}H = \phi_t + \phi_x\dot{x} + \phi_{\dot{x}}\ddot{x} - \ddot{x}\phi_{\dot{x}} - \dot{x}\left(\frac{d}{dt}\phi_{\dot{x}}\right) = \phi_t + \dot{x}\underbrace{(\phi_x - (\frac{d}{dt}\phi_{\dot{x}}))}_{=0\ (\textit{Euler-Lagrange}\ \text{eq.})} = \phi_t \tag{3.26}$$

If H is time-invariant, then $\phi_t = 0 \Leftrightarrow \frac{dH}{dt} = 0 \Leftrightarrow H = \text{const.}$ a.e.

□

Legendre-Clebsch condition and higher-order conditions

In static optimization, the well-known second-order necessary condition for a local minimum is $f''(x) \geq 0$. Similarly, for a second-order (or generally higher-order) necessary condition(s) in dynamic optimization, one has to look at the second variation and demand it to be positive semidefinite [71]

$$\left.\frac{d^2J}{d\epsilon^2}\right|_{\epsilon=0} = \int_{t_0}^{t_f} \phi_{xx}\delta x^2 + \phi_{x\dot{x}}\dot{\delta x}\delta x + \phi_{\dot{x}\dot{x}}\dot{\delta x}^2 dt \overset{!}{\geq} 0 \tag{3.27}$$

This leads (amongst others) to

$$\phi_{\dot{x}\dot{x}} \geq 0. \tag{3.28}$$

(3.28) was falsely proven by *Legendre* and correctly proven later on by *Alfred Clebsch*, therefore coining the term *Legendre-Clebsch condition*. It is a second-order necessary condition and can be simplified for optimal control. In general, higher-order necessary and/or sufficient conditions are difficult to pose and verify for real-world problems. Hence, they will not be considered in this thesis.

3.2 General Optimal Control Problem Formulation in Banach Spaces

Minimize

$$J = \int_{t_0}^{t_f} \mathcal{L}(x(t), u(t), t)dt \tag{3.29}$$

subject to

$$f(x(t), u(t), t) = \dot{x}, \tag{3.30a}$$
$$r_{\text{eq}}(t_0, x(t_0), t_f, x(t_f)) = 0, \tag{3.30b}$$
$$r_{\text{in}}(t_i, x(t_i), x(t_i^-), x(t_i^+)) = 0, \tag{3.30c}$$
$$C(x(t), u(t), t) \leq 0. \tag{3.30d}$$

(3.29) is the cost functional, (3.30a) a first-order ODE in explicit form (the dynamics), (3.30b) the initial and terminal boundary manifold, (3.30c) the interior point conditions and (3.30d) mixed inequality constraints (also: path constraints)[1]. The function x is called state with $x \in \mathcal{W}^{1,\infty}([t_0, t_f], \mathbb{R}^{n_x})$ and the function u is called control with $u \in L^\infty([t_0, t_f], \mathbb{R}^{n_u})$. Endowing these spaces with the strong norm $\|x\|_{1,\infty} = \|x(t_0)\|_2 + \|\dot{x}\|_\infty$ and the norm[2] $\|u\| := \text{ess sup}\{\|u\|_2 | t \in [t_0, t_f]\}$ the following Banach spaces are obtained [25]:

- $(\mathcal{W}^{1,\infty}([t_0, t_f], \mathbb{R}^{n_x}), \|x\|_{1,\infty})$, the *Sobolev* space of uniformly *Lipschitz*-continuous functions and
- $(L^\infty([t_0, t_f], \mathbb{R}^{n_u}), \|u\|)$, the *Banach* space of essentially bounded, measurable functions

Necessary conditions

For now, inequality constraints are neglected. In order to get admissible variations, the problem has to be transformed into a free problem (unconstrained problem). Initial and terminal conditions, as well as interior point conditions are adjoined as before such that they are incorporated in a function g preceding the integral term. This leads to the reformulated problem (for one interior point condition)

$$J(x(t), u(t), t) = g(t_0, t_J, t_f, x(t_0), x(t_J^-), x(t_J^+), x(t_f)) + \int_{t_0}^{t_f} \mathcal{L}(x(t), u(t), t)dt \to \text{min!} \tag{3.31}$$

subject to

$$\dot{x}(t) = f(x(t), u(t), t). \tag{3.32}$$

g is called *Mayer* term (also: *terminal cost*) and $\mathcal{L}$ *Lagrange* term (also: *running cost*). Optimal control problems are classified by these terms as

- *Mayer* problem, if $g \neq 0$ and $\mathcal{L} = 0$

[1] Note that this implies equality constraints on the entire domain by setting $C(x(t), u(t), t) \leq 0$ and $-C(x(t), u(t), t) \leq 0 \Rightarrow C(x(t), u(t), t) = 0$.

[2] In a measure space $(X, \sum, \mu_M)$, the essential supremum is defined as $\text{ess sup}\, f := \inf\{a \in \mathbb{R} : \mu_M(\{x : f(x) > a\})\}$.

- *Lagrange* problem, if $g = 0$ and $\mathcal{L} \neq 0$
- *Bolza* problem, if $g \neq 0$ and $\mathcal{L} \neq 0$

The problem classes are all equivalent and can be transformed into each other. The dynamics $\dot{x}(t) - f(x(t), u(t), t) = 0$ are adjoined by piecewise continuously differentiable *Lagrangian* functions[3] λ called *adjoints* or *costates* in order to obtain the first variation

$$\begin{aligned}
\delta J = &+ \left[\frac{\partial g}{\partial t_0} - H\right]\Big|_{t_0} \delta t_0 \\
&+ \left[\frac{\partial g}{\partial t_J} + H^- - H^+\right]\Big|_{t_J} \delta t_J \\
&+ \left[\frac{\partial g}{\partial t_f} + H\right]\Big|_{t_f} \delta t_f \\
&+ \left[\frac{\partial g}{\partial x_0} + \lambda\right]\Big|_{t_0} \delta x_0 \\
&+ \left[\frac{\partial g}{\partial x_J^-} - \lambda^-\right]\Big|_{t_J} \delta x_J^- + \left[\frac{\partial g}{\partial x_J^+} + \lambda^+\right]\Big|_{t_J} \delta x_J^+ \\
&+ \left[\frac{\partial g}{\partial x_f} - \lambda\right]\Big|_{t_f} \delta x_f \\
&+ \int_{t_0}^{t_f} \left[H_x + \frac{d}{dt}\lambda\right] \delta\lambda + H_u \delta u + \left[H_\lambda - \frac{d}{dt}x\right] \delta x dt.
\end{aligned} \tag{3.33}$$

With the Fundamental Lemma of CoV 3.1.1 (or the Lemma of *DuBois-Reymond*) the integral terms become

$$\dot{x} = H_\lambda(x, u, \lambda) = f(x, u, \lambda) \tag{3.34a}$$

$$\dot{\lambda} = -H_x(x, u, \lambda) \tag{3.34b}$$

$$H_u = 0, \tag{3.34c}$$

where H is the *Hamiltonian*, which is defined as $H = \mathcal{L} + \lambda^T f$ for optimal control. As in CoV, it is constant if the time does not appear explicitly. Moreover, if the final time does not appear explicitly in the *Mayer* term, then $H \equiv 0$. The equivalent to the *Legendre-Clebsch* condition (3.28) for optimal control is H_{uu} to be positive semidefinite.
(3.34a) is again the dynamics, (3.34b) the adjoint equations, and (3.34c) the *optimality condition*. Invoking the implicit function theorem for the assumption $H_u \neq 0$ and $H_{uu} > 0$ guarantees unique solvability w.r.t. the control u and so for some function $\tilde{g_1}$ the following holds: $u = \tilde{g_1}(x, \lambda)$. This function can be plugged into equations (3.34a) and (3.34b) to obtain

$$\begin{pmatrix} \dot{x} \\ \dot{\lambda} \end{pmatrix} = \begin{pmatrix} f(x, \lambda, \tilde{g_1}(x, \lambda)) \\ -H_x(x, \lambda, \tilde{g_1}(x, \lambda)) \end{pmatrix} = \begin{pmatrix} \tilde{f}(x, \lambda) \\ -\tilde{H}_x(x, \lambda) \end{pmatrix}. \tag{3.35}$$

The corresponding boundary and interior point conditions are drawn from the first variation (3.33) to complete the MPBVP. The case that it is not possible to extract a control this way will be discussed in the sequel.

[3] These functions are often called *Lagrange parameters* due to the similar adjoining approach in nonlinear optimization.

3.3 Singular Optimal Control Problems

Optimal control problems are defined to be singular if

$$\det(H_{uu}) = 0, \tag{3.36}$$

meaning that the Hessian of the *Hamiltonian* w.r.t. the control u is singular (hence the name, cf. [41]). The most prominent and dominant subclass of singular optimal control problems are those with a control-affine *Hamiltonian* (the control enters linearly into the *Hamiltonian*). These problems often arise in industrial problems, such as robotics and aerospace applications. In order to find candidates for the optimal control $u^* \in \mathcal{U}$, the domain $\mathcal{U}$ of admissible controls has to be bounded, closed, convex and with non-empty interior [83]. For this class of problems conditions (3.34c) and (3.28) are replaced with what is nowadays widely know as Pontryagin's[4] Minimum[5] Principle [85]

$$H(x^*, u^*, \lambda^*, t^*) \leq H(x^*, u, \lambda^*, t^*), \tag{3.37}$$

meaning that the optimal control minimizes the *Hamiltonian*

$$u^* = \arg\min_{u \in \mathcal{U}} H(x, u, \lambda, t). \tag{3.38}$$

For $u_{\min} \leq u \leq u_{\max}$ the control then takes the form of

$$u = \begin{cases} u_{\min} & \text{if } s > 0 \\ u_{\text{sing}} & \text{if } s \equiv 0 \\ u_{\max} & \text{if } s < 0, \end{cases} \tag{3.39}$$

where s is called switching function. It is defined as

$$s := \frac{\partial}{\partial u} H(x, u, \lambda, t). \tag{3.40}$$

If the switching function s exhibits only isolated zeros, then the control alternates purely between the lower bound $u_{\min}$ and the upper bound $u_{\max}$ and the isolated zeros of s determine the corresponding switching times. These type of controls are called *bang-bang* controls. If the switching function equals zero on at least one interval $t \in [t_a, t_b]$, so-called *singular arcs* u_{sing} occur. In this case the switching function is differentiated w.r.t. time until the control appears explicitly in order to obtain an analytical expression for u_{sing}. Let $i \in \mathbb{N}$ be the smallest integer for which the control u appears explicitly

$$\frac{\partial}{\partial u}\left(\frac{d^i}{dt^i}\frac{\partial}{\partial u} H(x, \lambda, u)\right) \neq 0 \tag{3.41}$$

The order of the singular control is then defined as $n_s := \frac{i}{2}$ and i is always an even number (for a proof refer to [63]). For non-scalar controls the switching function (3.40) becomes a

[4] An in-depth look into contributions of other famous mathematicians can be found in the historical paper in [84].

[5] Originally called Maximum Principle due to modeling differences.

vector field and (3.39) and (3.41) are understood componentwise w.r.t. each control.
Until now, no general assumption about existence or number of singular arcs can be made. Also, it is not guaranteed that n_s is finite, that means for the case of $n_s = \infty$ it is not possible to extract the control by differentiation as proposed in (3.41).
In [7, 66] the existence of singular arcs is eliminated by evaluating further necessary conditions, known as *Goh-Legendre* condition:
Let $u \in \mathbb{R}^l$ be a singular control on $t \in [t_a, t_b]$ and $n_{s,i}$ denote the order of the singular control u_i, then for each finite $n_{s,i}$

$$\frac{\partial}{\partial u_i}\left(\frac{d^k}{dt^k}\frac{\partial}{\partial u_j}H(x,\lambda,u)\right) = 0 \tag{3.42}$$

holds for all $k = 0, ..., (n_{s,i} + n_{s,j})$, $1 \leq i, j \leq l$ on $t \in [t_a, t_b]$ [48].
Furthermore, if $\forall i\ n_{s,i} < \infty$ then

$$(-1)^{n_{s,j}}\frac{\partial}{\partial u_{n_{s,i}}}\left(\frac{d^{n_{s,i}+n_{s,j}}}{dt^{n_{s,i}+n_{s,j}}}\frac{\partial}{\partial u_{n_{s,j}}}H(x,\lambda,u)\right) \tag{3.43}$$

must be symmetric and positive semidefinite ($1 \leq i, j \leq k$) [70]. For the case of a scalar control, (3.43) corresponds to the (strict for positive definiteness) generalized *Legendre-Clebsch* condition of singular optimal control problems (proven in [63]).
Since (3.42) and (3.43) are only necessary conditions, they can only be used to prove that singular arcs are non-optimal if the conditions are violated, however, otherwise no assumption can be made. A remedy can be found by introducing a regularization term or model the problem differently to avoid occurrences of singular arcs with infinite order.

3.4 Inequality Constraints

In general, solving optimal control problems with inequality constraints is a cumbersome task. To alleviate and structurize the handling of such constraints, the following classification is made

- Mixed inequality constraints $C(x(t), u(t), t) \leq 0$ (see (3.30d))
- (Pure) control inequality constraints $C(u(t), t) \leq 0$ with $\frac{\partial}{\partial x}C \equiv 0$
- (Pure) state inequality constraints $C(x(t), t) \leq 0$ with $\frac{\partial}{\partial u}C \equiv 0$

Without loss of generality it is always possible to transform time-variant optimal control problems into time-invariant ones by parameterizing the time as new additional state. Therefore, state inequality constraints will be given in the form of $C(x(t))$ and control inequality constraints in the form of $C(u(t))$ for the next subsection to enhance readability. Subsequently, state inequality constraints will be examined.

State inequality constraints

A boundary arc occurs if $C(x) \equiv 0$ holds for an interval $t \in [t_{entry}, t_{exit}]$, otherwise the extremal is said to be *free* ($C(x) < 0$). If $C(x) = 0$ holds only at discrete points t_c, then a

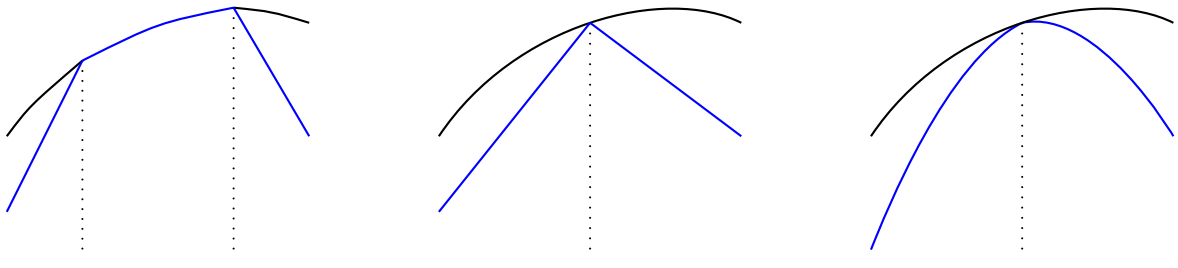

(a) Boundary arc (b) Contact point (c) Touch point

Figure 3.5: Constraint is active on (a) $t \in [t_{entry}, t_{exit}]$ and (b)-(c) $t = t_c$, i.e. $C(x(t)) = 0$ $\forall t \in [t_{entry}, t_{exit}] \cup t_c$, otherwise $C(x(t)) < 0$

contact point occurs, or a touch point if additionally $\frac{d}{dt}C(x)\big|_{t_c} = 0$ holds (see Figure 3.5). Let n_q denote the order of the state inequality constraint, i.e. n_q is the smallest integer $i \in \mathbb{N}$ such that

$$\frac{\partial}{\partial u}C^i(x(t)) := \frac{\partial}{\partial u}\frac{d^i}{dt^i}C(x(t)) \neq 0. \tag{3.44}$$

In the sequel, only one state inequality constraint is considered. The basic idea, pioneered by *Pontryagin* is to form the *extended Lagrangian*

$$\mathcal{L}_{ex}(x(t), u(t), \mu(t), t) := \mathcal{L}(x(t), u(t), t) + \mu(t) \cdot C^{n_q}(x(t), u(t), t), \tag{3.45}$$

with $\mu \in L^\infty([t_0, t_f], \mathbb{R})$ and adjoin the lower derivatives to the *Mayer* term at the entry point (*tangency constraints*) with $\nu \in \mathbb{R}^{n_q}$

$$\tilde{g} := g(...) + \nu^T N(x(t))\Big|_{t_{entry}} \qquad N(x(t)) := \begin{pmatrix} C(x(t)) \\ \vdots \\ C^{n_q-1}(x(t)) \end{pmatrix} \tag{3.46}$$

so that the functional becomes

$$J(x(t), u(t), t) = \tilde{g}(...) + \int_{t_0}^{t_f} \mathcal{L}_{ex}(x(t), u(t), t)dt \to \min! \tag{3.47}$$

With the *extended Hamiltonian*

$$H_{ex}(x, u, \lambda, \mu, t) := \mathcal{L}_{ex} + \lambda^T f = \mathcal{L} + \mu C^{n_q} + \lambda^T f \tag{3.48}$$

and by applying the familiar apparatus of CoV, the following necessary conditions for an optimal control problem with one state inequality constraint of order n_q are obtained [21, 55, 81]

1. Adjoint equations and dynamics

$$\dot{\lambda} = -H_{ex,x}(x, u, \lambda, \mu, t) \tag{3.49a}$$
$$\dot{x} = f(x, u) \tag{3.49b}$$

2. Minimum Principle

$$u^* = \arg\min_{u \in \mathcal{U}} H_{ex}(x, u, \lambda, \mu, t) \tag{3.50}$$

3. Jump conditions

$$\lambda^T(t^+_{entry}) = \lambda^T(t^-_{entry}) - \sum_{i=1}^{n_q} \nu_i \frac{\partial}{\partial x(t_{entry})} C^i(x)\Big|_{t_{entry}} \tag{3.51a}$$

$$\lambda^T(t^+_{exit}) = \lambda^T(t^-_{exit}) \tag{3.51b}$$

4. Switching conditions

$$N(x)\Big|_{t_{entry}} = 0 \tag{3.52a}$$

$$C^{n_q}(x, u_b)\Big|_{t^+_{entry}} = 0 \tag{3.52b}$$

$$H_{ex}\Big|_{t^+_{entry}} = H_{ex}\Big|_{t^-_{entry}} + \sum_{i=1}^{n_q} \nu_i \frac{\partial}{\partial t_{entry}} C^i(x)\Big|_{t_{entry}} \tag{3.52c}$$

$$H_{ex}\Big|_{t^+_{exit}} = H_{ex}\Big|_{t^-_{exit}} \tag{3.52d}$$

5. Sign conditions

$$\forall i = 0...n_q - 1 \qquad \nu_i \geq 0 \tag{3.53a}$$

$$\forall i = 0...n_q - 1 \qquad (-1)^i \frac{d^i}{dt^i}\mu(t) \geq 0 \qquad \mu C = 0 \tag{3.53b}$$

The missing interior point, initial and end conditions are drawn from the first variation. The sign conditions and *Hamiltonian* are used as test functions that are evaluated a-posteriori to assess numerical discrepancies. Due to the fact that the inequality constraint is adjoined by its derivative, this approach is known as *indirect adjoining approach*. Intuitively, if adjoined directly without differentiating, it is called *direct adjoining approach*.
Similar conditions can be established for

- the direct adjoining approach (see [69] for a relation of the parameter between the two approaches)
- touch and contact points
- boundary arcs where the adjoints are continuous across the entry point and exhibit jumps at the exit points
- multiple state inequality constraints

An excellent survey covering these topics can be found in [55]. Inequality constraints that involve the control can be treated as state inequality constraint of order zero.

3.5 Numerical Treatment

Since optimal control problems are seldomly analytically solvable (mostly only if the problem at hand is linear, time-invariant and low-dimensional) the focus heavily relies on good numerical algorithms. Three approaches exist and are introduced in the following.

Hamilton-Jacobi-Bellman equation

Around the same time as *Lev Pontryagin* (1908-1988) developed the *Maximum Principle*, *Richard Bellman* (1920-1984) approached the optimal control problem via *Dynamic Programming*, which led for infinitely small time steps to

$$-\frac{\partial J}{\partial t}(x,t) = \min_u \left(\mathcal{L}(x,u) + \frac{\partial J}{\partial x}(x,t) \cdot f(x,u) \right) \tag{3.54}$$

subject to a boundary condition relating to the *Mayer* term.
The partial differential equation (3.54) is called *Hamilton-Jacobi-Bellman* (HJB) equation and is the continuous-time analogon to the discrete-time dynamic programming algorithm [12]. It might be enticing to favor this approach because evaluating (3.54) over the whole state-space is not only a necessary but also sufficient condition (cf. [15]). Unfortunately, for higher dimensions Bellman's "curse of dimensionality" occurs, meaning that the computational effort grows exponentially in the dimensions of the state and control [77].
If the problem exhibits an easy structure, such as the *Linear Quadratic Regulator*, where the state and the control appear linearly in the dynamics and quadratic in the cost function, solving the HJB equation leads to the *Riccati* differential/algebraic equation for a finite/an infinite horizon [71].

Direct methods

Direct methods share the common principle of discretizing the control and/or the state in order to transform the infinite-dimensional optimal control problem into a finite-dimensional *Nonlinear Programming* (NLP) problem.

- *Discrete Mechanics*
  A novel approach for mechanical structures is presented in [79] by discretizing *Hamilton*'s principle prior to the evaluation of the *Euler-Lagrange* equations and optimizing with the resulting discrete equations.
- *Direct Single Shooting*
  The method relies on control discretization by substituting the control vector with an approximation of linearly combined basis functions, such as constant, linear, cubic B-splines followed by numerical integration of the dynamics (see [54]).
- *Collocation*
  Discretizations of the controls and states with collocation techniques are used to satisfy the dynamics, which leads to a large-scale, sparse NLP.

- *Direct Multiple Shooting*
  This is a combination of *Direct Single Shooting* and *Collocation* techniques. A control discretization takes place as in *Direct Single Shooting*, together with a state discretization.
- *Pseudospectral Methods*
  Will be discussed shortly in more detail due to its usage in this thesis.

These methods benefit from recent advantages in NLP optimization and powerful state-of-the-art *sequential quadratic programming* (SQP) (sparse if needed) or *interior point* (IP) methods can be employed. Also, neither system knowledge (e.g. switching structure in singular optimal control problems) nor theory of CoV is required a-priori. The burdensome task of setting up a MPBVP in the presence of inequality constraints and multiple interior point constraints is therefore avoided. This makes direct methods easily applicable even for highly complex systems where the dynamic behavior cannot be estimated beforehand, so it is clear that the overwhelming majority of optimal control problems was solved by these so-called "*first discretize, then optimize*" methods lately. This comes at a price: Due to the early discretization the solution is only suboptimal.

Excursus in spectral methods

Spectral methods originate from fluid dynamics and the problem of numerically solving partial differential equations [26]. Similar to a local approach in finite element methods, where linear combinations of non-smooth functions with small local support are chosen, spectral methods linearly combine functions that are (generally) nonzero on the entire domain. Together with an appropriate choice of support points this global collocation approach is beneficial for the convergence property of smooth functions, so called *spectral convergence/accuracy* [60].
For the numerical integration, the *Gauss Quadrature* is defined as

$$\int_{-1}^{1} f(\tau)d\tau \approx \sum_{i=1}^{N} w_i f(\tau_i), \tag{3.55}$$

where N is the number of support points $\tau_i \; \forall i = 1, ..., N$. The integration limits pose no loss of generality since the domain can always be scaled via the affine-transformation

$$\tau := \frac{2}{t_f - t_0} t - \frac{t_f + t_0}{t_f - t_0} \tag{3.56}$$

from $t \in [t_0, t_f]$ to $\tau \in [-1, 1]$. A popular choice are *Legendre-Gauss* (LG) points where the support points τ_i are roots of the (L^2-orthogonal) *Legendre* polynomials

$$P_N(x) = \frac{1}{2^N N!} \frac{d^N}{dx^N}(x^2 - 1)^N \tag{3.57}$$

and the weights are determined by

$$w_i = \frac{2}{(1 - \tau_i^2)(P_N'(\tau_i))^2} \tag{3.58}$$

so that polynomials of degree $2N-1$ are integrated exactly. Other choices are *Legendre-Gauss-Radau* (LGR) points and *Legendre-Gauss-Lobatto* (LGL) points where the main difference is that

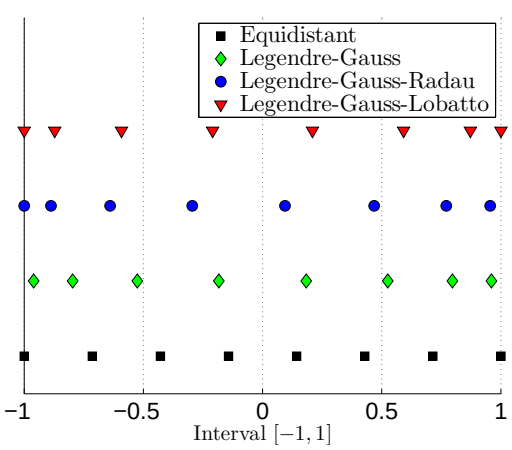

(a) 8 support points on the interval $[-1, 1]$

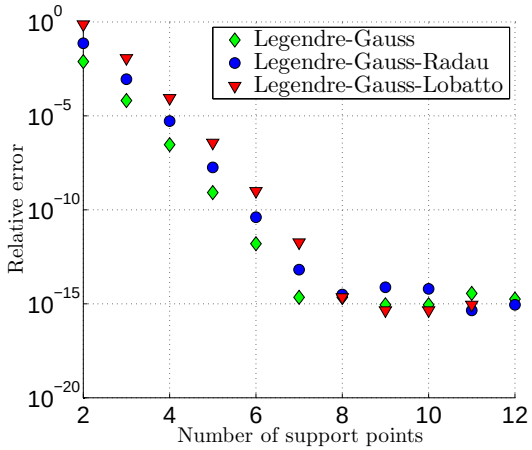

(b) Relative error on a logarithmic scale, machine accuracy achieved after 8 support points

Figure 3.6: (a) Distribution of 8 support points, (b) Spectral convergence of the *Gauss Quadrature* for $\int_{-1}^{1} e^t dt$ using LG, LGL and LGR points

- LG collocation points lie in the open interval $\tau \in (-1, 1)$
- LGR collocation points are roots of $P_N(x) + P_{N-1}(x)$ and lie in the half-open interval $\tau \in [-1, 1)$ or $\tau \in (-1, 1]$ (exact for polynomials of degree $2N - 2$)
- LGL collocation points are roots of $(1 - x^2)P'_{N-1}(x)$ and lie in the closed interval $\tau \in [-1, 1]$ (exact for polynomials of degree $2N - 3$)

The distribution of the support points is depicted in Figure 3.6(a) for polynomials of degree 8. All exhibit the spectral convergence property, i.e. after a relatively low number of support points the machine accuracy is already achieved. Figure 3.6(b) shows an example, where the integral $\int_{-1}^{1} e^t dt$ is solved numerically.

Pseudospectral methods in optimal control

The motivation behind pseudospectral methods in optimal control is to obtain a highly accurate approximation of the cost functional by *Gauss Quadrature* with only a small number of support points. The state and control functions are approximated by

$$y(\tau) \approx Y(\tau) = \sum_{i=1}^{N} L_i(\tau) Y(\tau_i), \tag{3.59}$$

where L_i denote *Lagrange* polynomials[6] with the corresponding *isolation property*

$$L_i(\tau) = \prod_{i=1}^{N} \frac{\tau - \tau_j}{\tau_i - \tau_j} \qquad L_i(\tau_j) = \begin{cases} 1 & \text{for } i = j \\ 0 & \text{for } i \neq j \end{cases} \tag{3.60}$$

[6]State and control discretization do not necesarily share the same polynomials or even support points.

Due to occurences of the well-known *Runge phenomenon*, equidistant points are an unfortunate choice for support points and so the support points mentioned previously are selected to nullify this undesired effect. The choice of support points coines the names *Gauss pseudospectral method*, *Radau pseudospectral method* and *Lobatto pseudospectral method*, respectively. With (3.55) and (3.59) the optimal control problem can be transcribed to a nonlinear optimization problem that needs to satisfy the first-order optimality conditions, so called *Karush-Kuhn-Tucker* (KKT) conditions. Either SQP or IP methods are used to solve the NLP numerically.

Obviously, non-smooth solutions arise in optimal control problems (e.g. a bang-bang control) so that the spectral convergence property does not hold anymore. *Multidomain techniques* address this problem and try to recover some of the advantages of the spectral methods (hence pseudospectral). The basic idea is to divide the domain into smaller segments, so called *meshes*, and scale these again to $[-1, 1]$ in order to apply aforementioned techniques. According to [88], *Radau* pseudospectral methods are superior in a multiple interval formulation due to the fact that

- no overlapping/redundant points occur as in *Lobatto* pseudospectral methods (where LGL collocation points are used) and
- the endpoint within a mesh is collocated as opposed to *Gauss* pseudospectral methods (where LG points are used), see Figure 3.6(a). Since the LGR points are in $\tau \in [-1, 1)$, the endpoint collocation is achieved by flipping the LGR points.

The multiple mesh formulation leads to a sparse differentiation matrix resulting from the NLP discretization that should be exploited when choosing a nonlinear optimizer to enhance computational speed. Moreover, the differentiation matrix is rectangular and has full rank for LG and LGR points, whereas the differentiation matrix is singular for LGL points [43].

A particulary interesting property of *Gauss* and *Radau* pseudospectral methods is that the resulting costates arising from the NLP optimality conditions are algebraically related to the costates of the discretized BVP at the collocation points. Therefore, they yield a discrete representation of the continuous-time first-order optimality conditions with a costate mapping as long as the costates are continuous (see Figure 3.7). If the costates are discontinuous, then the approximation of the costates depends on the location of the collocation points. By placing the mesh points at discontinuities the approximation of the costates is improved significantly [31].

A strategy to obtain better solutions (in the sense of accuracy and computational speed) in pseudospectral methods is the *hp-adaptive*[7] *mesh refinement* technique. An algorithm is presented in [33] that decides in each iteration step whether it is better to further subdivide the meshes or to increase the number of collocation points within a segment until a certain tolerance is met. However, the drawback of

- an increasing number of meshes is that the NLP problem will become very large and therefore difficult to compute a solution (although the sparsity will increase as well)
- increasing the polynomial degree is that the NLP problem will become more dense and computationally intractable

[7] h stands for the number of meshes and p for the polynomial degree.

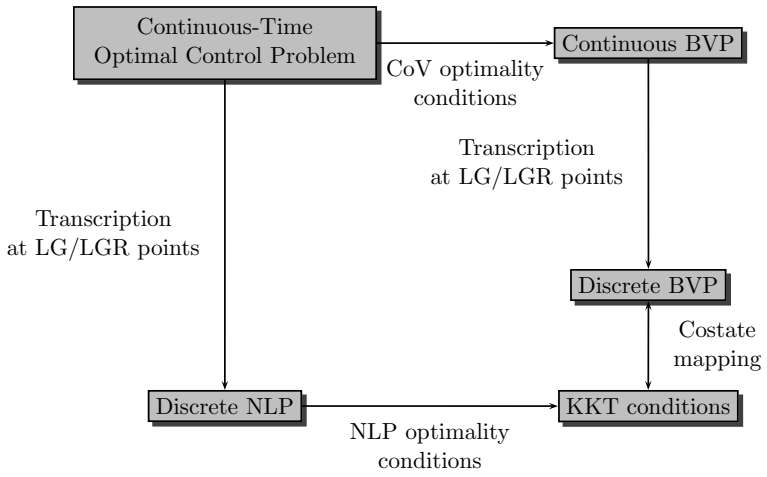

Figure 3.7: Direct and indirect methods in optimal control and how the costate mapping comes into play in pseudospectral methods [60].

Efficient implementations should use as few mesh intervals as possible and the lowest possible polynomial degree approximation in each mesh interval.

The underlying heuristic of the algorithm is that subdivions of the meshes are preferable if the solution is discontinuous/rapidly changing in order to place the mesh points at locations of nonsmoothness (exemplified in Figure 3.8), whereas a polynomial increase in a mesh is preferable if the solution is smooth in order to exploit the spectral convergence. Since the

(a) (b)

Figure 3.8: Optimal solution (blue) with (a) initial mesh grid and (b) a mesh grid considered "best fit"

structure of the solution is in general not clear a-priori, the algorithm initially starts with a uniform (coarse) distribution of mesh points with low polynomial order. To asses smoothness within each mesh interval the curvature

$$\kappa^{(k)} = \frac{|\ddot{x}_m^{(k)}|}{\left|\left[1 + (\dot{x}_m^{(k)})^2\right]^{3/2}\right|} \tag{3.61}$$

serves as a primary tool, where x_m is the component of the state approximation that corresponds to the maximum (absolute) error of the discretized dynamic equation in the k-th

mesh interval

$$e_{\max}^{(k)} := \max_{i,j} \left| \dot{x}_i^{(k)}(\bar{t}_j^{(k)}) - f_i^{(k)}(X_j^{(k)}, U_j^{(k)}, \bar{t}_j^{(k)}) \right|, \tag{3.62}$$

where $i \in 1, ..., n$ and $\bar{t}_j$ with $j \in 1, ..., L$ are L arbitrary chosen points within a mesh interval. More precisely, the decision process is based on the ratio between maximum curvature and average curvature $r_k := \kappa_{\max}^{(k)}/\kappa_{\text{avg}}^{(k)}$. Algorithm 1 outlines the concept where $r_{\max} > 0$ is a

Algorithm 1 *hp-adaptive mesh refinement*

```
for k=1...K do
    while e_max^(k) > TOL do
        if r ≥ r_max or N_k > M then
            Refine k-th mesh into n_k subintervals and set degree of the polynomials on
            each of the subintervals to be M
        else
            Set the degree of the polynomials on the k-th subinterval to be N_k
        end if
    end while
end for
```

user-specified parameter, N_k/n_k the number of collocation points within each mesh interval/subinterval with

$$N_k = M + \left\lceil \log_{10}\left(\frac{e_{\max}^{(k)}}{TOL}\right) \right\rceil + 1 \qquad n_k = \left\lceil 2\log_{10}\left(\frac{e_{\max}^{(k)}}{TOL}\right) \right\rceil \tag{3.63}$$

for each iteration and M the (pre-specified) initial polynomial degree. A more detailed description is given in [33, 88], e.g. how to find the locations of the new mesh points using the integral of a curvature density function. This is beyond the scope of this thesis. An alternative *hp*-adaptive mesh refinement method without the curvature approach is proposed in [32].

Subsequently, the open-source *MATLAB* toolbox *GPOPS* will be used as indirect solver of choice. It uses the *Radau* pseudospectral method[8] and incorporates useful features as the *hp* mesh refinement technique, the costate estimation and the option to pass the analytic derivatives of the dynamics and cost function, which improves the speed of the calculations considerably. Additionally, the user is able to define *phases*, where different dynamics or cost functions can be specified within each phase. The corresponding interior point conditions between the phases are then passed in a so called *linkage* file. *GPOPS* comes with a restricted version of *SNOPT* [47], an NLP solver utilizing a sparse SQP *Quasi-Newton* method.
For more on pseudospectral methods refer to [13, 43, 60, 88]. Other software tools that employ pseudospectral methods are e.g. *DIDO* [89], *PROPT* [90] and *PSOPT* [11].

[8]The first version employed the *Gauss* pseudospectral method and coined the name, the advantages of LQR collocation points became apparent later.

Indirect methods

Indirect methods are characterized by making explicit use of the optimality conditions arising from the theory of CoV.

- *Gradient Methods*
  The method relies on iterative optimization of the optimal control by maximizing the *Hamiltonian* subject to the according MPBVP [34, 62, 67].
- *Collocation*
  The MPBVP is solved using collocation techniques [8, 37].
- *Shooting Methods*
  In single shooting the BVP problem is solved forward in time with initial guesses for the states and the adjoints. A function that calculates the difference between the exact end values and the values found by the forward integration (the so-called *shooting*) then needs to be minimized. The algorithm of choice to find the roots of this function is often *Newton*'s method, which is known to converge fast if the initial values are sufficiently close to the optimal solution. This is the main drawback of shooting methods since the adjoints cannot be estimated easily and convergence is not guaranteed. *Multiple shooting* methods try to minimize this by dividing the domain into multiple smaller segments and "shoot" in each of those and assemble a solution on the entire domain [23, 35, 81, 102]. Also, *Homotopy techniques/Continuation methods* are often employed to overcome the difficulty of finding the switching structure (i.e. the sequence of boundary-, bang- or singular arcs) and reasonable initial values [24, 36, 57, 83].

The main advantage of indirect methods is that the solution is highly accurate. This is due to the control structure (e.g. number of switching points, boundary or singular control in a certain interval) that has to be found in order to apply these methods and so the optimality conditions are already satisfied to a certain degree. As already hinted previously, it may not always be possible to find a closed-form expression for the optimal control, e.g. in singular optimal control problems if the order is not finite, and so one cannot establish a MPBVP. Solving the problem by these so-called "*first optimize, then discretize*" methods is nullified in this case. For low dimensional and not too complex problems these methods are often a good choice.

In conclusion to this chapter, so-called *hybrid methods* should be mentioned as well, where the optimal control problem is first solved via a direct approach and the resulting information about the switching structure and adjoints is fed to an indirect solver in order to obtain a solution with high precision.

Chapter 4

Mass Spring Systems

Mass spring systems are simple multibody systems consisting, as the name already implies, only of masses and springs, here concatenated in alternation and only free to move in one dimension. The harmonic oscillator as a special case is by far the most popular example and has been already analyzed in depth (e.g. see [6] for an energetic contemplation in the context of optimal control). Their simplicity allows (to an extent) to retrieve analytical solutions and understand basic properties, eventually providing heuristics for (highly) nonlinear cases, such as the double pendulum, where a closed-form solution cannot be obtained.
The systems will subsequently be classified by the number of masses (indicated by n). This is equivalent here to the DoF due to the fact that one translational coordinate is sufficient to describe the configuration because the rotation is not considered and no kinematic constraints are prevalent. The *Kutzbach* criterion (2.3) therefore yields

$$n = (1 + 0) \cdot n_b - n_c = n_b. \tag{4.1}$$

Throughout this chapter the goal will be to maximize the velocity of the last mass, where the system rests at initial time $t_0 = 0$.
According to [56] the mass proportions of the "standard" human arm (see Table 4.1) are usually arranged in a descending kinematic chain, i.e. $m_1 > m_2 > ....$

Body part	% of total body mass	% of total arm	absolute weight [kg]
Upper arm	2.8	56	1.96
Forearm	1.6	32	1.12
Hand	0.6	12	0.42
Total arm	5	100	3.5

Table 4.1: Arm proportions of the "standard" human. The total body mass is 70 [kg] (taken from [56]).

For numerical examples, the mass ratios are chosen to be similar to the human arm, i.e. for examples involving

- two masses $m_1 = m_2 = 2$ kg (Upper arm : Forearm+Hand $\approx 0.5 : 0.5$)
- three masses $m_1 = 2$ kg, $m_2 = 1.5$ kg and $m_3 = 0.5$ kg (Upper arm : Forearm : Hand $\approx 0.5 : 0.35 : 0.15$)

Retrieving the stiffness from the human body is still a matter of current research. Here, the stiffness is assumed to be linear and mechanical reasonable values $k \in [25, 80]$ [N/m] are chosen that are of the same order of magnitude as the HASy after scaling appropriately. For analytical calculations the stiffness values will always be assumed to be greater than zero because this will turn out to be helpful for later assumptions. The boundaries for the input force are chosen to be at $u_{\max} = -u_{\min} = 4$ [N] and nonzero for analytical calculations. These values will be used for numerical examples if not explicitly specified otherwise.
For convenience, all values used in numerical evaluations are summarized in Table A.1 in Appendix A.

4.1 Constant Stiffness

First, mass spring systems with constant stiffness are considered. They can be seen as the equivalent to intrinsically elastic/compliant robots without stiffness actuation mentioned in Chapter 2.5.

2 DoF mass spring system

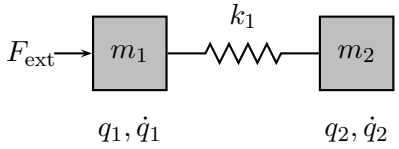

Figure 4.1: 2 DoF mass spring system

The most basic system with force input is a system with two masses, a constant spring connecting them and an external force acting on the first mass, see Figure 4.1. By deriving the equations of motion with *Newton's second law*

$$\begin{aligned} m_1\ddot{q_1} &= k_1(q_2 - q_1) + F_{\text{ext}} \\ m_2\ddot{q_2} &= k_1(q_1 - q_2) \end{aligned} \tag{4.2}$$

and defining the states as $x := (q_1, q_2, \dot{q}_1, \dot{q}_2)$ and the control as $u := F_{\text{ext}}$ the state-space equation can be written as

$$\dot{x} = \frac{d}{dt}\begin{pmatrix} q_1 \\ q_2 \\ \dot{q}_1 \\ \dot{q}_2 \end{pmatrix} = \begin{bmatrix} 0 & 0 & 1 & 0 \\ 0 & 0 & 0 & 1 \\ -\frac{k_1}{m_1} & \frac{k_1}{m_1} & 0 & 0 \\ \frac{k_1}{m_2} & -\frac{k_1}{m_2} & 0 & 0 \end{bmatrix} x + \begin{pmatrix} 0 \\ 0 \\ \frac{1}{m_1} \\ 0 \end{pmatrix} u =: Ax + bu, \tag{4.3}$$

where q_1, q_2 is the position and $\dot{q}_1$, $\dot{q}_2$ the velocity of the first and second mass respectively. $k_1 > 0$ denotes the stiffness constant. Additionally, the control is constrained by

$$u_{\min} \leq u \leq u_{\max} \tag{4.4}$$

with $u_{\min} < 0 < u_{\max}$. Aiming to maximize the velocity of the final mass, the cost function reads as

$$J = -\dot{q}_2(t_f) = -x_4(t_f) = g(x(t_f)) \to \min! \tag{4.5}$$

The necessary conditions for the optimal control problem (4.3)-(4.5) can be set up in accordance with Chapter 3.2.
The final time is fixed at t_f and the necessary conditions are drawn from (3.33) with $\delta t_0 = 0$, $\delta x_0 = 0$ (fixed initial time and state), $\delta t_f = 0$ (fixed end time) and $\delta t_J = \delta x_J^- = \delta x_J^+ = 0$ (no jumps considered). The system is resting at initial time, hence $x_0 = (0,0,0,0)^T$. Since no *Lagrange* term is prevalent, the *Hamiltonian* results in $H = \lambda^T f = \lambda^T(Ax+bu) = \lambda^T Ax + u\lambda^T b$ and due to the control-affine *Hamiltonian*, the problem belongs to the class of singular optimal control problems. The costate differential equations are

$$\dot{\lambda} = -\frac{\partial H}{\partial x} = -f_x^T \lambda = -A^T \lambda, \tag{4.6}$$

with the corresponding boundary (transversality) conditions

$$\lambda(t_f) = \frac{\partial g(x(t_f))}{\partial x(t_f)} = (0,0,0,-1)^T. \tag{4.7}$$

The switching conditions for the control arise from the *Minimum Principle* (3.38)

$$s = H_u = \lambda^T b = \frac{\lambda_3}{m_1} \Rightarrow u = \begin{cases} u_{\max} & \text{if } \frac{\lambda_3}{m_1} < 0 \\ u_{\min} & \text{if } \frac{\lambda_3}{m_1} > 0 \\ u_{\text{sing}} & \text{if } \frac{\lambda_3}{m_1} \equiv 0 \end{cases} \tag{4.8}$$

For linear systems, the adjoint equations (4.6) neither depend on the control nor the state and can be solved separately and backwards in time with the corresponding boundary conditions (4.7). The switching function results in

$$s = \frac{\lambda_3^*}{m_1} = \underbrace{\frac{k_1}{\omega^2 m_1 m_2}}_{>0} \underbrace{(\cos(\omega^2(t-t_f)) - 1)}_{\leq 0} \leq 0 \tag{4.9}$$

and is only zero at isolated points, otherwise negative, therefore an optimal control is found by $u^* = u_{\max}$. The natural eigenfrequency is denoted by $\omega := \sqrt{\frac{k_1}{m_1} + \frac{k_1}{m_2}}$. Now the state-space equations (4.3) can be integrated forward in time together with the optimal control and initial values x_0. For a full solution of the states and costates, the reader is referred to Appendix A.1 where the initial value problem for the dynamics (4.3) with initial values $x_0 = (0,0,0,0)^T$ and the end value problem for the costates (4.6) with end values (4.7) are solved analytically. The velocity of the second mass is then

$$x_4^* = \frac{u_{\max}}{m_1 + m_2} \left(t - \frac{1}{\omega} \sin(\omega t) \right), \tag{4.10}$$

where $\frac{u_{\max}}{m_1+m_2}$ is the total acceleration of the system. Local extrema can be located by calculating the first derivative of the velocity

$$\dot{x}_4^* = \frac{u_{\max}}{m_1 + m_2} (1 - \cos(\omega t)) \tag{4.11}$$

and by evaluating the second derivative saddle points are found at $t \in \frac{2\pi}{\omega} l \; \forall l \in \mathbb{N}$, i.e. integer multiplicities of the period of the eigenfrequency. In this case, the deflection between the masses is zero and no potential energy is prevalent.

If a desired velocity needs to be achieved at final time (now free to choose instead of fixed) then

$$\left[\frac{u_{\max}}{m_1+m_2}\left(t-\frac{1}{\omega}\sin(\omega t)\right)\right]\Bigg|_{t=t_f} \stackrel{!}{=} v_d \tag{4.12}$$

needs to hold. For integer multiplicities of $\frac{\pi}{\omega}$ this can be used to find a closed-form solution for k_1 by choosing the final time there as $t_f = \frac{\pi l}{\omega}$

$$-\frac{1}{\omega}\sin(\omega t_f) + t_f = -\frac{1}{\omega}\underbrace{\sin(2\pi l)}_{=0} + \frac{2\pi l}{\omega} = \frac{v_d(m_1+m_2)}{u_{\max}} \Rightarrow \omega = \frac{2\pi u_{\max} l}{v_d(m_1+m_2)} \tag{4.13}$$

and solving for k_1

$$\Rightarrow k_1 = \left(\frac{2\pi l u_{\max}}{v_d(m_1+m_2)\sqrt{\frac{1}{m_1}+\frac{1}{m_2}}}\right)^2 \tag{4.14}$$

For more arbitrary final times a numerical solver will provide a solution. From now on, only fixed final times will be considered for the rest of this chapter.

3 DoF mass spring system

Adding another spring and mass leads to the 3 DoF mass spring system, see Figure 4.2. The

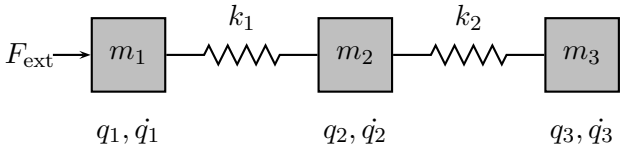

Figure 4.2: 3 DoF mass spring system

equations of motion can be derived as previously seen

$$\begin{aligned} m_1\ddot{q_1} &= k_1(q_2-q_1) + F_{\text{ext}} \\ m_2\ddot{q_2} &= k_1(q_1-q_2) + k_2(q_3-q_2) \\ m_3\ddot{q_3} &= k_2(q_2-q_3) \end{aligned} \tag{4.15}$$

and brought into the form of (2.25)

$$M\ddot{q} + Kq = F, \tag{4.16}$$

with

$$M = \begin{bmatrix} m_1 & 0 & 0 \\ 0 & m_2 & 0 \\ 0 & 0 & m_3 \end{bmatrix} \quad K = \begin{bmatrix} k_1 & -k_1 & 0 \\ -k_1 & k_1+k_2 & -k_2 \\ 0 & -k_2 & k_2 \end{bmatrix} \quad F = \begin{pmatrix} F_{\text{ext}} \\ 0 \\ 0 \end{pmatrix} = \begin{pmatrix} u(t) \\ 0 \\ 0 \end{pmatrix} \tag{4.17}$$

The necessary conditions are the same as before. Albeit innocent looking, straightforward computation of the analytical solution with a computer algebra system leads to a large, complex and unstructured solution. *Modal analysis* provides a helpful tool to unveil the structure of the solution and gain more insight. The basic idea is to introduce a transformation $q = Qp$ that decouples the ODE (4.15) so that it decomposes into multiple second-order ODEs. Q consists of eigenvectors[1] (so-called *eigenmodes*) of $M^{-1}K$ so that

$$\begin{aligned} MQ\ddot{p} + KQp &= F \qquad / \cdot Q^T \\ \underbrace{Q^T MQ}_{=:\tilde{M}}\ddot{p} + \underbrace{Q^T KQ}_{=:\tilde{K}}p &= \underbrace{Q^T F}_{=:\tilde{F}}, \end{aligned} \tag{4.18}$$

where $\tilde{M}, \tilde{K}$ are diagonal matrices[2] (for proofs and more on modal analysis see e.g. [72]). Let ω_i^2 and $\tilde{\omega}_i^2$ denote the eigenvalues of $M^{-1}K$ and $\tilde{M}^{-1}\tilde{K}$ respectively, then the transformed system $\tilde{m}_i\ddot{p}_i + \tilde{k}_i p_i = \tilde{f}_i(u(t))\ \forall i \in \{1,2,3\}$ can be written as

$$\ddot{p}_i + \frac{\tilde{k}_i}{\tilde{m}_i}p_i =: \ddot{p}_i + \tilde{\omega}_i^2 p_i = \ddot{p}_i + \omega_i^2 p_i = \frac{\tilde{f}_i(u(t))}{\tilde{m}_i}. \tag{4.19}$$

The equality $\tilde{\omega}_i^2 = \omega_i^2$ holds because $M^{-1}K$ and $\tilde{M}^{-1}\tilde{K}$ share the same spectrum since the matrices are similar to each other [58]

$$\tilde{M}^{-1}\tilde{K} = (Q^{-1}MQ)^{-1}(Q^{-1}KQ) = Q^{-1}M^{-1}KQ \tag{4.20}$$

There are two complex conjugated eigenvalue pairs corresponding to $\omega_{1/2}^2 = \left(\frac{C_2 \pm C_1}{2m_1m_2m_3}\right)^2$ where C_1 and C_2 are constants that can be found in Appendix A.2 and an eigenvalue at zero with algebraic multiplicity two that corresponds to $\tilde{\omega}_3^2 = \omega_3^2 = 0$. From a mechanical point of view it is reasonable that one eigenvalue will always be at zero since the system is free to move in one dimension (in this case horizontally) [38] and that the constants C_1 and C_2 vanish only for pathological cases such as $k_1 = k_2 = 0$ and $m_1 = m_2 = m_3 = 0$ because the system can not oscillate anymore.

The initial conditions for (4.19) are given by $p(t_0) = Q^{-1}q(t_0)$ and $\dot{p}(t_0) = Q^{-1}\dot{q}(t_0)$. The solution of the new states p can now easily be calculated with the principle of superposition[3]

- for initial conditions $q(t_0) = \vec{0}, \dot{q}(t_0) = \vec{0} \Rightarrow p(t_0) = \vec{0}, \dot{p}(t_0) = \vec{0}$ (system rests at the beginning) with

$$\begin{aligned} &\bullet\ \omega_i^2 \neq 0 \text{ as } p_i(t) = -\frac{\tilde{f}_i(u)}{\tilde{k}_i}\cos(\omega_i t) + \frac{\tilde{f}_i(u)}{\tilde{k}_i} \\ &\bullet\ \omega_i^2 = 0 \text{ as } p_i(t) = \frac{\tilde{f}_i(u)}{2\tilde{m}_i}t^2 \end{aligned} \tag{4.21}$$

[1] The columns of Q can be scaled and interchanged.

[2] However, $\tilde{F}$ is now fully occupied here.

[3] The subsequent step assumes that the control is constant a.e. so that the solution holds for each interval between two control switches.

- and for arbitrary initial conditions at t_1: $p_{i0} = Q^{-1}q(t_1)$ and $\dot{p}_{i0} =: p_{i1} = Q^{-1}\dot{q}(t_1)$ with

$$\begin{aligned} &\bullet\ \omega_i^2 \neq 0 \text{ as } p_i(t) = \left(p_{i0} - \frac{\tilde{f}_i(u)}{\tilde{k}_i}\right)\cos(\omega_i t) + \frac{p_{i1}}{\omega_i}\sin(\omega_i t) + \frac{\tilde{f}_i(u)}{\tilde{k}_i} \\ &\bullet\ \omega_i^2 = 0 \text{ as } p_i(t) = p_{i0} + p_{i1}t + \frac{\tilde{f}_i(u)}{2\tilde{m}_i}t^2 \end{aligned} \tag{4.22}$$

The solution for the initial states can now conveniently be expressed as

$$q_i = q_{i1}p_1 + q_{i2}p_2 + q_{i3}p_3. \tag{4.23}$$

The transformation matrix Q has been computed with the computer-algebra software *MAPLE*

$$Q = \begin{bmatrix} q_{11} & q_{12} & 1 \\ q_{21} & q_{22} & 1 \\ 1 & 1 & 1 \end{bmatrix} \tag{4.24}$$

Due to large and complex entries, the interested reader is referred to the Appendix A.2 for a detailed description of the matrix. Of major interest is the velocity of the final mass

$$\begin{aligned} x_6 = \dot{q}_3 &= \frac{d}{dt}\{q_{31}p_1 + q_{32}p_2 + q_{33}p_3\} \qquad\qquad q_{3i} = 1 \forall i \in \{1,2,3\} \\ &= \dot{p_1} + \dot{p_2} + \dot{p_3} \\ &= \omega_1 \frac{\tilde{f}_1(u)}{\tilde{k}_1}\sin(\omega_1 t) + \omega_2 \frac{\tilde{f}_2(u)}{\tilde{k}_2}\sin(\omega_2 t) + \frac{\tilde{f}_3(u)}{\tilde{m}_3}t \end{aligned} \tag{4.25}$$

For arbitrary initial values the cosine terms are added accordingly.

A particularly interesting aspect arises when looking at the adjoint system

$$\dot{\lambda} = \begin{bmatrix} 0 & M^{-1}K \\ -\mathbb{1} & 0 \end{bmatrix}\lambda \tag{4.26}$$

and writing it as a second-order ODE by defining

$$\tilde{\lambda}_1 := (\lambda_1, \lambda_2, \lambda_3)^T \qquad\qquad \tilde{\lambda}_2 := (\lambda_4, \lambda_5, \lambda_6)^T \tag{4.27}$$

to obtain

$$M\ddot{\tilde{\lambda}}_2 + K\tilde{\lambda}_2 = 0. \tag{4.28}$$

This system is equivalent to the unforced system (4.16) [82] and so the same transformation can be applied with $\tilde{\lambda}_2 = Q\tilde{p}$ and no recalculation of the matrix Q is necessary. The end conditions expressed in the new modal coordinates are $\tilde{p}(t_f) = Q^{-1}\tilde{\lambda}_2(t_f) = Q^{-1}\cdot(0,0,-1)^T$ and $\dot{\tilde{p}}(t_f) = Q^{-1}\tilde{\lambda}_1(t_f) = Q^{-1}\cdot(0,0,0)^T = \vec{0}$ and the costates λ_{i+3} $i \in \{1,2,3\}$ can be derived as follows

$$\lambda_{i+3} = \tilde{\lambda}_{2i} = \tilde{p}_1(t_f)q_{1i}\cos(\omega_1(t-t_f)) + \tilde{p}_2(t_f)q_{2i}\cos(\omega_2(t-t_f)) + \underbrace{q_{3i}}_{=1}\tilde{p}_3(t_f) \tag{4.29}$$

The switching function is then obtained as

$$s = \frac{\lambda_4}{m_1} = \frac{\tilde{\lambda}_{21}}{m_1} = \frac{\tilde{p}_1(t_f)q_{11}}{m_1}\cos(\omega_1(t-t_f)) + \frac{\tilde{p}_2(t_f)q_{21}}{m_1}\cos(\omega_2(t-t_f)) + \frac{\tilde{p}_3(t_f)}{m_1}. \tag{4.30}$$

This makes evident that although a closed-form solution can be obtained, the zeros of the switching function, in general, cannot be found analytically anymore. However, after finding them numerically (e.g. *Newton*'s method), a solution can be assembled piecewise with (4.21) and (4.22), and there is no need to use a full-blown (direct or indirect) optimal control solver.

Example

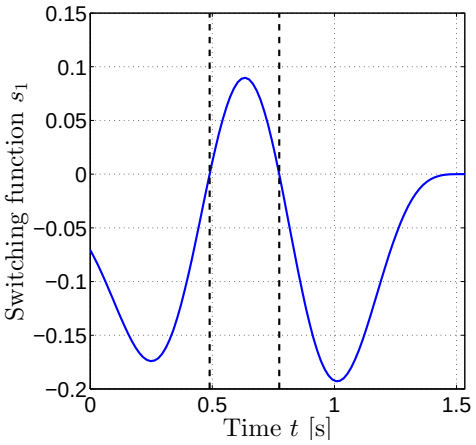

(a) Switching function s_1

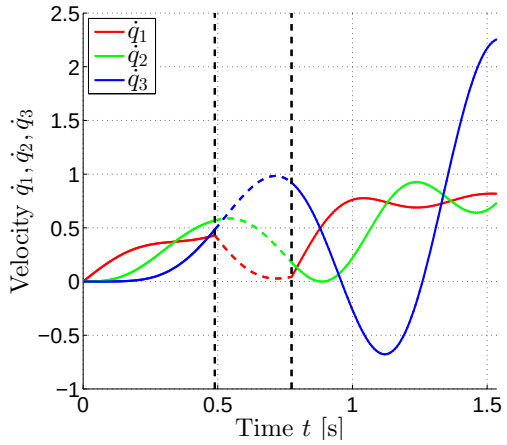

(b) Analytical subsolutions in Phase 1 and 3 (solid) and Phase 2 (dashed)

Figure 4.3: High precision (quasi-analytical) solution of for the 3 DoF mass spring system with constant stiffness calulated with *MAPLE*.

Figure 4.3 depicts an example with the values mentioned in the beginning of this chapter and the stiffness set to $k_1 = 80$ [N/m] for the first and $k_2 = 25$ [N/m] for the second spring. The final time is chosen in a similar manner as for the 2 DoF case as

$$t_f = \frac{2\pi}{\sqrt{\frac{k_1}{m_1} + \frac{k_1}{m_2+m_3}}} + \frac{2\pi}{\sqrt{\frac{k_2}{m_3} + \frac{k_2}{m_1+m_2}}} =: \frac{2\pi}{\omega_1} + \frac{2\pi}{\omega_2} \tag{4.31}$$

The zeros of the switching function have been found numerically using the `solve` command implemented on *MAPLE* as $t_1 = 0.4891$ and $t_2 = 0.7740$. It is easy to find them with high precision because they are nicely separated and reasonable initial values can be taken from the plot of the switching functions, see Figure 4.3(a). Afterwards, the three initial value problems are solved analytically and stitched together for a solution on the entire domain (see Figure 4.3(b) for the velocities). A switching of the control invokes a rapid change in the velocity of the first mass and the corresponding trajectory exhibits edges at control switches, whereas the other two masses are connected via springs and the solution is smoother.

It does not look like there is an obvious pattern that seems intuitive for the switchings of the control. By choosing extremer values, here $m_1 = m_2 = 2$ [kg], $m_3 = 8$ [kg], $k_1 = 40$ [N/m] and $k_2 = 10$ [N/m], a pattern will become apparent. Figure 4.4 depicts the velocities of the masses for this new problem and the background color indicates which control is active at the time. It seems like the control tries to keep the first to masses inversely phased for as

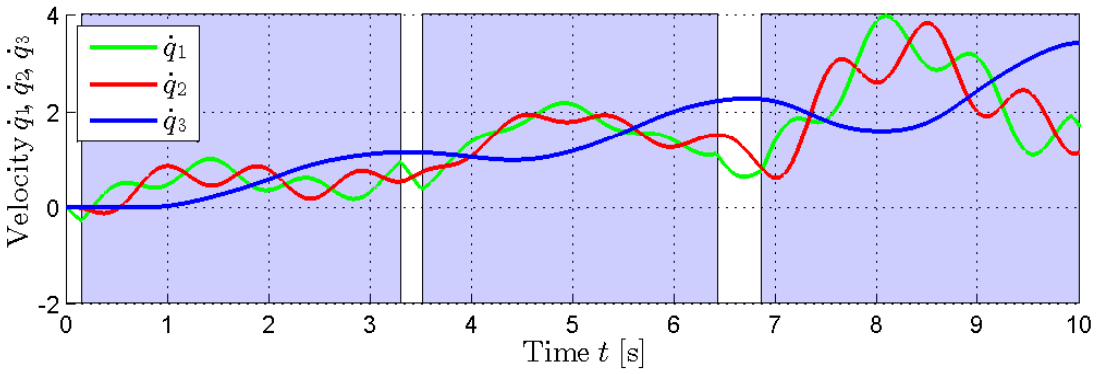

Figure 4.4: Velocities of the masses, the light purple background denotes $u = u_{\max}$ and the white one $u = u_{\min}$, the switchings occur between the color changes.

long as possible. Because there is a third mass attached, this will change after some time. A switching is invoked as soon as these masses go out of phase and the control is switched to guarantee that the two masses are in phase opposition again. A physical interpretation would be that the maximal possible energy can be transferred to the third mass by this excitation with eigenfrequency. For the 2 DoF case where only 2 masses are involved, this is always the case. By attaching another mass via a spring this is not always guaranteed anymore, and depending on spring stiffness and mass, the influence on the first two masses varies.

Controllability

Controllability plays an important role in the context of time-optimal control problems. In this class, every linear system $\dot{x} = Ax + Bu$ that is controllable does not exhibit singular arcs, i.e. the optimal control will be of bang-bang type [67, 71]. The controllability condition for linear system can be tested by evaluating if $(B, AB, A^2B, ..., A^{n-1}B)$ has full rank (also known as *Kalman's criterion*).

Hence, an n DoF mass spring system with only one external force acting on the first mass is now examined with respect to the controllability property. It will be convenient here to define the states as $x := (\dot{q}_1, q_1 - q_2, \dot{q}_2, \dots, , q_{n-1} - q_n, \dot{q}_n)^T$, so that the state-space equation takes the (reduced) form

$$\dot{x} = \begin{pmatrix} \ddot{q}_1 \\ \dot{q}_1 - \dot{q}_2 \\ \ddot{q}_2 \\ \dot{q}_2 - \dot{q}_3 \\ \vdots \\ \dot{q}_{n-1} - \dot{q}_n \\ \ddot{q}_n \end{pmatrix} = \begin{bmatrix} 0 & -\frac{k_1}{m_1} & 0 & 0 & 0 & 0 & 0 \\ 1 & 0 & -1 & 0 & 0 & 0 & 0 \\ 0 & \frac{k_1}{m_2} & 0 & -\frac{k_2}{m_2} & 0 & 0 & 0 \\ 0 & 0 & 1 & 0 & -1 & 0 & 0 \\ 0 & 0 & 0 & \ddots & 0 & \ddots & 0 \\ 0 & 0 & 0 & 0 & 1 & 0 & -1 \\ 0 & 0 & 0 & 0 & 0 & \frac{k_{n-1}}{m_n} & 0 \end{bmatrix} x + \begin{pmatrix} \frac{1}{m_1} \\ 0 \\ 0 \\ 0 \\ \vdots \\ 0 \\ 0 \end{pmatrix} u, \tag{4.32}$$

where $A \in \mathbb{R}^{2n-1 \times 2n-1}$ is a tridiagonal matrix with zeros in the main diagonal. The controllability matrix $C = [b, Ab, A^2b, A^3b, \dots, A^{2n-2}b] \in \mathbb{R}^{2n-1 \times 2n-1}$ is then upper triangular and

its diagonal elements are (proof see Appendix A.3):

$$\mathrm{diag}(C) = \{b_1, b_1 \cdot a_{21}, b_1 \cdot a_{21} \cdot a_{32}, \ldots, b_1 \cdot \prod_{k=1}^{2n-2} a_{k+1,k}\} \tag{4.33}$$

The determinant of a triangular matrix is the product of its diagonal elements [58]:

$$\det(C) = \left(\frac{1}{m_1}\right) \cdot \left(\frac{1}{m_1} \cdot 1\right) \cdot \left(\frac{1}{m_1} \cdot 1 \cdot \frac{k_1}{m_2}\right) \cdot \ldots \cdot \left(b_1 \cdot \frac{k_1 \cdots k_{n-1}}{m_1 \cdots m_n}\right) \tag{4.34}$$

If any k_i, $i \in \{1, ..., n-1\}$ vanishes, then $\det(C) = 0$ and the matrix is singular, the full rank condition is violated and the system is not fully controllable anymore[4]. This is intuitively clear, one or more vanishing springs decouple the mechanical system and the subsequent masses cannot be influenced by a torque only acting on the first mass.
Consequences are twofold:

Every n DoF mass spring system with a torque acting on the first mass

- is fully controllable and every point in the state-space reachable by a continuous control function
- can be brought to any configuration in state-space in minimum time by a bang-bang control

Same properties hold for the simplification (2.43), i.e. instead of a torque acting on a mass, a point whose velocity can be directly controlled is assumed (see Figure 4.5). Having found a continuous function for the force input, the desired control function is immediately obtained for a velocity input by integration of *Newton's second law* (function will then be even in C^1) and the system is guaranteed to be controllable.

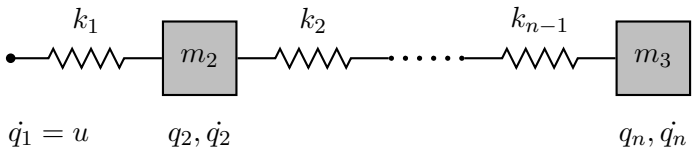

Figure 4.5: n DoF mass spring system with velocity input

4.2 2 DoF Constant Stiffness Mass Spring System with Deflection Constraint

As mentioned in Chapter 2 the deflection of the spring is of vital importance for the systems health. Subsequently, this constraint is considered for the 2 DoF mass spring system with

[4]Same holds of course for multiple vanishing k_i $i \in \{1, ..., n-1\}$, even more, the rankloss of the controllability matrix increases the more proximal the springs to the torque input vanish (no proof, see diagonal elements of C).

constant stiffness. Assume the deflection is constrained by $\varphi = q_1 - q_2 = x_1 - x_2 \leq \varphi_{\max}$ with $\varphi_{\max} > 0$ or written in the familiar form $C(x) := x_1 - x_2 - \varphi_{\max} \leq 0$ from Chapter 3.4. To gain more understanding of the problem at hand, it will be helpful here to reformulate the cost functional with the help of (4.2) as

$$\begin{aligned} J &= -\dot{q}_2(t_f) = \int_0^{t_f} -\ddot{q}_2 dt = -\frac{1}{m_2}\int_0^{t_f} m_2 \ddot{q}_2 dt \\ &= -\frac{1}{m_2}\int_0^{t_f} k_1 \underbrace{(q_1 - q_2)}_{=\varphi} dt = \underbrace{\frac{k_1}{m_2}}_{>0} \int_0^{t_f} -\varphi(t) dt \to \min \end{aligned} \tag{4.35}$$

The implication is that, in order to maximize the velocity of the final mass, the deflection needs to be maximized over time. Therefore, ideally, the deflection should be kept at $\varphi = \varphi_{\max}$. However, at initial time the deflection is zero so the maximal deflection still has to be reached as fast as possible. If $\varphi = \varphi_{\max} = \text{const.}$, both masses move with the same velocity so that $\dot{q}_1 \equiv \dot{q}_2 \Rightarrow \ddot{q}_1 \equiv \ddot{q}_2$ follows. The control u_b that keeps the deflection at the boundary then can be calculated with (4.2) and the aforementioned properties

$$\begin{aligned} m_1 \ddot{q}_1 &= k_1(q_2 - q_1) + F_{\text{ext}} = -k_1 \varphi_{\max} + u_b \\ m_2 \ddot{q}_2 &= m_2 \ddot{q}_1 = k_1(q_1 - q_2) = k_1 \varphi_{\max} \end{aligned} \tag{4.36}$$

by solving the equations above for $\ddot{q}_1$ and subtracting them to be

$$u_b = m_1 \frac{k_1}{m_2}\varphi_{\max} + k_1 \varphi_{\max} = m_1 \varphi_{\max}\left(\frac{k_1}{m_1} + \frac{k_1}{m_2}\right) = m_1 \omega^2 \varphi_{\max}. \tag{4.37}$$

This is consistent with the optimal control theory from Chapter 3.4 and the boundary control u_b derived with tools of optimal control by solving equation (3.52b) for u_b

$$\begin{aligned} \frac{d}{dt}C(x) &= \frac{d}{dt}(x_1 - x_2 - \varphi_{\max}) = x_3 - x_4 \\ \frac{d^2}{dt^2}C(x) &= \frac{d^2}{dt^2}(x_1 - x_2 - \varphi_{\max}) = \dot{x}_3 - \dot{x}_4 = \underbrace{\left(\frac{k_1}{m_1} + \frac{k_1}{m_2}\right)}_{=\omega^2} \underbrace{(x_2 - x_1)}_{-\varphi} + \frac{u}{m_1} \\ &= -\omega^2 \varphi + \frac{u}{m_1} \stackrel{!}{=} 0 \Rightarrow u_b = m_1 \varphi_{\max} \omega^2 \end{aligned} \tag{4.38}$$

yields the same result. Due to the fact that the constraint needs to be differentiated twice for u to appear explicitly, it is of second order. This makes the extended *Hamiltonian*

$$H_{ex}(x, u, \lambda, \mu) = \lambda^T f(x, u) + \mu\left(\frac{d^2}{dt^2}C(x)\right) = \lambda^T(Ax + bu) + \mu\left(\frac{d^2}{dt^2}C(x)\right), \tag{4.39}$$

where $\frac{d^2}{dt^2}C(x)$ depends explicitly on u now and the derivative of the extended *Hamiltonian* w.r.t. u is

$$H_{ex,u}(x, u, \lambda, \mu) = \lambda^T \frac{\partial}{\partial u}(Ax + bu) + \mu \cdot \frac{\partial}{\partial u}\left(\frac{d^2}{dt^2}C(x)\right) = \lambda^T b + \mu \frac{1}{m_1} = \frac{\lambda_3}{m_1} + \frac{\mu}{m_1}. \tag{4.40}$$

The *Lagrangian* function μ for the boundary arc $\mu_b = -\lambda_3$ can be obtained by solving $H_{ex,u} = 0$ for μ. If the state constraint is not active, i.e. $x_1 - x_2 < 0$, then $\mu \equiv 0$ vanishes.

For this case, no singular arcs occur as shown previously. The state and costate ODEs result in the piecewise-defined ODEs

$$\dot{x} = \begin{cases} Ax + bu & \text{for } C < 0 \text{ with } u = u_{\max} \vee u_{\min} \\ Ax + bu_b & \text{for } C \equiv 0 \end{cases}$$
$$\dot{\lambda} = \begin{cases} -A^T\lambda & \text{for } C < 0 \\ -A^T\lambda - \mu_b \left(\frac{\partial}{\partial x}\frac{d^2}{dt^2}C(x)\right)\Big|_{u=u_b} = -A^T\lambda + \lambda_3 \cdot \left(-\omega^2, \omega^2, 0, 0\right)^T & \text{for } C \equiv 0 \end{cases} \tag{4.41}$$

All quantities for the MPBVP are now known except the switching structure that is necessary to fully determine the interior point conditions. What further assumptions can be made? As mentioned before, a state where the deflection is kept at $\varphi_{\max}$ should be reached as fast as possible. From this time on, the integral in the reformulated cost functional (4.35) is maximized. Hence, the part with the boundary arc should occur in the last part of the MPBVP and the switching times are independent from final time[5]. How many times does the control need to switch in order to obtain a state with the deflection at the maximum value and the masses moving with the same velocity? Is one switch already sufficient, i.e. going from $u_{\max}$ to u_{b}? From the analytical solution of the 2 DoF case without state inequality constraints that has $u^* = u_{\max}$ as optimal control, it is known that the velocities are identical at integer multiplicities of $\frac{\pi}{\omega}$, see for example Figure 4.16(a). However, at these points the deflection is at $\frac{2u_{\max}}{m_1\omega^2}$. If the constraint is below that value it is not possible without switching another time to obtain a state with equal velocities of the masses without violating the constraint. This makes already evident that the value of the deflection influences the switching structure significantly. From the 2 DoF case without state inequality constraint it is known that the deflection obtained from the analytical solution (see Appendix A.1) is bounded by

$$\varphi^* = x_1^* - x_2^* = -\frac{u_{\max}}{m_1\omega^2}(\cos(\omega t) - 1) = \underbrace{\frac{u_{\max}}{m_1\omega^2}}_{>0}\underbrace{(1 - \cos(\omega t))}_{\leq 2} \leq \frac{2u_{\max}}{m_1\omega^2}. \tag{4.42}$$

Hence, for $\varphi_{\max} \geq \frac{2u_{\max}}{m_1\omega^2}$ the state inequality will not affect the system and the case without state inequality constraint is obtained, which was already analyzed in Chapter 4.1.

Until now, the control constraint $u \leq u_{\max}$ was not taken into account. Of course the boundary control should not violate this constraint, so that

$$u_b = m_1\omega^2\varphi_{\max} \overset{!}{\leq} u_{\max} \tag{4.43}$$

needs to hold[6]. Solving for $\varphi_{\max}$ makes evident that this is only valid for

$$\varphi_{\max} \leq \frac{u_{\max}}{m_1\omega^2}. \tag{4.44}$$

This means that if greater values are chosen for $\varphi_{\max}$, it is not possible to keep the deflection constant and incurring oscillations are an immediate consequence. Therefore, the following three cases arise

[5] As long as the final time is greater than the switching time required to bring the mass spring system into the desired state.

[6] The constraint $u \geq u_{\min}$ needs to considered as well but ultimately leads to the same condition: $m_1\omega^2\varphi_{\max} \geq u_{\min} \Rightarrow \varphi_{\max} \geq \frac{u_{\min}}{m_1\omega^2} = -\frac{u_{\max}}{m_1\omega^2} \Rightarrow \varphi_{\max} \leq \frac{u_{\max}}{m_1\omega^2}$.

1. Case: $\varphi_{\max} \geq \frac{2u_{\max}}{m_1\omega^2}$
   This is case is equivalent to the system without inequality constraint analyzed in Chapter 4.1.

2. Case: $\frac{u_{\max}}{m_1\omega^2} < \varphi_{\max} < \frac{2u_{\max}}{m_1\omega^2}$
   In this case, the deflection cannot be kept constant, hence oscillations occur.

3. Case: $\varphi_{\max} \leq \frac{u_{\max}}{m_1\omega^2}$
   Here, keeping the deflection at the maximum possible value and achieving this state as fast as possible is optimal from the considerations of the cost functional (4.35).

In the following, the third case will be discussed in detail to retrieve more analytical information. The necessary conditions from Chapter 3.4 complete the piecewise-defined ODEs (4.41) with the missing interior point conditions. As mentioned before, one switch is not sufficient. Therefore, it will be assumed that it takes two control switches to bring the mass spring system into the desired state of constant deflection starting with $u_{\max}$, i.e. the assumed control structure is $u_{\max} \to u_{\min} \to u_{\mathrm{b}}$. Let t_1 denote the switching time belonging to the transition from $u_{\max}$ to $u_{\min}$ and the switching time t_2 to the transition from $u_{\min}$ to u_b. States and costates are continuous across t_1 because the constraint has not been reached yet. Since the state constraint is of second order, the multiplier ν is two dimensional $\nu \in \mathbb{R}^2$. Evaluating the jump conditions (3.51) and switching conditions (3.52) at t_2 leads to

$$\begin{aligned}
\lambda_1(t_2^+) &= \lambda_1(t_2^-) - \nu_1 \\
\lambda_2(t_2^+) &= \lambda_2(t_2^-) + \nu_1 \\
\lambda_3(t_2^+) &= \lambda_3(t_2^-) - \nu_2 \\
\lambda_4(t_2^+) &= \lambda_4(t_2^-) + \nu_2 \\
x_1(t_2) - x_2(t_2) &= \varphi_{\max} \\
x_3(t_2) - x_4(t_2) &= 0 \\
\lambda_3(t_2^+) &= \frac{2k_1\varphi_{\max} - u_{\min}}{u_{\min} - u_b}\nu_2
\end{aligned} \tag{4.45}$$

The MPBVP for the third case is comprised of (4.41) and (4.45) along with the trivial ODEs $\dot{\nu}_1 = 0$ and $\dot{\nu}_2 = 0$. Even for this simple system, consisting of two masses and one spring, adding only one constraint results in a ten-dimensional system of piecewise-defined differential equations with four initial values, four end values, four jump conditions and three switching conditions. Since there is no way to find reasonable initial values for the adjoint variables and the MPBVP is already complex, convergence issues arise as mentioned in Chapter 3.5 using indirect methods. An alternative approach via energy-based considerations is presented here for the third case.

The performed work at t_2 calculates from integration of the performance with $u_{\min} = -u_{\max}$ as

$$\begin{aligned}
W(t_2) &= \int_0^{t_1} u_{\max}\dot{q}_1 dt + \int_{t_1}^{t_2} u_{\min}\dot{q}_1 dt \\
&= u_{\max}(q_1(t_1) - \underbrace{q_1(0)}_{=0}) + u_{\min}(q_1(t_2) - q_1(t_1)) = u_{\max}(2q_1(t_1) - q_1(t_2))
\end{aligned} \tag{4.46}$$

The total energy of the system at t_2 is

$$E(t_2) = \frac{1}{2}m_1\dot{q}_1^2(t_2) + \frac{1}{2}m_2\dot{q}_2^2(t_2) + \frac{1}{2}k_1\varphi_{\max}^2(t_2) \tag{4.47}$$

As a necessary condition $E(t_2) - W(t_2) = 0$ needs to hold. Additionally, the masses need to move with same velocity from t_2 on, so that

$$\dot{q}_1(t_2) - \dot{q}_2(t_2) = 0 \tag{4.48}$$

is a further condition. The switching times t_1 and t_2 can be obtained by solving the nonlinear system of equations

$$\begin{aligned} \frac{1}{2}m_1\dot{q}_1^2(t_2) + \frac{1}{2}m_2\dot{q}_2^2(t_2) + \frac{1}{2}k_1\varphi_{\max}^2(t_2) - u_{\max}(2q_1(t_1) - q_1(t_2)) &= 0 \\ \dot{q}_1(t_2) - \dot{q}_2(t_2) &= 0 \end{aligned} \tag{4.49}$$

where $\dot{q}_1(t_1), \dot{q}_1(t_2), \dot{q}_1(t_2), \dot{q}_2(t_2)$ can be found by analytically solving the state ODE for $t \in [0, t_1]$ with $u = u_{\max}$ and for $t \in [t_1, t_2]$ with $u = u_{\min}$. While this approach also leads to a nonlinear system of equations as indirect methods, the dimensionality has been reduced immensely and the remaining unknowns are t_1 and t_2 instead of $t_1, t_2, \nu_1, \nu_2, \lambda_1, \lambda_2, \lambda_3, \lambda_4$.

To get more information about the missing quantities, the *Hamiltonian* plays an important role. Let the assumption be that the *Hamiltonian* is constant on the entire domain with $H \equiv -\frac{k_1}{m_1}\varphi_{\max}$, then following conditions have to be shown

(i) Continuity across a control switch if no state constraint is active.

(ii) Continuity across an entry point, i.e. the beginning of a state constrained arc.

(iii) Value $-\frac{k_1}{m_1}\varphi_{\max}$ at final time.

Proof

(i) Consider a general optimal control problem in *Mayer* form and control-affine dynamics. Let u be one-dimensional for the sake of short notation. The extension is straightforward but not of interest here. The *Hamiltonian* takes the form

$$H = \lambda^T f(x,u) = \lambda^T f_1(x) + u\lambda^T f_2(x). \tag{4.50}$$

At a control switch the following holds

$$s = H_u = \lambda^T f_2(x) = 0. \tag{4.51}$$

With the continuity of the states and adjoints, a jump in the *Hamiltonian* calculates as

$$\begin{aligned} H\Big|_{t_1^-} - H\Big|_{t_1^+} &= \lambda^T f_1(x)\Big|_{t_1^-} + u^-\lambda^T f_2(x)\Big|_{t_1^-} - \lambda^T f_1(x)\Big|_{t_1^+} - u^+\lambda^T f_2(x)\Big|_{t_1^+} \\ &= (u^- - u^+)\cdot\lambda(t_1)^T f_2(x(t_1)), \end{aligned} \tag{4.52}$$

where $u^{\pm} = \lim_{t\to t_1^{\pm}} u(t)$. Due to (4.51) the right-hand side is always zero at a control switch, hence yielding continuity.

(*ii*) Looking at (3.52c), this holds if the state constraint does not depend explicitly on time, which is the case in the considered problem.

(*iii*) The *Hamiltonian* at final time is

$$H\Big|_{t_f} = \lambda^T f(x,u)\Big|_{t_f} = (0,0,0,-1)\cdot(\dot{x}_1(t_f),\dot{x}_2(t_f),\dot{x}_3(t_f),\dot{x}_4(t_f))^T = -\dot{x}_4(t_f). \quad (4.53)$$

This corresponds to the acceleration of the second mass. As mentioned previously, the last part in the MPBVP is the one with the active state constraint. Therefore, it is possible to solve the second equation of (4.36) for $\ddot{q}_2$. This yields $\ddot{q}_2 = \frac{k_1}{m_1}\varphi_{\max}$, hence

$$H\Big|_{t_f} = -\dot{x}_4(t_f) = -\ddot{q}_2(t_f) = -\frac{k_1}{m_1}\varphi_{\max} \quad (4.54)$$

□

Having found the value of the *Hamiltonian* it is possible to obtain the multiplier (jump parameter) ν_1 and ν_2. For the first multiplier, the implicit equation

$$H\Big|_{t_1^-}(x,\lambda,u,\nu_1,\nu_2) = -\frac{k_1}{m_1}\varphi_{\max} \quad (4.55)$$

needs to be solved for ν_1. The analytical solution has been computed with *MAPLE* and is not shown due to its length. Although it would be more obvious to solve $H|_{t_2^-}(x,\lambda,u,\nu_1,\nu_2) = -\frac{k_1}{m_1}\varphi_{\max}$ for ν_1, this is not possible because a cancellation of the multiplier ν_1 occurs. For the second jump parameter, the last equation of (4.45) needs to be solved for ν_2 yielding

$$\nu_2 = \frac{u_{\min} - u_b}{2k_1\varphi_{\max} - u_{\min}}\lambda_3(t_2^+), \quad (4.56)$$

where $\lambda_3(t_2^+)$ can be found by analytical integration with the adjoint ODE from (4.41) for the case $C \equiv 0$ and the familiar end value $\lambda(t_f) = (0,0,0,-1)^T$.

Quantity	Method	Value
Switching times t_1,t_2	numerical via energetic approach	-
Hamiltonian H	analytic	$-\frac{k_1}{m_1}\varphi_{\max}$
Jump parameter ν_1	analytic	$H\big\|_{t_1^-}(x,\lambda,u,\nu_1,\nu_2) = -\frac{k_1}{m_1}\varphi_{\max}$
Jump parameter ν_2	analytic	$\frac{u_{\min}-u_b}{2k_1\varphi_{\max}-u_{\min}}\lambda_3(t_2^+)$
Lagrangian function μ	analytic	$-\lambda_3$
Control u	analytic/assumption	$u_{\max} \to u_{\min} \to u_{\mathrm{b}}$
States x	analytic	Not displayed for readability
Costates λ	analytic	Not displayed for readability

Table 4.2: Overview over the different quantities and the method to obtain them.

Example

Figure 4.6 depicts a numerical solution obtained with *GPOPS* for $m_1 = m_2 = 2, u_{\max} = 4, k_1 = 25$ and $t_f = 2$. The deflection is constrained by $\varphi_{\max} \in \{0.18, 0.12, 0.05\}$ in order to display the three cases, since $\frac{2u_{\max}}{m_1\omega^2} = 0.16$. The numerical results correspond nicely

to the previously formulated statements, such as the boundary control $u_b = m_1\omega^2\varphi_{\max} = 2 \cdot \left(\frac{25}{2} + \frac{25}{2}\right) \cdot 0.05 = 2.5$ appearing in the third case. However, the control as calculated by

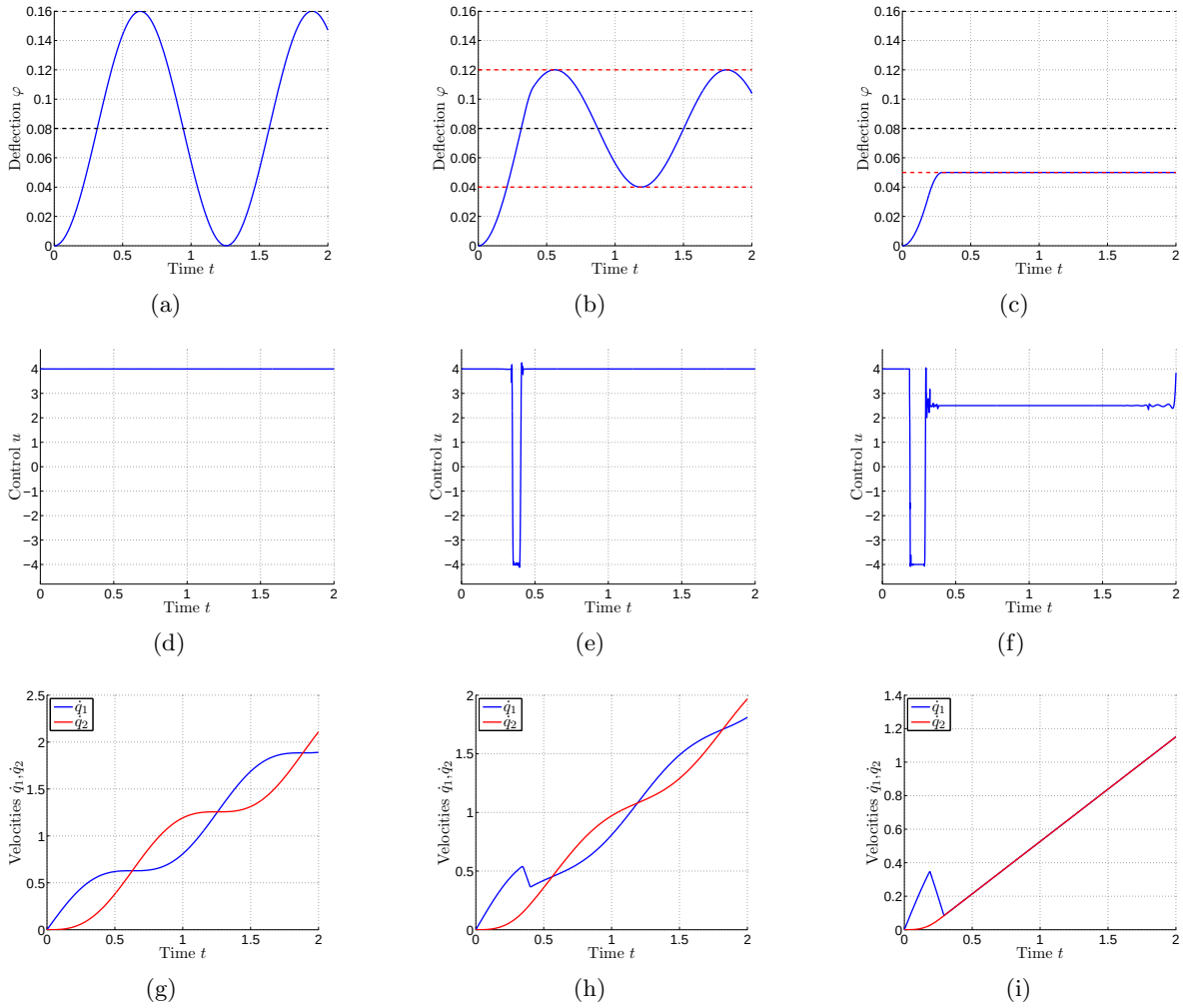

Figure 4.6: Deflection (a)-(c), control (d)-(f) and mass velocities (g)-(i) for the three cases.

GPOPS deviates from its expected solution, especially near the switching times and the final time, see Figure 4.6(f). As mentioned in Chapter 3.5, discontinuous solutions are problematic in pseudospectral methods. It is a well-known phenomenon caused by the (automatic) placement of collocation points in a mesh interval formulation. Since the locations of non-smoothness are not known a-priori, in general, numerical artifacts occur at transitions of constituent arcs. A possible explanation for the numerical discrepancies at final time could be that the point at final time is uncollocated due to the usage of flipped LGR points.
To improve the solution, the aforementioned approach with the energetic considerations is chosen.

First, the switching times need to be computed. Figure 4.7 depicts the nonlinear system (4.49) for these values graphically. It should be noted that since $t_2 > t_1$, only one half space is relevant. Numerical solver, such as *MAPLE*'s `solve` or *MATLAB*'s `fsolve`, both find the

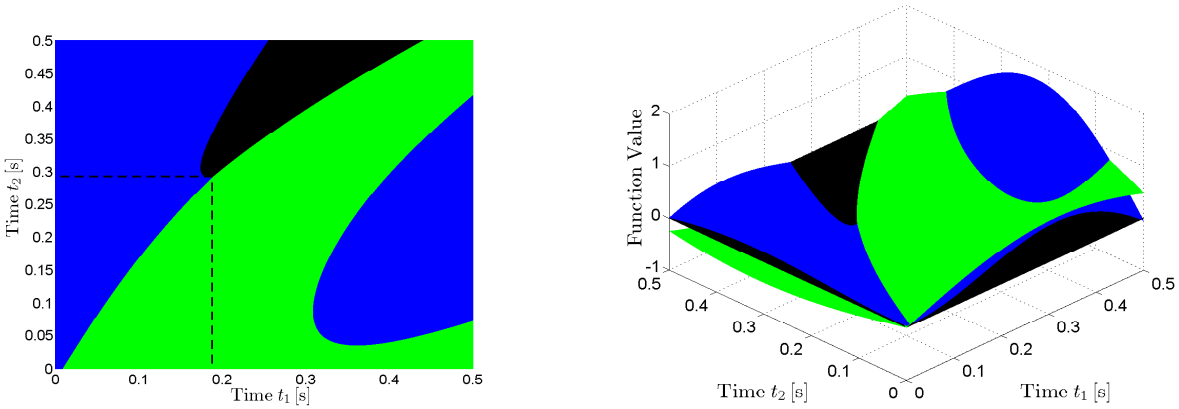

(a) (b)

Figure 4.7: Visualization of the nonlinear system of equations (4.49). Blue indicates $E(t_2) - W(t_2)$, green $\dot{q}_1(t_2) - \dot{q}_2(t_2)$ and black $g(t_1, t_2) = 0$. Left: Top view with dashed lines that show the intersection of the equations. Right: 3D view.

zeros at $t_1 = 0.1880$ and $t_2 = 0.2920$ with the additional assumptions $t_2 > t_1 > 0$. In the subsequent step the jump parameters are calculated, yielding $\nu_1 = 22.0151$ and $\nu_2 = 18.2329$. Finally, the states and costates can be found by integration which completes the solution (depicted in Figure 4.8). The numerical chattering effects of the control are nullified. As mentioned in Chapter 3.4 the sign conditions (3.53) and *Hamiltonian* serve as tool for a-posteriori analysis. The non-negativity of both multiplier stated in (3.53a) is readily apparent: $\nu_1 = 22.0151 \geq 0$, $\nu_2 = 18.2329 \geq 0$. The *Lagrangian* function also complies with (3.53b):

$$\mu = \begin{cases} 0 \geq 0 & \text{for } t \in [0, t_2[\quad (C < 0) \\ -\lambda_3 = \frac{1}{2}\frac{k_1}{m_2} t_f (\frac{1}{t_f} t^2 - 2t + t_f) \geq 0 & \text{for } t \in [t_2, t_f] \quad (C \equiv 0) \end{cases} \tag{4.57a}$$

$$\frac{d}{dt}\mu = \begin{cases} 0 \leq 0 & \text{for } t \in [0, t_2[\quad (C < 0) \\ -\dot{\lambda}_3 = \lambda_1 = \frac{k_1}{m_2}(t - t_f) \leq 0 & \text{for } t \in [t_2, t_f] \quad (C \equiv 0) \end{cases} \tag{4.57b}$$

Figure 4.9 depicts the deviation of the *Hamiltonian* from its expected value. As opposed to the solution with the numerical solver *GPOPS* (cf. Figure 4.9(a)) it can be seen that the energy approach is significantly closer to the exact solution. The reason is that the control is already deviating from the optimal solution due to its discretization and the costates are only approximated and not solved for explicitly. These inaccuracies are reflected in the *Hamiltonian*.

Case 2 is even more complicated due to the fact that the deflection hits the constraint periodically and therefore touch point conditions need to be evaluated at the corresponding points. The structure of the MPBVP also depends on the final time.

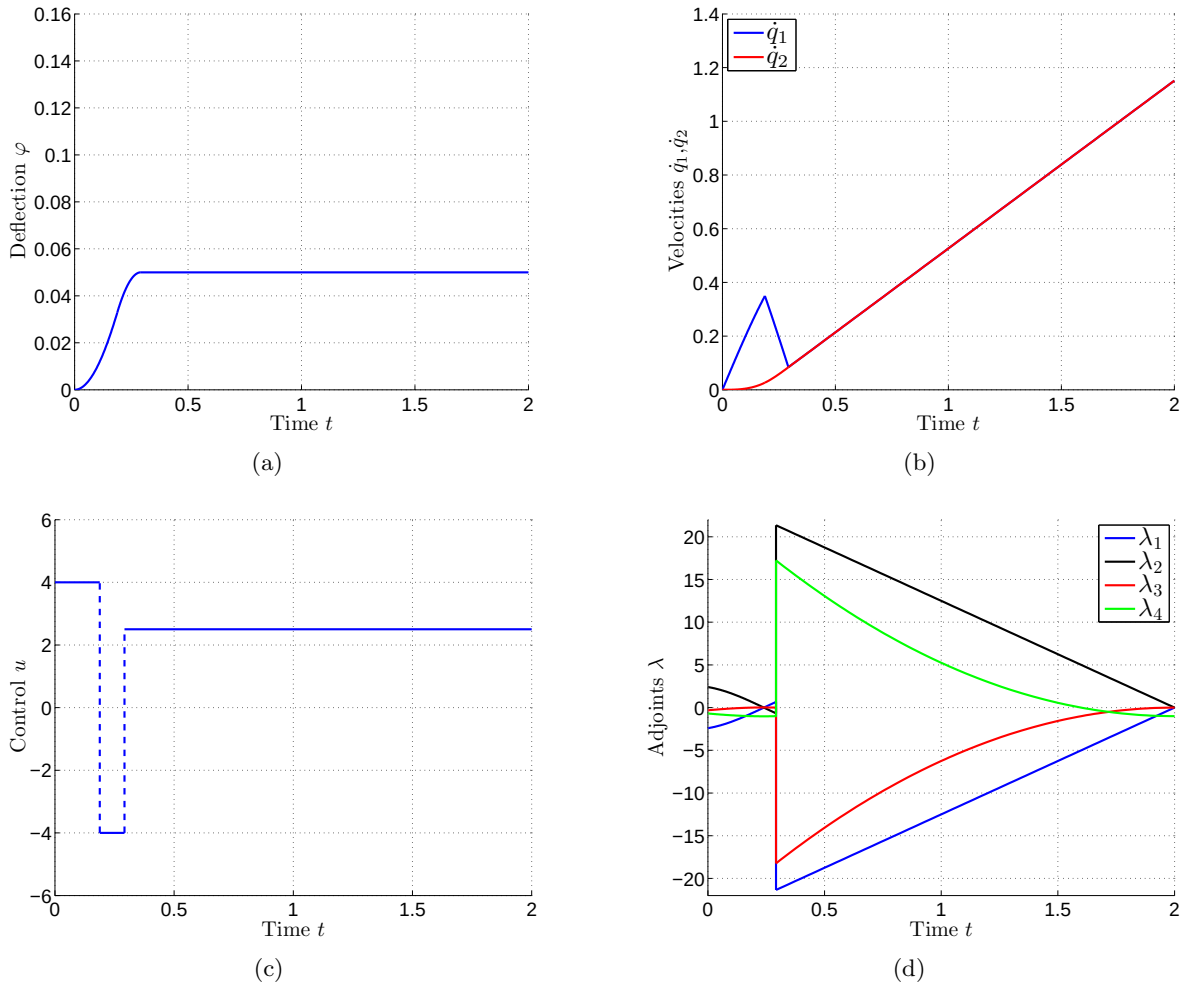

Figure 4.8: Solution of the third case via energetic considerations arising in the 2 DoF mass spring system with deflection constraint. While the switching points are found numerically, the solution within each phase is found analytically here.

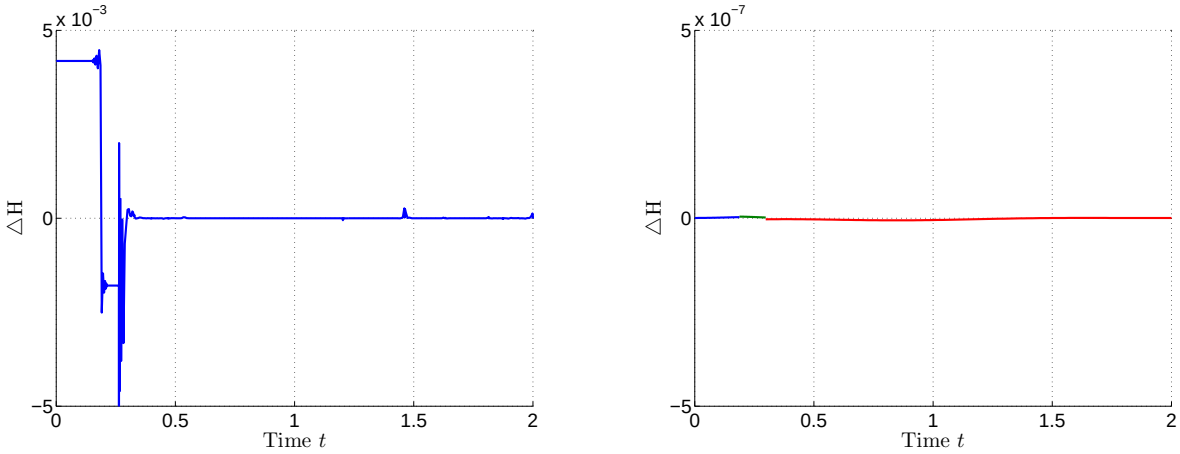

(a) *GPOPS* (b) Energy approach

Figure 4.9: $\triangle H := H - H^* = H + \frac{k_1}{m_1}\varphi_{\max}$ is the error of the computed *Hamiltonian* and its optimal constant value. The reader should not overlook the different scaling of (a) and (b).

4.3 Variable Stiffness

For the variable stiffness case, in addition to the torque control u_1 (former u) acting on the first mass, it is assumed that additional controls can directly adjust the stiffness of the corresponding springs, i.e. $u_i = k_{i-1}$ for $i \in \{2, ..., n\}$, see Figure 4.10. These systems correspond to robots with variable stiffness/impedance actuators mentioned in Chapter 2.5. Without any

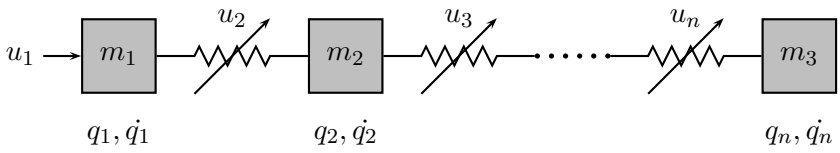

Figure 4.10: n DoF mass spring system with variable stiffness

effort, the state-space equations can be carried over for the 2 DoF case from (4.3) by simply replacing k_1 with u_2

$$\dot{x} = \frac{d}{dt}\begin{pmatrix} q_1 \\ q_2 \\ \dot{q_1} \\ \dot{q_2} \end{pmatrix} = \begin{bmatrix} 0 & 0 & 1 & 0 \\ 0 & 0 & 0 & 1 \\ -\frac{u_2}{m_1} & \frac{u_2}{m_1} & 0 & 0 \\ \frac{u_2}{m_2} & -\frac{u_2}{m_2} & 0 & 0 \end{bmatrix} x + \begin{pmatrix} 0 \\ 0 \\ \frac{1}{m_1} \\ 0 \end{pmatrix} u_1 =: A(u_2)x + bu_1. \tag{4.58}$$

Since the system matrix A also incorporates the stiffness controls for higher-dimensional cases (see (4.32)), the state-space equations obviously take the form

$$\dot{x} = A(u_2, ..., u_n)x + bu_1. \tag{4.59}$$

These are not linear systems anymore, in fact, one has to deal with bilinear systems of the form

$$\dot{x} = Ax + \sum_{j=1}^{n} G_j x u_j + Bu. \tag{4.60}$$

More precisely, following the notation of [40], (4.60) is a biaffine system. It reduces to a (pure) bilinear[7] system for $B = 0$. This makes the adjoint equations (in general) homogeneous, linear, time-variant ODEs

$$\dot{\lambda} = -H_x = \left(-A - \sum_{j=1}^{n} G_j u_j(t) \right)^T \lambda =: \tilde{A}(u(t))\lambda \tag{4.61}$$

and the switching functions

$$s_i = H_{u_i} = f_{u_i}^T \lambda = (G_i x + b_i)^T \lambda = s_i(x, \lambda), \tag{4.62}$$

where b_i is the i-th column of B.
Adjoint equations and switching functions are now coupled in the sense that in order to solve the adjoint equations, the optimal control has to be known, whereas in the linear case the adjoint equations could be solved independently of the control.

Exclusion of singular arcs for the 2 DoF variable stiffness mass spring system

In order to make assumptions about the existence of singular arcs one has to look at the switching function and (possibly) its higher derivatives. It turns out, that the *Goh-Legendre* conditions (3.42) and (3.43) are satisfied and therefore not suited for the exclusion due to reasons mentioned in Chapter 3.3 (this can be verified easily, omitted for brevity here). For the 2 DoF case, the switching functions s_1 and s_2 for the controls u_1 and u_2 can be calculated from (4.58), with

$$\begin{aligned} s_1 &= \lambda^T \frac{\partial}{\partial u_1} \left(A(u_2)x + bu_1 \right) = \frac{\lambda_3}{m_1} \\ s_2 &= \lambda^T \frac{\partial}{\partial u_2} \left(A(u_2)x + bu_1 \right) = (x_1 - x_2) \left(\frac{\lambda_4}{m_2} - \frac{\lambda_3}{m_1} \right) \end{aligned} \tag{4.63}$$

It is crucial to assume that $u_2 > 0$ and $u_{1,\max} \neq 0 \neq u_{1,\min}$ as mentioned in the beginning of this chapter. In order to show that no singular arcs exist, it needs to be proven that for both switching functions (4.63) no intervals exist where they are zero. As a direct consequence, it needs to be shown that each of the following terms

(*i*) λ_3

(*ii*) $\frac{\lambda_4}{m_2} - \frac{\lambda_3}{m_1}$

(*iii*) $x_1 - x_2$

[7] Terminology not consistent throughout literature.

are only zero at discrete points. Recalling the dynamics for the states and adjoints from (4.58) and (4.61) as

$$\begin{aligned} \dot{x}_1 &= x_3 & \dot{\lambda}_1 &= u_2\left(\frac{\lambda_3}{m_1} - \frac{\lambda_4}{m_2}\right) \\ \dot{x}_2 &= x_4 & \dot{\lambda}_2 &= u_2\left(\frac{\lambda_4}{m_2} - \frac{\lambda_3}{m_1}\right) \\ \dot{x}_3 &= \frac{u_2}{m_1}(x_2 - x_1) + \frac{u_1}{m_1} & \dot{\lambda}_3 &= -\lambda_1 \\ \dot{x}_4 &= \frac{u_2}{m_2}(x_1 - x_2) & \dot{\lambda}_4 &= -\lambda_2 \end{aligned} \tag{4.64}$$

Using these dynamic equations, it can be shown that singular arcs do not occur and the proof is as follows

(*i*) Assume that $s_1 = \frac{\lambda_3}{m_1} \equiv 0$. It follows immediately

$$\begin{aligned} &\lambda_3 \equiv 0 \Rightarrow \dot{\lambda}_3 \equiv 0 \Rightarrow \lambda_1 \equiv 0 \Rightarrow \dot{\lambda}_1 \equiv 0 \\ &\Rightarrow \underbrace{u_2}_{>0}\Bigg(\underbrace{\frac{\lambda_3}{m_1}}_{=0} - \frac{\lambda_4}{m_2}\Bigg) \equiv 0 \Rightarrow \lambda_4 \equiv 0 \Rightarrow \dot{\lambda_4} \equiv 0 \Rightarrow \lambda_2 \equiv 0 \end{aligned} \tag{4.65}$$

If $\lambda \equiv 0$ holds for some interval, then λ would remain at zero, and since the transversality condition is $\lambda(t_f) = (0, 0, 0, -1)^T$ this is a contradiction. In other words, s_1 can never stay at zero and $u_1^* = u_{1,\min} \vee u_{1,\max}$.

(*ii*) Assume that $x_1 - x_2 \equiv 0$. Then

$$\begin{aligned} &\frac{d}{dt}(x_1 - x_2) = x_3 - x_4 \equiv 0 \\ &\frac{d^2}{dt^2}(x_1 - x_2) = \dot{x}_3 - \dot{x}_4 = \left(\frac{u_2}{m_1} + \frac{u_2}{m_2}\right)\underbrace{(x_2 - x_1)}_{=0} + \frac{u_1}{m_1} = \frac{u_1}{m_1} \neq 0 \end{aligned} \tag{4.66}$$

and u_1 is never at zero due to (*i*). Consequently, $x_1 - x_2$ cannot stay at zero in a finite time interval.

(*iii*) This leaves only the case of $\frac{\lambda_4}{m_2} - \frac{\lambda_3}{m_1} \equiv 0$ that needs to be excluded.

$$\begin{aligned} &\frac{d}{dt}\left(\frac{\lambda_4}{m_2} - \frac{\lambda_3}{m_1}\right) = \frac{\lambda_1}{m_1} - \frac{\lambda_2}{m_2} \\ &\frac{d^2}{dt^2}\left(\frac{\lambda_4}{m_2} - \frac{\lambda_3}{m_1}\right) = \left(\frac{\dot{\lambda}_1}{m_1} - \frac{\dot{\lambda}_2}{m_2}\right) = \left(\frac{u_2}{m_1} + \frac{u_2}{m_2}\right)\underbrace{\left(\frac{\lambda_3}{m_1} - \frac{\lambda_4}{m_2}\right)}_{=0} \equiv 0 \end{aligned} \tag{4.67}$$

Due to the adjoint dynamics (4.64), $\dot{\lambda}_1$ and $\dot{\lambda}_2$ are zero and λ_1 and λ_2 are constants as a consequence. The adjoints dynamics are not influenced by either control and will remain at these constant values. With the transversality conditions the solution beginning at a singular arc is $\forall t \in [t_{entry}, t_f]$ $\lambda^* = (0, 0, 0, -1)^T$. The cost function can be rewritten

as in [82] with t_{entry} denoting the beginning of a singular arc as

$$\begin{aligned} J &= -x_4(t_f) = \lambda(t_f)^T x(t_f) = \int_0^{t_f} \frac{d}{dt}(\lambda^T x)dt = \int_0^{t_f} \dot{\lambda}^T x + \lambda^T \dot{x} dt \\ &= \int_0^{t_f} (-A^T\lambda)^T x + \lambda^T(Ax+bu)dt = \int_0^{t_f} -\lambda^T Ax + \lambda^T Ax + \lambda^T b u dt \\ &= \int_0^{t_f} \lambda^T b u dt = \int_0^{t_f} \frac{\lambda_3}{m_1} u dt = \int_0^{t_{entry}} \frac{\lambda_3}{m_1} u dt + \int_{t_{entry}}^{t_f} \underbrace{\frac{\lambda_3}{m_1}}_{=0} u dt = \int_0^{t_{entry}} \frac{\lambda_3}{m_1} u dt \end{aligned} \tag{4.68}$$

It can be seen that the cost cannot be minimized further if a singular arc occurs and is therefore nonoptimal. If $\lambda_3 \neq 0$ the control can always be chosen accordingly so that the integral is negative.

□

A physical interpretation for singular arcs would be for example that the deflection between the two masses needs to vanish for a certain amount of time. This would make the masses move with the same velocity and $x_3 - x_4$ would equal zero in that interval. By looking at the first derivative

$$\dot{s}_2 = (x_1 - x_2)\left(\frac{\lambda_1}{m_1} - \frac{\lambda_2}{m_2}\right) + (x_3 - x_4)\left(\frac{\lambda_4}{m_2} - \frac{\lambda_3}{m_1}\right) \tag{4.69}$$

it is confirmed in a mathematical sense that this is a further necessary condition for a singular arc to occur. Physically speaking, a singular arc for the stiffness control only occurs if no spring force is exerted due to a vanishing deflection and adjusting the stiffness leaves the system unaffected. Mechanical reasoning suggests that the deflection between two masses is never zero for an interval if the system is under permanent excitation, which it is, because $u_1 \in \{u_{\min}, u_{\max}\}$ and $u_{\min} \neq 0 \neq u_{\max}$.

This argumentation and the proof is readily formulated for different cost functions, such as maximizing the kinetic energy $J = \frac{1}{2} m_2 \dot{q}_2^2(t_f)$ or the deflection $J = -\varphi(t_f) = -(q_1(t_f) - q_2(t_f))$ at final time and both lead to bang-bang solutions. A counter-example would be an energy-minimal criterion $J = \int_0^{t_f} u^2 dt$ that has a regular *Hamiltonian*. Intuitively, switchings from $u_{\min}$ to $u_{\max}$ are not reasonable from an energetic perspective.

A peculiar, but pathological case is left for future work where the stiffness or the torque input can be zero on its boundary. For the exclusion of singular arcs it was necessary to rule out these cases. It is not evidently clear how the optimal solution will behave and if singular arcs occur.

However, both controls are constant a.e. here and this can be used to make further assumptions about the control nearing the final time. Let $\varepsilon > 0$ be small enough so that in $(t_f - \varepsilon, t_f]$ no control switch occurs. The solution of the constant stiffness (Appendix A.1) can be used

now to evaluate the switching functions near final time

$$s_1\Big|_{t=t_f-\varepsilon} = \frac{\lambda_3^*}{m_1}\Big|_{t=t_f-\varepsilon} = \frac{1}{m_1+m_2}[\cos(-\varepsilon)-1] < 0 \tag{4.70a}$$

$$s_2\Big|_{t=t_f-\varepsilon} = (x_1^*-x_2^*)\left(\frac{\lambda_4^*}{m_2}-\frac{\lambda_3^*}{m_1}\right)\Big|_{t=t_f-\varepsilon} \tag{4.70b}$$

$$= \frac{u_{\max}}{k_1(m_1+m_2)}\cos(\omega\varepsilon)\left(\cos(\omega(\varepsilon-t_f))-1\right) \leq 0 \tag{4.70c}$$

The equality sign in "$\leq$" of (4.70c) holds only if a switching occurs which was excluded, so that at final time, both controls are at their upper boundary.

Example

Due to (4.63) and the choice $m_1 = m_2$ for the 2 DoF case, the switching times for u_2 only occur when the deflection $x_1 - x_2$ is zero or $\lambda_3 - \lambda_4$ is zero. This is visualized in Figure 4.11 for the (fixed) final time $t_f = 1.2$. More interestingly, zeros of $x_1 - x_2$ correspond to a negative edge and zeros of $\lambda_3 - \lambda_4$ to a positive edge. Taking a look at the dual system (4.28) that describes the same undamped mass spring system but without external force and in terms of the states λ_3, λ_4

$$\begin{bmatrix} m_1 & 0 \\ 0 & m_2 \end{bmatrix}\begin{pmatrix}\ddot{\lambda}_3 \\ \ddot{\lambda}_4\end{pmatrix} + \underbrace{\begin{bmatrix} u_2 & -u_2 \\ -u_2 & u_2 \end{bmatrix}}_{=K(u_2)}\begin{pmatrix}\lambda_3 \\ \lambda_4\end{pmatrix} = 0, \tag{4.71}$$

then $\lambda_3 - \lambda_4$ is the deflection of the dual system. Since it is undamped, unforced and the end condition is not identical zero, it must be always in motion and the same argument for the deflection is applicable. In conclusion, for u_2 to switch, either the deflection of the mechanical or the dual system is zero. If both are compressed or pushed apart simultaneously at a specific time, then the control is at its upper boundary $u_{\max}$, else at its lower boundary $u_{\min}$ (cf. 4.11(b) and 4.11(d)). Moreover, both controls are at the upper boundary near final time as shown previously, see Figures 4.11(a) and 4.11(b).

Assumptions for the n DoF case

The system dynamics of an n DoF mass spring system with varying stiffness is as follows:

$$\dot{x} = \begin{pmatrix} x_{n+1} \\ \vdots \\ x_{2n} \\ \frac{u_1}{m_1} + \frac{u_2}{m_1}(x_2 - x_1) \\ \frac{u_2}{m_2}(x_1 - x_2) + \frac{u_3}{m_2}(x_3 - x_2) \\ \vdots \\ \frac{u_{n-1}}{m_{n-1}}(x_{n-2} - x_{n-1}) + \frac{u_n}{m_{n-1}}(x_n - x_{n-1}) \\ \frac{u_n}{m_n}(x_{n-1} - x_n) \end{pmatrix} \tag{4.72}$$

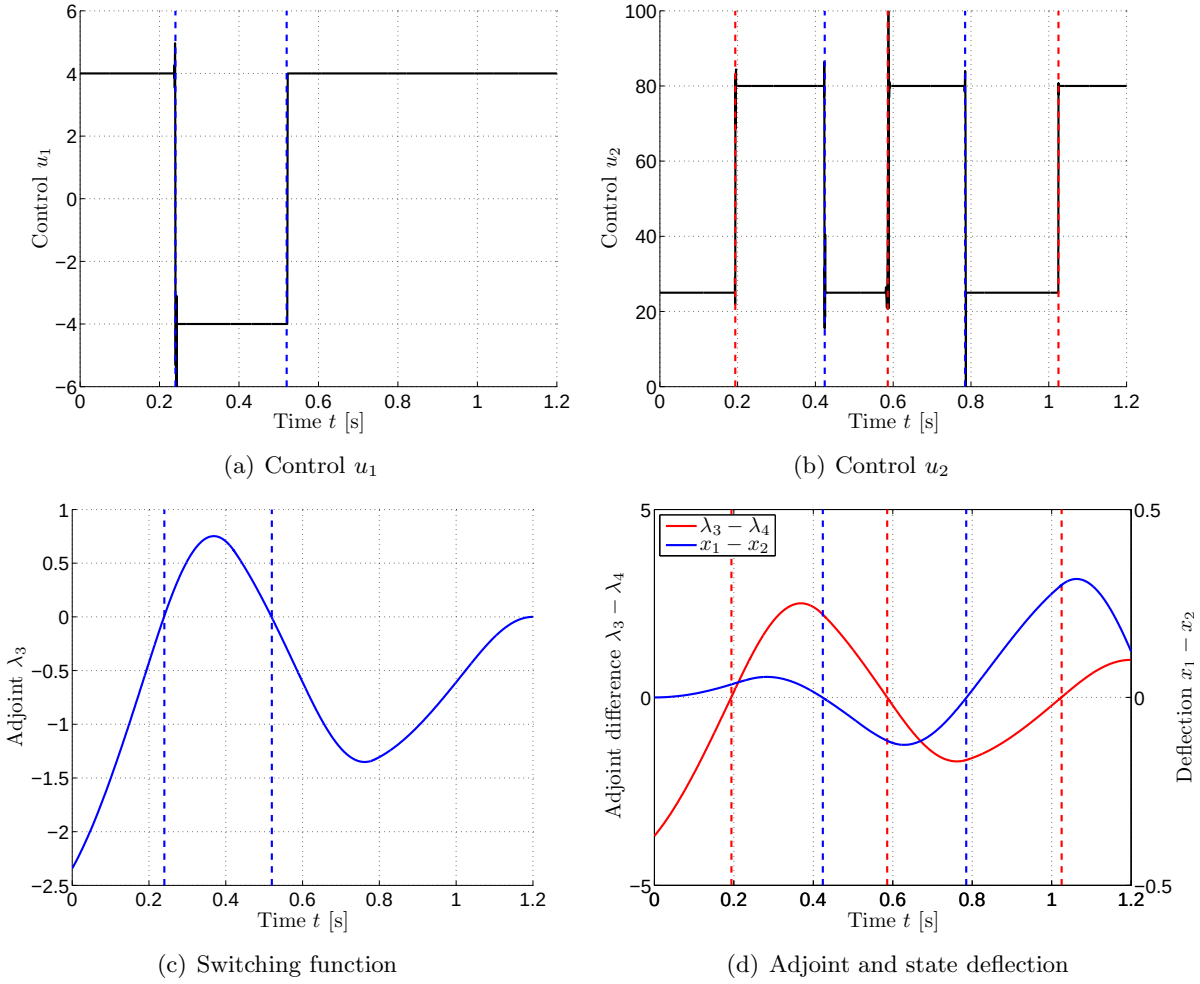

(a) Control u_1

(b) Control u_2

(c) Switching function

(d) Adjoint and state deflection

Figure 4.11: Top row: Controls u_1 and u_2. Bottom row: Functions that cause a switching.

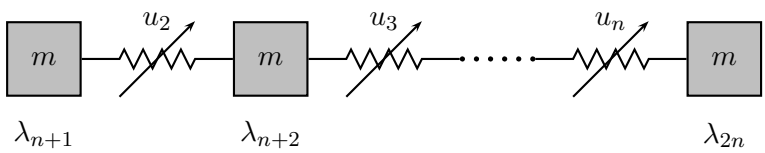

Figure 4.12: Dual system with equal masses (unforced)

The switching functions therefore are:

$$\begin{aligned} s_1 &= \frac{\lambda_{n+1}}{m_1} \\ s_i &= (x_{i-1} - x_i)\left(\frac{\lambda_{n+i}}{m_i} - \frac{\lambda_{n+i-1}}{m_{i-1}}\right) \qquad\qquad i \in \{2, ..., n\} \end{aligned} \tag{4.73}$$

A closer look at (4.73) reveals, if all masses are equal, the assumption from the 2 DoF system is even valid for n DoF systems:
Switchings of the stiffness controls occur as soon as the deflection of the (real) mechanical system is zero or the one of the dual system (see Figure 4.12) for the corresponding spring. By introducing a transform $\hat{\lambda} = M^{-1}\tilde{\lambda}$, the difference of $\hat{\lambda}_i - \hat{\lambda}_{i-1}$ corresponds to a switching for arbitrary masses even if they are not equal. The system becomes

$$M\ddot{\hat{\lambda}} + KM\hat{\lambda} = 0. \tag{4.74}$$

However, this is a virtual system and not a mechanical system anymore due to fact that the units are transformed as well. A zero deflection $\hat{\lambda}_i - \hat{\lambda}_{i-1}$ of the virtual system or a zero deflection in $x_{i-1} - x_i$ then causes a switching in the stiffness control u_i.

4.4 Comparison

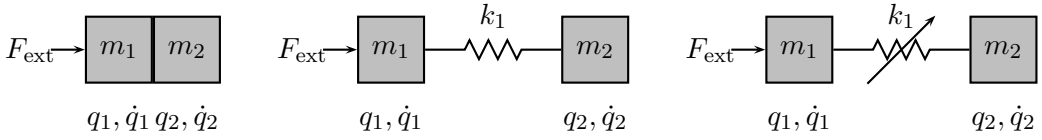

Figure 4.13: From left to right: Rigid, constant stiffness and variable stiffness mass spring systems with 2 masses.

After discussing some properties of mass spring systems with constant and variable stiffness, they will subsequently be compared to each other. In addition to the two mentioned systems, a rigid robot is emulated by directly connecting the masses (or motor and link so to say) without any spring at all (see Figure 4.13). For the rigid case, the velocity is readily found by integration of *Newton's second law*

$$F_{\text{ext}} = m \cdot a \Rightarrow a = \frac{F_{\text{ext}}}{m} \Rightarrow v_{\text{rigid}} = \int_{t_0}^{t} \frac{F_{\text{ext}}}{m} d\xi + \underbrace{v_0}_{=0} = \frac{F_{\text{ext}}}{m} t \tag{4.75}$$

The maximal deviation between the velocity of the last mass of the rigid system and the

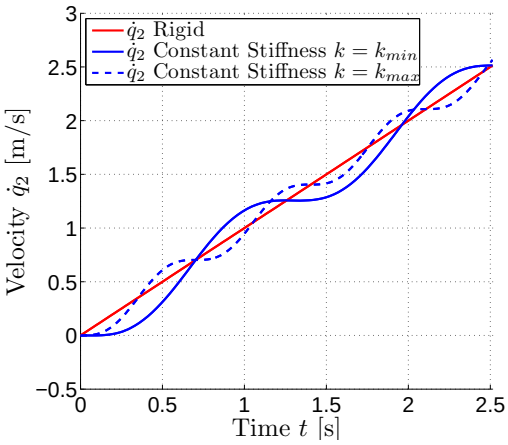

(a) Comparison of rigid and constant stiffness

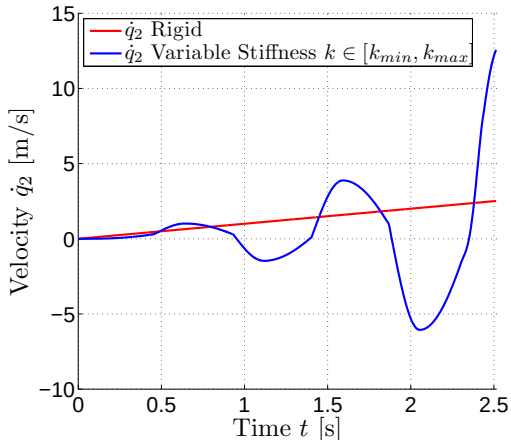

(b) Comparison of rigid and variable stiffness

Figure 4.14: Comparing the velocity of the three cases for a fixed end time.

constant system can then be calculated with (4.10) and (4.75)

$$\begin{aligned} d_{\max} &= |v_{\text{constant}} - v_{\text{rigid}}| = |-\frac{u_{\max}}{\omega(m_1+m_2)}\sin(\omega t) + \frac{u_{\max}}{m_1+m_2}t - \frac{u_{\max}}{m_1+m_2}t| \\ &= |-\frac{u_{\max}}{\omega(m_1+m_2)}\sin(\omega t)| = \underbrace{|-1|}_{=1}|\underbrace{\frac{u_{\max}}{\omega(m_1+m_2)}}_{>0}| \cdot |\underbrace{\sin(\omega t)}_{\leq 1}| \leq \frac{u_{\max}}{\omega(m_1+m_2)} \qquad (4.76) \\ &= \text{const.} \end{aligned}$$

In the constant stiffness, case the eigenfrequeny ω is constant as well and so the maximal deviation is bounded. This means the velocity of the final mass in the constant stiffness case is oscillating around the one of the rigid case

$$v_{\text{rigid}} - d_{\max} \leq v_{\text{constant}} \leq v_{\text{rigid}} + d_{\max}. \qquad (4.77)$$

The deviation decreases with increasing eigenfrequency but higher oscillations occur (see e.g. Figure 4.14(a) for two different constant stiffness cases) and for $\omega \to \infty \Rightarrow d_{\max} = 0$ the constant stiffness case converges to the rigid one as one would expect. For the variable stiffness case there happens a built up that seems to grow beyond any fixed boundary with increasing time. The end velocity is not strictly monotonic increasing anymore but zero crossing instead.

If the control domain $\mathcal{U}_2 \in [u_{2,\min}, u_{2,\max}]$ degenerates to a point it would obviously yield the case of constant stiffness and the maximum achievable velocity would be equal or less than $\frac{F_{\text{ext}}}{m}t_f + d_{\max}$ [m/s] in the given time span[8]. This leads in a natural way to the question of how much effect is taken by shrinking/expanding the control domain.
In the sequel, two variants are considered where one expands from $u_{2,\min}$ and the other from $u_{2,\max}$.

1. $\mathcal{U}_{L2}(\gamma) = [u_{2,\min}, u_{2,\min} + \gamma(u_{2,\max} - u_{2,\min})]$

[8] In Figure 4.14(a) the end velocities seem to be almost identical, this is a mere coincidence and not true in general.

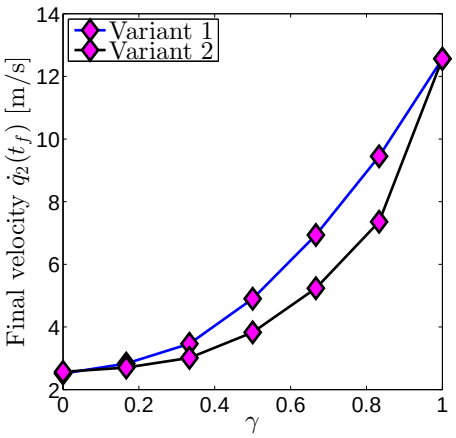

(a) Expansion of the control domain.

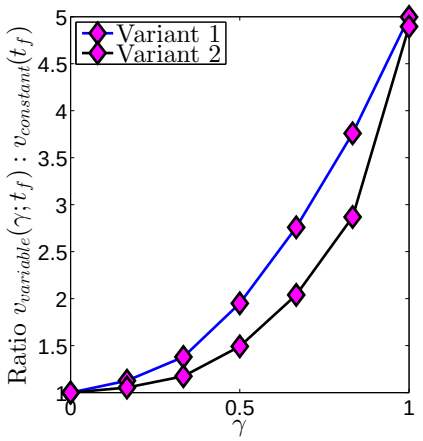

(b) Ratio variable vs. constant stiffness

Figure 4.15: Left: Comparing the end velocity of the two variants for a fixed end time. Although the end velocities appear identical for $\gamma = 0$ this is not the case and is due to scaling. Right: The ratio of the variable stiffness mass spring system end velocity and the constant stiffness one is depicted. For $\gamma = 0$ the variable and constant stiffness systems collaps to the same system and the ratio is 1.

2. $\mathcal{U}_{R2}(\gamma) = [u_{2,\max} + \gamma(u_{2,\min} - u_{2,\max}), u_{2,\max}]$

The percentual factor $\gamma \in [0, 1]$ indicates how much the domain is expanded, i.e. $\gamma = 0$ % corresponds to one of the constant stiffness cases (depending on the chosen variant) and $\gamma = 100$ % to the (full domain) variable stiffness case. Figure 4.15(a) depicts the end velocity of the last mass with respect to the size of the control domain $\mathcal{U}_{L2}(\gamma)$ and $\mathcal{U}_{R2}(\gamma)$. As expected, both variants end up with the end velocity of the constant stiffness cases and the variable stiffness case for $\gamma = 0$ % and $\gamma = 100$ %, respectively (cf. Figure 4.14). Furthermore, with the expansion of the control domain, the corresponding end velocity of the last mass increases immensely. In Figure 4.15(b) the ratio between the constant stiffness end velocity and the end velocity of the variable stiffness case is shown with respect to the modified control domain. It ends at a factor 5 between the two cases.
The fact that variable stiffness is so much faster can be assigned to the idealized assumption that the stiffness can be adjusted directly, so it is possible to pump potential energy instantaneously into the system. At a control switch t_1, the increase/decrease in potential energy is given by $\pm\frac{1}{2}(k_{\max} - k_{\min})\varphi^2(t_1)$. Due to the lack of constraints, this instantaneous increase is not bounded by any means. The surplus of energy can be calcutated as difference between the total energy at final time of the constant stiffness robot

$$E_{\text{const}} = U_{\text{const}} + T_{\text{const}} = \sum_{i=1}^{n-1} \frac{1}{2} k_i \varphi_i^2(t_f) + \sum_{l=1}^{n} \frac{1}{2} m_l \dot{q}_l^2(t_f) \tag{4.78}$$

and the variable stiffness robot[9]

$$\begin{aligned}
E_{\text{var}} &= U_{\text{variable}} + T_{\text{variable}} \\
&= \int_{\varphi(t_0)}^{\varphi(t_f)} k\varphi(t)d\varphi + \sum_{l=1}^{n} \frac{1}{2} m_l \dot{q}_l(t_f) = \int_{t_0}^{t_f} k\varphi(t)\dot{\varphi}(t)dt + \sum_{l=1}^{n} \frac{1}{2} m_l \dot{q}_l^2(t_f) \\
&= \int_{t_0}^{t_1^-} k\varphi(t)\dot{\varphi}(t)dt + \sum_{i=1}^{j-1} \int_{t_i^+}^{t_{i+1}^-} k\varphi(t)\dot{\varphi}(t)dt + \int_{t_j^+}^{t_f} k\varphi(t)\dot{\varphi}(t)dt + \sum_{l=1}^{n} \frac{1}{2} m_l \dot{q}_l^2(t_f) \\
&= \frac{1}{2}\left[-k_{\min}\varphi^2(t_0) + \sum_{i=1}^{j-1} (-1)^i (k_{\min} - k_{\max})\varphi^2(t_i) + k_{\max}\varphi^2(t_f) \right] + \sum_{l=1}^{n} \frac{1}{2} m_l \dot{q}_l^2(t_f),
\end{aligned} \tag{4.79}$$

where j denotes the number of switches. For this specific example here $j = 5$ (see Figure 4.11(b)) and $n = 2$ (Variant 1 chosen due to vanishing deflection at final time) the difference in energy at final time results in

$$\triangle E = |E_{\text{variable}} - E_{\text{const}}| = |144.1463 - 12.5000| = 131.6463. \tag{4.80}$$

Although one could think of mechanical realizations where the stiffness changes rapidly, e.g. if two masses are connected by two springs and one is detached by pulling a bolt, a gradual change of the stiffness is not very likely realizable without additional mechanism as it would require to change and control the material properties themselves as desired. Usually, there is a mechanical mechanism involving a motor (see Chapter 2.5) behind the stiffness actuation and the energy that can be brought into the system is limited. To keep the comparison fair, the energy will now be constrained so that the same amount of energy is used by both systems at the final time. This can be expressed mathematically as a condition at final time[10] for the variable stiffness case as

$$\frac{1}{2} k_{\max}\varphi^2(t_f) + \frac{1}{2} m_1 x_3^2(t_f) + \frac{1}{2} m_2 x_4^2(t_f) = E_{\text{const}}. \tag{4.81}$$

The optimal control problem is then solved again along with the new condition. Figure 4.16 depicts the velocities of both masses for the constant stiffness case (left) and the variable stiffness case with the energetic constraint (right). It is surprising that the variable stiffness mass spring system is still more optimal, although both systems consume the same energy. While the last mass is not a factor 5 times faster as previously (see Figure 4.15(b)), it still exceeds the velocity of the constant stiffness case by a factor ≈ 1.4. How can this be interpreted? Bilinear system have the beneficial property that they are more controllable than linear systems and therefore offer a better performance overall [74]. Due to the additional control it is possible to minimize the kinetic energy that dissipates into the first mass by adjusting the stiffness accordingly. In Figure 4.16(b) it can be seen that the velocity of the first mass could be decelerated to zero, whereas in the constant stiffness case the first mass still moves with 2.46 [m/s] due to the inability of the system to somehow divide the energy between the two masses. For both cases, the deflection (not depicted) is almost zero at final time and hence the potential energy that contributes to the total amount of energy at final time is negligible.

[9] The fact that the stiffness is constant a.e. is exploited for the subsequent calculation.

[10] It has been shown in Chapter 4.3 that both controls are at their upper boundary at final time, therefore $u_2(t_f) = k_{\max}$.

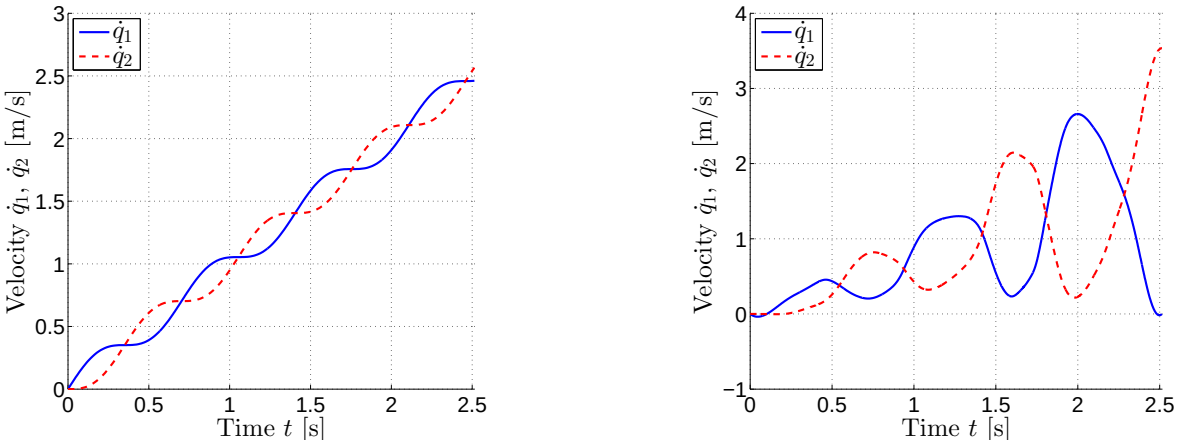

Figure 4.16: Comparing the constant stiffness case with the variable stiffness case and the additional constraint.

Chapter 5

Nonlinear Dynamics

In the previous chapter, mass spring systems interconnected by springs with constant and variable stiffness were analyzed. For the constant stiffness, the dynamics were linear and for variable stiffness bilinear, which is a type of "weak" nonlinearity. In this chapter, (fully) nonlinear dynamics are analyzed. The nonlinearity results from the consideration of gravity and nonlinear effects due to the inertial coupling, when the masses (more precisely the links) are allowed to move in more than one dimension.

5.1 Single Pendulum

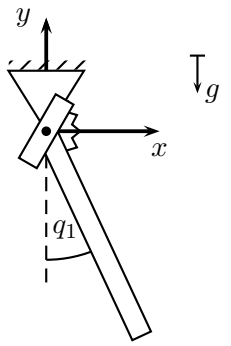

Figure 5.1: Elastic single pendulum

First, an elastic single pendulum will be considered. The motor is connected via a spring to the link and the gravitational force points in $-y$ direction, see Figure 5.1. Similar to the example of Chapter 2, the equations of motion can be derived with the *Lagrange* equations of the second kind. The only difference here is that the center of gravity is assumed to be in the middle of the link and the inertia is taken into account for both the motor and the link, i.e. for the inertia tensor $I \not\equiv 0$. The moments of inertia can be obtained from modeling the link as thin rods and the motors as solid disks. For the link with rotation axis through the tip, this yields with the well-known formula and the axis parallel theorem $I_{zz1} = \frac{1}{3} m_1 l_1^2$, with m_1 and l_1 being the link mass and length and for the motor with rotation axis in the

center of mass $b_1 = \frac{1}{2} m_m l_m^2 i_g^2$, with motor mass m_m, rotor length l_m and gear ratio i_g. The gear ratio term is necessary because the link-side inertia is of interest. The dynamics for the elastic single pendulum are then obtained as

$$\begin{aligned} \underbrace{\left(\frac{1}{4} m_1 l_1^2 + I_{zz1}\right)}_{=:m_{11}} \ddot{q}_1 + \underbrace{\frac{1}{2} m_1 l_1 g \sin(q_1)}_{=:g(q)} - k_1(\theta_1 - q_1) = 0 \\ b_1 \ddot{\theta}_1 + k_1(\theta_1 - q_1) = \tau_m, \end{aligned} \tag{5.1}$$

where q_1 and θ_1 are link and motor positions, k_1 the joint stiffness constant, g the gravity constant and $u = \tau_m$ the motor torque that serves as control input. Due to constant link and motor inertia matrices (here: scalars), the only difference to the previously examined mass spring system is the sine term arising due to gravity. Therefore, for small q_1, the solution is expected to be similar to previously formulated statements.

Similar to the previous chapter, maximizing the link velocity at final time is expressed via the cost function

$$J = -\dot{q}_1(t_f) \rightarrow \min! \tag{5.2}$$

and the well-known control constraint is

$$-u_{\max} \leq u \leq u_{\max}. \tag{5.3}$$

In Chapter 4.2, it could be observed that three cases occur if a spring deflection constraint is imposed on the 2 DoF mass spring system. Since the third case was analyzed in more detail, a small deflection bound is intentionally chosen here to invoke this case as well. The spring deflection is defined as $\varphi_1 := \theta_1 - q_1$ and the corresponding (symmetric) constraint is

$$-\varphi_{\max} \leq \varphi \leq \varphi_{\max}. \tag{5.4}$$

In Chapter 4.2, the boundary control u_b was calculated in two different ways. First, by physical reasoning and secondly by means of optimal control. Choosing the latter here as well, the state constraint $\varphi \leq \varphi_{\max}$ is still of second order $n_q = 2$ and solving (3.52b) for u_b yields

$$u_b^+(t) = b_1 \left(\frac{k_1}{b_1} + \frac{k_1}{m_{11}}\right) \varphi_{\max} - \underbrace{\frac{b_1}{m_{11}}}_{=:R} \underbrace{\frac{1}{2} m_1 l_1 g \sin(q(t))}_{=g(q)} \tag{5.5}$$

For $g = 0$, this is equivalent to (4.37) and the boundary control is constant, see also the examples in Figures 4.6(f) and 4.8(c). However, taking gravity into account, (5.5) shows that the boundary control is influenced by a new term depending on the link position, which makes it non-constant. In fact, the new term is just the gravitational force vector times the inertial ratio R. In Chapter 4, it was sufficient to consider only an upper bound $\varphi \leq \varphi_{\max}$. However, for the nonlinear elastic single pendulum, upswinging motions can occur and both constraint boundaries need to be considered. It is straightforward to calculate the boundary control for $\varphi \geq -\varphi_{\max}$, which yields

$$u_b^-(t) = -b_1 \left(\frac{k_1}{b_1} + \frac{k_1}{m_{11}}\right) \varphi_{\max} - \underbrace{\frac{b_1}{m_{11}}}_{=R} \underbrace{\frac{1}{2} m_1 l_1 g \sin(q(t))}_{=g(q)} \tag{5.6}$$

The optimal boundary control must lie within the following boundaries

$$\pm b_1 \left(\frac{k_1}{b_1} + \frac{k_1}{m_{11}} \right) \varphi_{\max} - \underbrace{\frac{b_1}{2m_{11}} m_1 l_1 g}_{>0} \leq u_b^{\pm}(t) \leq \pm b_1 \left(\frac{k_1}{b_1} + \frac{k_1}{m_{11}} \right) \varphi_{\max} + \underbrace{\frac{b_1}{2m_{11}} m_1 l_1 g}_{>0} \quad (5.7)$$

as well as the control constraint (5.3)

$$-u_{\max} \leq u_b^{\pm}(t) \leq u_{\max} \quad (5.8)$$

Figure 5.2 depicts the numerical solution of the optimal control problem (5.1)-(5.4) with initial values $(q_0, \dot{q}_0, \theta_0, \dot{\theta}_0) = (0, 0, 0, 0)$, $t_f = 0.65$ [s], $\varphi_{\max} = 2$ [°] and $u_{\max} = 70$ [Nm]. The remaining values for the elastic single pendulum can be found in Table B.1 in Appendix B. The usual numerical fluctuations for the control around switching times and at final time can be observed as in Chapter 4, here amplified due to the nonlinearity. The analytic expressions u_b^+ and u_b^- of equations (5.5) and (5.6) are plotted in Figure 5.2(b) and comply with the numerical solution of the controls at the deflection boundary.

The switching structure is fairly similar to the 2 DoF mass spring system of Chapter 4.2. There, two switchings were needed to get to a state with maximal deflection which was being held until final time. Here, two control switchings occur to bring the system in a state that reaches maximal negative deflection and afterwards, another two switchings in order to bring the system to a state with maximal positive deflection. Of course, for increasing final time, this switching structure will not always prevail. For greater deflections of the link, the gravity plays an important role and will have significant impact on the solution/switching structure. To maximize link velocity, the gravity can be used intentionally as an accelerating factor and by switching back and forth, an upswinging motion may be optimal in order to minimize the work that otherwise has to be exerted against gravity.

The results for the boundary control from previous calculations and of Chapter 4.2 can be easily extended for higher dimensional robotic systems with elastic joint transmission elements. Consider the reduced flexible joint model of (2.37)

$$\begin{aligned} M(q)\ddot{q} + c(q, \dot{q}) + g(q) + K(q - \theta) &= 0 \\ B\ddot{\theta} + K(\theta - q) &= \tau_m, \end{aligned} \quad (5.9)$$

which also holds for intrinsically compliant robots without stiffness adjusting mechanism. The deflection constraint is assumed to be

$$-\varphi_{\max} \leq \theta - q \leq \varphi_{\max}. \quad (5.10)$$

(5.10) should be understood component-wise, since $\varphi_{\max} \in \mathbb{R}^n$ here. As usual, the motor torque is the control input $u = \tau_m$. Subtracting motor and link accelerations yields

$$\ddot{\theta} - \ddot{q} = B^{-1}u - B^{-1}K(\theta - q) - M^{-1}K(\theta - q) + M^{-1}c(q, \dot{q}) + M^{-1}g(q). \quad (5.11)$$

At a boundary, $\ddot{\theta} - \ddot{q}$ needs to vanish and the boundary control can be calculated for the upper or lower bound with $\varphi = \theta - q = \pm\varphi_{\max}$ respectively, as

$$\Rightarrow B^{-1}u_b^{\pm} - B^{-1}K\underbrace{(\theta - q)}_{\pm\varphi_{\max}} - M^{-1}K\underbrace{(\theta - q)}_{\pm\varphi_{\max}} + M^{-1}c(q, \dot{q}) + M^{-1}g(q) \stackrel{!}{=} 0 \quad (5.12)$$

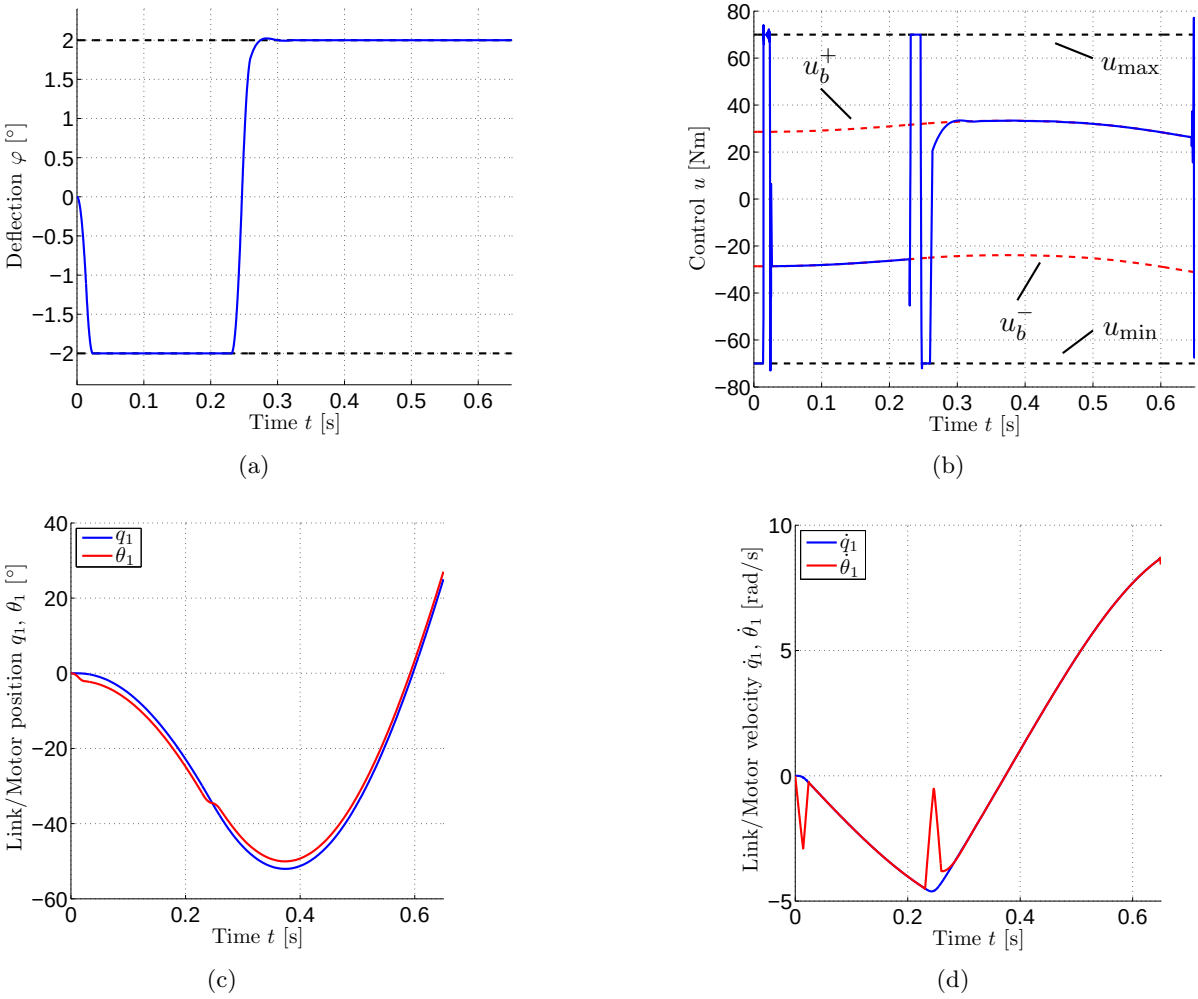

Figure 5.2: Numerical solution for the elastic single pendulum with deflection constraint.

$$\Rightarrow u_b^{\pm}(t) = B(B^{-1}K + M^{-1}(q)K) \cdot (\pm\varphi_{\max}) - BM^{-1}(q)\left(c(q,\dot{q}) + g(q)\right), \tag{5.13}$$

where $\pm\varphi_{\max} = (\pm\varphi_{1\max}, \pm\varphi_{2\max}, ..., \pm\varphi_{n\max})$ is the vector of (mixed) boundary limits which are active at the current time instance, and $R := BM^{-1}$ is the inertial ratio. It shall be noted that formula (5.13) is only valid if the spring deflection is in the limit for every joint, which is of course a special case. The case where only some deflections are in their limits, while others are not, is left for future work.

5.2 Double Pendulum

For the double pendulum, a full set of constraints will be taken into account that is reasonable for real-world applications.

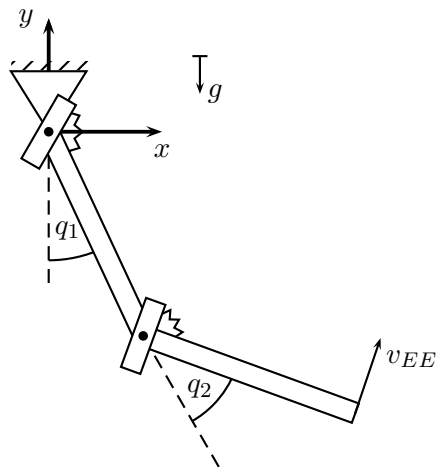

Figure 5.3: Elastic double pendulum

Singular optimal control problem

Here, a different cost function is necessary. Choosing $J = -\dot{q}_2(t_f)$ would lead to unnatural and jerky movements without any further restriction (such as a pre-specified area for the end position of the pendulum). This is due to the fact that maximizing the link velocity for the second link does not imply anything for the first link. This may result in unnatural movements when the first joint is counter reacting with the second link. Therefore, from now on, the goal will be to maximize the end-effector velocity. The end-effector velocity results from kinematic considerations

$$\|v_{EE}\| = \|\frac{d}{dt} r_{EE}\| = \sqrt{l_1^2\dot{q}_1^2 + 2l_1 l_2 \dot{q}_1(\dot{q}_1 + \dot{q}_2)\cos(q_2) + l_2^2(\dot{q}_1 + \dot{q}_2)^2} \tag{5.14}$$

The new cost function then reads as

$$J = -\|v_{EE}(t_f)\| \rightarrow \min! \tag{5.15}$$

Again, the *Lagrange* equations of the second kind yield the dynamics in the subsequent form

$$M\ddot{q} + c(q,\dot{q}) + g(q) - K(\theta - q) = 0 \tag{5.16a}$$

$$B\ddot{\theta} + K(\theta - q) = \tau_m, \tag{5.16b}$$

where $K = diag\{k_1, k_2\}$ is the diagonal positive definite stiffness matrix with constant values. The derivation is straightforward but tedious and will not be displayed. A detailed description of the matrices and vectors of (5.16) can be found in Appendix B. In addition to the control constraints, several state constraints are now considered. Besides the deflection constraint that was already imposed several times before, new constraints on the motor and link position, as well as on the motor velocity, are introduced. The full set of constraints reads as

$$-u_{1\max} \leq u_i \leq u_{1\max} \tag{5.17a}$$

$$-q_{\max} \leq q_i \leq q_{\max} \tag{5.17b}$$

$$-\theta_{\max} \leq \theta_i \leq \theta_{\max} \tag{5.17c}$$

$$-\varphi_{\max} \leq \varphi_i \leq \varphi_{\max} \tag{5.17d}$$

$$-\dot{\theta}_{\max} \leq \dot{\theta}_i \leq \dot{\theta}_{\max}, \tag{5.17e}$$

where $i \in \{1, 2\}$ denotes the number of the corresponding joint.

For numerical examples, the constraint boundaries are chosen as $u_{1\max} = 70$ [Nm], $q_{\max} = 135$ [°], $\theta_{\max} = 120$ [°], $\varphi_{\max} = 15$ [°], $\dot{\theta}_{\max} = 4$ [rad/s]. The remaining numerical values for the elastic double pendulum can be found in Table B.1 in Appendix B. As always, initial state, initial time and end time are fixed and the final state is free. The initial configuration is $(q, \dot{q}, \theta, \dot{\theta}) = (0, 0, 0, 0)^T$ at initial time $t_0 = 0$ [s] and the final time is chosen as $t_f = 0.2$ [s].

For the numerical solver *GPOPS*, the dynamics are brought into first-order form $\dot{x} = f(x, u)$ by introducing the control $u = \tau_m$ and state vector as $x = (q, \dot{q}, \theta, \dot{\theta})^T$. Also, the first derivative of the right-hand side of the first-order dynamics w.r.t. the states and controls is calculated with the computer algebra system *MAPLE* and passed on to the software. Overall, this improves solution accuracy and calculation speed significantly.

For the variable stiffness case, the dynamics (5.16) change only marginally. The stiffness matrix K is replaced with $K(u) = diag\{u_3, u_4\}$, where u_3 and u_4 are the additional control variables that are able to directly change the stiffness. The corresponding constraints for the stiffness controls are

$$u_{2\min} \leq u_{1/2} \leq u_{2\max}, \tag{5.18}$$

with the numerical values $u_{2\min} = 400$ [Nm/rad] and $u_{2\max} = 800$ [Nm/rad] for the subsequent examples[1].

Figures 5.4 and 5.5 depict the numerical solutions of the optimization problems for the constant stiffness case (5.15)-(5.17) and the variable stiffness case ($K = K(u)$) (5.15)-(5.18) with the additional initial/end conditions, respectively.

Following observations can be made

[1]This is a simplification because for real-world robotic systems as the HASy, the stiffness can not be controlled directly. There, a stiffness adjusting mechanism is prevalent which needs its own dynamic modeling, cf. Chapter 2.5.

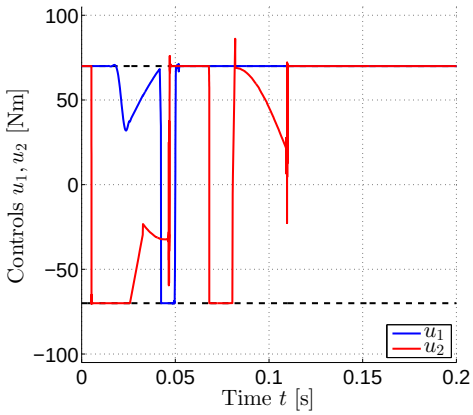

(a) Torque Controls

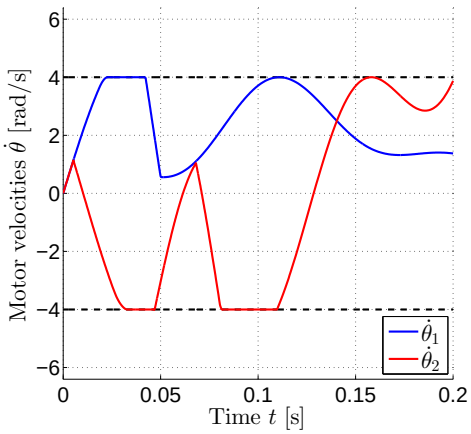

(b) Motor Velocities

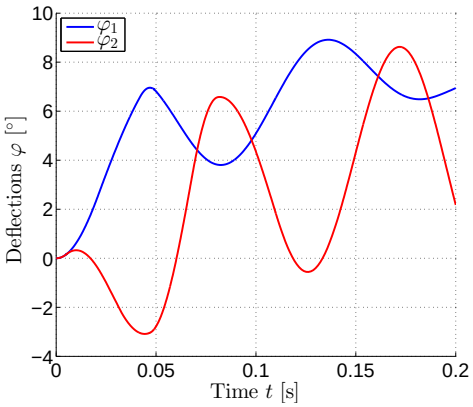

(c) Deflections

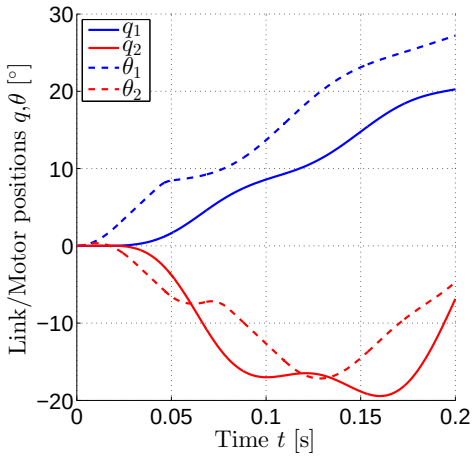

(d) Link and Motor Positions

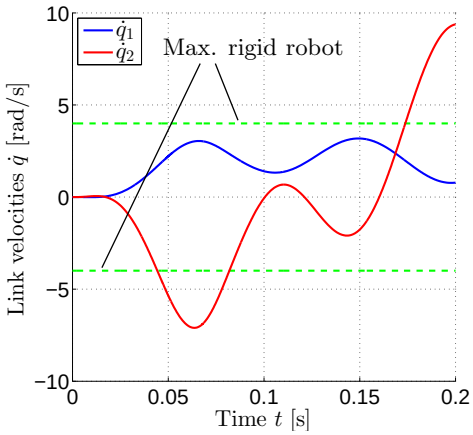

(e) Link Velocities

Figure 5.4: Solution of the optimal control problem for the elastic double pendulum with constant stiffness.

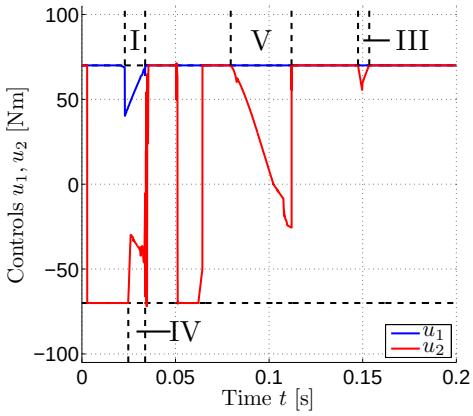

(a) Torque Controls

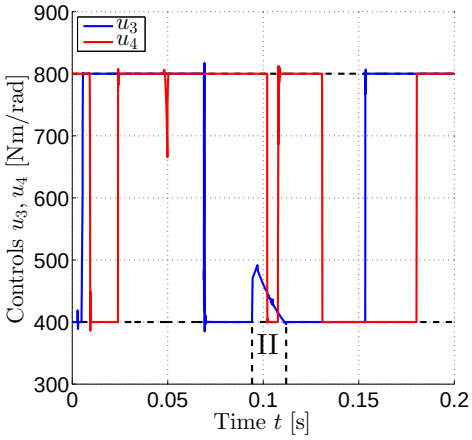

(b) Stiffness Controls

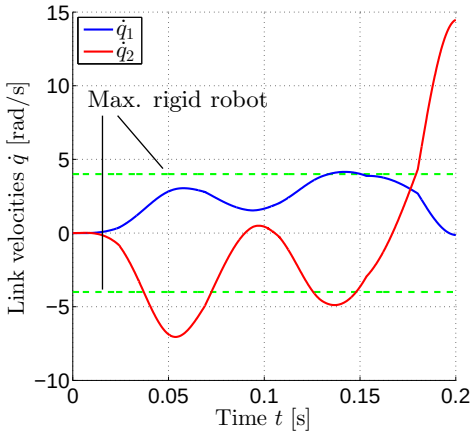

(c) Link velocities

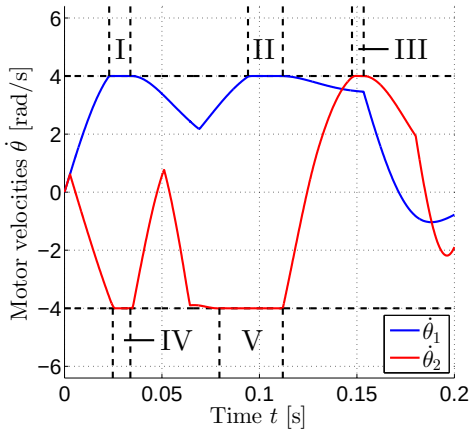

(d) Motor Velocities

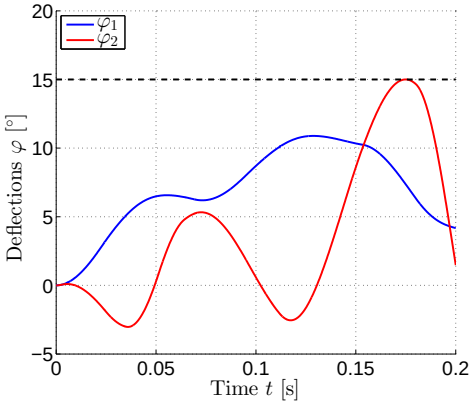

(e) Deflections

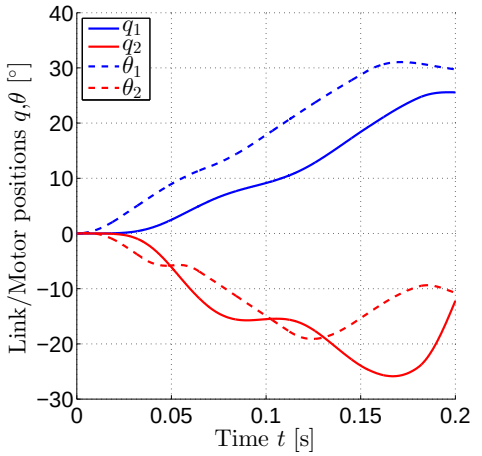

(f) Link and Motor Positions

Figure 5.5: Solution of the optimal control problem for the elastic double pendulum with variable stiffness.

- For a rigid robot, the maximal link velocity equals the maximal motor velocity due to the stiff coupling. In Figures 5.4(e) and 5.5(c) the maximal link velocity for a rigid robot is indicated by a green dashed line. For the case of constant as well as variable stiffness, this velocity is exceeded by far.

- Figure 5.6 shows the end-effector velocity for the constant and variable stiffness case. At final time, the end-effector velocity for the variable stiffness case is 30% faster than the end-effector velocity for the constant stiffness case. For a rigid robot, the maximal end-effector velocity would be $v_{\text{rigid,EE}} = \dot{q}_{\max}(l_1 + l_2) = \dot{\theta}_{\max}(l_1 + l_2) = 3.64$ [m/s].

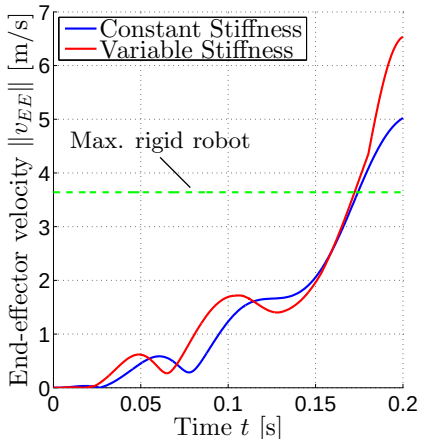

Figure 5.6: End-effector velocity of the actuated double pendulum with variable and constant stiffness transmission elements.

- The bang-boundary-bang structure is clearly observable, see Figures 5.4(a), 5.5(a) and 5.5(b). Apparently, no singular arcs occur, i.e. for every part in the control which is non-constant, there is a corresponding boundary arc in the state constraints. For example, in the variable stiffness case, there are five boundary arcs which occur due to the constraint in the motor velocity, see Figure 5.5(d) segments I-V. Two times, the maximum motor velocity is reached for the first motor, which then invokes a boundary control for the torque input (Figure 5.5(a), segment I) and a boundary control for the stiffness adjusting input (Figure 5.5(b), segment II). For the second motor velocity, there are three boundary arcs which all lead to a boundary torque control, cf. segments III-V in Figures 5.5(a) and 5.5(d). The same can be observed for the constant stiffness case, where three boundary arcs occur, see Figures 5.4(a) and 5.4(b).

- Here, the crucial constraint seems to be the motor velocity. Since the torque inputs are always at their maximum value, the motor velocities are rapidly brought to their limits. Due to the relatively short final time, the other state constraints do not seem to play an important role. For larger values of the final time, the system will obviously be brought into more of its limitations. To an extent, this already becomes apparent for the deflection in the variable stiffness case. In Figure 5.5(e), it can be seen that the deflection touches the constraint. However, since a touch point can be seen as a boundary arc of length zero, the control is still constant before and after the touch point.

- None of the state constraints are violated and all kept within their boundaries. For the control constraint, however, there are overshoots that occur in transitions between the constituent arcs. This phenomenon has already been observed a couple of times in this thesis. It is a well-known problem in pseudospectral methods [60]. The reason therefore is the placement of the LGR collocation points in pseudospectral methods. In general, there is no a-priori knowledge about the switching times that cause the discontinuities in the control. As mentioned in Chapter 3.5, by placing the mesh points at locations of nonsmoothness, the solution accuracy can be improved immensely. Unfortunately, the option to manually place mesh points at critical points is not supported yet.

Double pendulum with regularization term in the cost functional

For real-world applications, the controls should not violate their boundaries and the change in the slope should be bounded by a constant given by the dynamics. This enables the motor to track the desired trajectory. Since jumps are critical for the numerical calculations, a well-known trick in optimal control is to add a *Lagrange* term[2] $\int_{t_0}^{t_f} \varepsilon_r u^2 dt$ to the cost functional in order to smooth out discontinuous control trajectories. According to Chapter 3.2, the *Hamiltonian* for control-affine dynamics becomes

$$H = \varepsilon_r u^2 + \lambda^T f(x,u) = \varepsilon_r u^2 + \lambda^T f_1(x)u + \lambda^T f_2(x) \tag{5.19}$$

and the *Hessian* results in $H_{uu} = diag\{2\varepsilon_r, ..., 2\varepsilon_r\}$, which is regular for $\varepsilon_r \neq 0$. Henceforth, ε_r will be called regularization factor. Whereas the control could be discontinuous at transitions from the constituent arcs (bang, boundary or singular) before, the continuity of the control is guaranteed now [81]. The new cost functional for the constant stiffness case becomes

$$J_{r_1} = -\|v_{EE}(t_f)\| + \int_{t_0}^{t_f} \varepsilon_{r_1}(u_1^2 + u_2^2)dt \tag{5.20}$$

and for the variable stiffness case

$$J_{r_2} = -\|v_{EE}(t_f)\| + \int_{t_0}^{t_f} \varepsilon_{r_1}(u_1^2 + u_2^2) + \varepsilon_{r_2}(u_3^2 + u_4^2)dt \tag{5.21}$$

Again, solving the same optimal control problems for the constant stiffness (5.16)-(5.17), (5.20) and for the variable stiffness case ($K = K(u)$) (5.16)-(5.18),(5.21) as before with the new cost functionals leads to the solutions depicted in Figures 5.7 and 5.8. The regularization factors are chosen as $\varepsilon_{r_1} = 10^{-3}$ and $\varepsilon_{r_2} = 10^{-5}$.

The most noticeable difference is of course the continuity of the control. As a consequence, the undesired overshoot in the control is avoided, which makes this approach accessible for real-world applications. However, due to the new cost functional term, the descriptive bang-boundary-bang structure is lost here. The link velocities still exceed the link velocities of a rigid robot by far, see Figures 5.7(e) and 5.8(c). The end-effector velocities are depicted in Table 5.1 and one can see that variable stiffness is still superior to constant stiffness with

[2]The subsequent squared notation of a vector here is of course a shorthand for the dot product and serves visualization purposes.

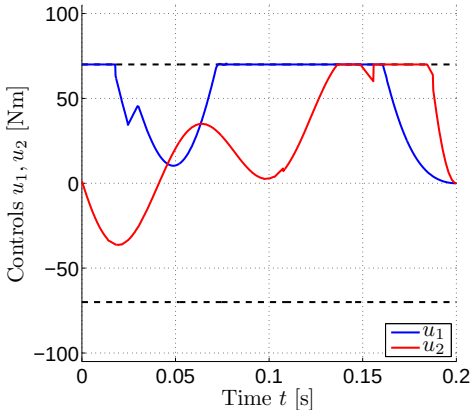

(a) Torque Controls

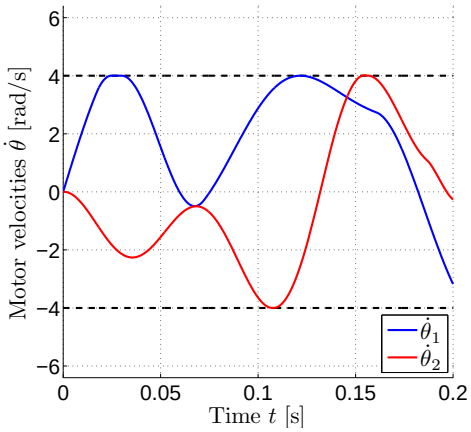

(b) Motor Velocities

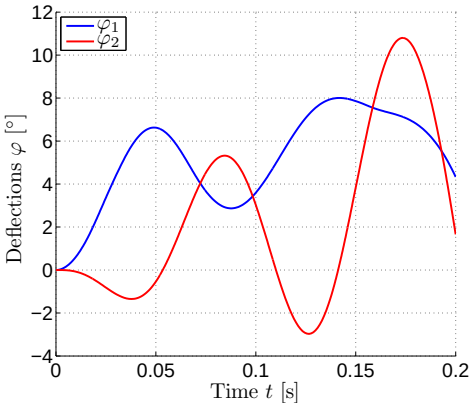

(c) Deflections

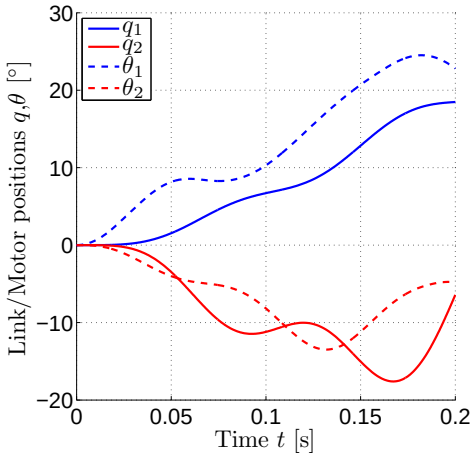

(d) Link and Motor Positions

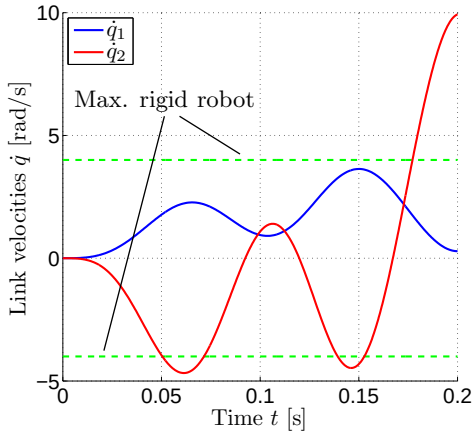

(e) Link Velocities

Figure 5.7: Solution of the optimal control problem for the elastic double pendulum with constant stiffness and regularization factor.

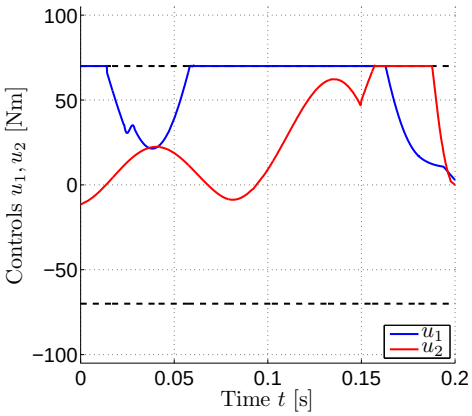

(a) Torque Controls

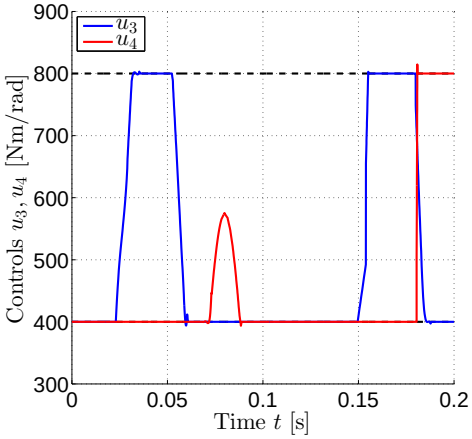

(b) Stiffness Controls

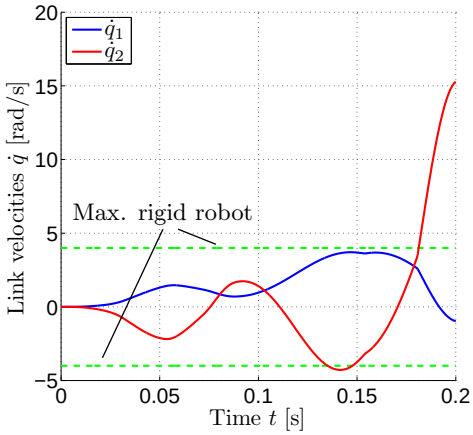

(c) Link velocities

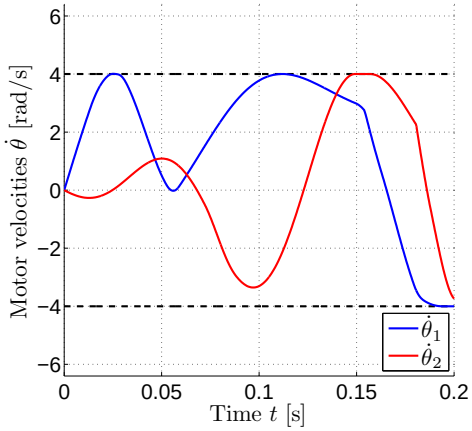

(d) Motor Velocities

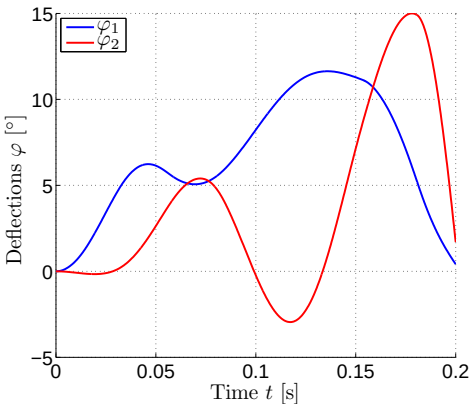

(e) Deflections

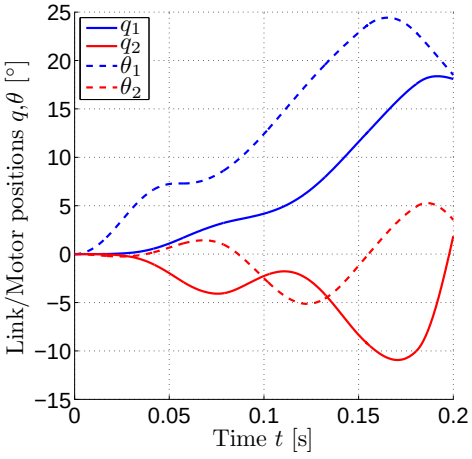

(f) Link and Motor Positions

Figure 5.8: Solution of the optimal control problem for the elastic double pendulum with variable stiffness and regularization factors in the cost functional.

	Constant Stiffness $\|v_{EE}(t_f)\|$	Variable Stiffness $\|v_{EE}(t_f)\|$	Velocity gain
Singular	5.0241 [m/s]	6.5359 [m/s]	30.09 %
Regularized	4.8266 [m/s]	6.1460 [m/s]	27.34 %

Table 5.1: End-effector velocities at final time for the constant and variable stiffness case as well as different cost functionals.

a velocity gain of 27 %. Furthermore, one can extract the unsurprising fact that the final velocities are both lower than for the singular optimal control case.

Since there are small overshoots in the stiffness control, see Figure 5.8, one could think of increasing the second regularization factor ε_{r_2}. This leads in a natural way of asking how much impact the regularization factors will have with respect to the achievable performance.

Figure 5.9 depicts the dependencies of the end-effector velocity on the regularization factors for the constant and variable stiffness case. In the constant stiffness case, a rapid decline of the end-effector velocity can be seen, see Figure 5.9(a). For the variable stiffness case, the performance seems to be more prone to the stiffness regularization term ε_{r_2}, while ε_{r_1} affects it less as opposed to the constant stiffness case. Therefore, it is advised to rather lower the boundaries for the maximal allowed stiffness rather than increasing ε_{r_2}.

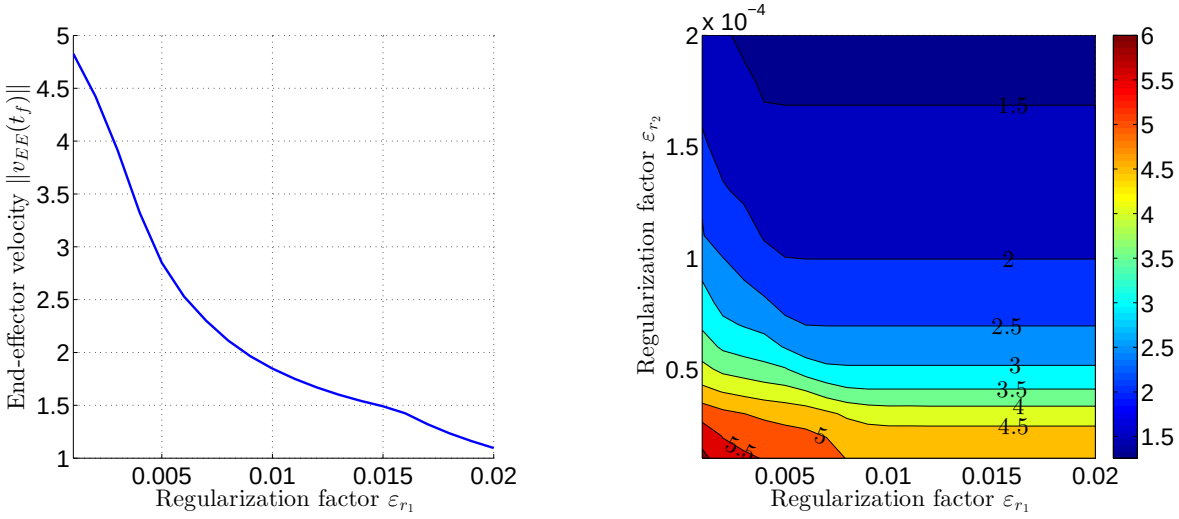

(a) Case of constant stiffness

(b) Case of variable stiffness

Figure 5.9: Dependencies of the end-effector velocity at final time on different regularization factors.

Chapter 6

Conclusion and Outlook

This thesis aimed at investigating multibody robotic systems that have elastic transmission elements with the objective to maximize the velocity of the final mass/the last link. Furthermore, the impacts of variable stiffness actuation with regard to performance were examined and compared to the performance of rigid and elastic systems.

For a well-defined problem formulation, control constraints and a fixed final time are at least necessary. Later on, for a more realistic approach, state constraints were imposed as well. The most important one is the spring deflection constraint, which should not be violated for intrinsically compliant robots and therefore plays an important role throughout the thesis.

Mass spring systems with torque input (with or without stiffness adjusting property) can be regarded as simplified models for intrinsically compliant robots. Hence, it was reasonable to examine those systems first to gain a basic understanding of the underlying behavior of this class of robots. Subsequently, it has been analyzed to what extent the found results can be transferred to intrinsically compliant robots that exhibit nonlinear dynamics.

Since the control will enter linearly for rigid and intrinsically compliant robots, a large class of cost functions leads to singular optimal control problems. The inherent numerical problems that arise for the control have been tackled as follows. For a subcase, an approach via energetic considerations has been chosen to find the switching times numerically, while the remaining quantities could be retrieved analytically, yielding a solution with high precision. This approach falls under the category of indirect methods. For nonlinear dynamics, a regularization strategy led to smoother control trajectories that are less prone to numerical artifacts using direct methods. Consequently, both strategies nullified the undesired overshoot of the control over its boundaries.

The key results of this thesis can be summarized as

- A 2 DoF mass spring system with constant stiffness and deflection constraint has been analyzed. Depending on the maximal allowed deflection, a distinction between three cases can be made. A focus was laid on the third case, where via an energetic approach the switching times are retrieved numerically. With the theory of optimal control, the remaining quantities could be obtained analytically. The assumed switching structure was verified later on with (direct) numerical methods.

- A similar pattern of the switching structure could be observed for the elastic single pendulum for a (sufficiently) small final time. However, due to gravitational effects, the boundary control is deformed by a nonlinear term. The formula for it could be obtained analytically and was verified by a numerical example. For the generalization of an n DoF intrinsically compliant robot that is at all deflection limits at a time instance, a formula for the boundary control depending on the link positions and velocities could be obtained in a straightforward manner.
- The controllability property for an n DoF mass spring system with constant stiffness and only one force input acting on the first mass has been proven. This has immediate consequences for the control structure of time-optimal control problems, meaning they will be of bang-bang type.
- For the n DoF variable stiffness mass spring system, the switchings of the torque control are induced by zeros in the deflection of the mass spring system or the corresponding virtual system. For equal masses the virtual system degenerates to the dual system of previous works.
- A direct comparison of a 2 DoF mass spring system with either constant, varying stiffness or stiff coupling has led to the observation that the speed of the last mass at final time is the greatest for the variable stiffness case, which speaks in favor for variable stiffness actuation. Moreover, it is rapidly increasing with the expansion of the stiffness control domain. Surprisingly, the last mass for the varying stiffness case was faster at final time as opposed to the constant stiffness case although the same energy consumption was imposed by an additional constraint. This can be accredited to the bilinear nature of the dynamics that allows more controllability over the system.
- For the elastic double pendulum, the link velocity exceeds the link velocity of a rigid robot for both constant and variable stiffness. Furthermore, the end-effector velocity is greater for the variable stiffness than for the constant stiffness, which again speaks in favor for variable stiffness actuation. In order to diminish numerical artifacts and avoid overshooting of the control over the control boundaries, regularization terms were used. It is advised to choose regularization factors carefully, since there is a significant degradation in performance with increasing regularization. For the variable stiffness case, the performance is more prone to the regularization factor that corresponds to the stiffness actuation than the one that corresponds to the torque control.

Although a large variety of different aspects has been considered and analyzed, numerous open issues remain, which shall be treated in future work, such as

- The exclusion of singular arcs for the n DoF mass spring system. For this generalization, an elegant proof without the (tedious) procedure of differentiating and case-by-case analysis would be preferable.
- For the 2 DoF mass spring system with constant stiffness and deflection constraint, the second case has not been covered extensively and only a numerical solution with a direct solver is presented in this thesis. Setting up a TPBVP for the second case requires the treatment of contact points and furthermore the structure is also depending on the final time as opposed to the third case.
- Under idealized assumptions (an instantaneous change in the control is possible), the

controls will be driven to their limits if no state constraints are active. This leads to the consideration of $k \in [0, \infty]$ as a degenerated case. This was excluded in the theoretical analysis of mass spring systems, where it was necessary for analytical results, such as the exclusion of singular arcs. For intrinsically compliant robots, $k = 0$ corresponds to an underactuated robot due to the decoupling of motor and link and $k = \infty$ to a rigid robot due to the stiff coupling. However, since the control domain needs to be closed, $k = \infty$ needs to be treated differently. Therefore, the dynamics should be modeled for each case of $k = \infty \vee 0$ in a joint separately and proper switching between the dynamics needs to be ensured. This leads to the theory of optimal control of hybrid systems.

- Time-optimal control problems with free final time for mass spring systems, or nonlinear robot dynamics with torque input have not yet been discussed thoroughly.
- Similar to the expansion of the control domain in the 2 DoF mass spring systems, one could observe the effects for expanding the control domain for the double pendulum and analyze the limitations of variable stiffness actuation.

Chapter A

Appendix to Chapter Mass Spring Systems

A.1 Analytic Solution for the 2 DoF Mass Spring System with Constant Stiffness

The analytical solution of the states and costates belonging to the boundary value problem (4.3),(4.6),(4.7) with $x_0 = (0,0,0,0)^T$ considered in Chapter 4.1 is displayed subsequently

$$x^* = \begin{pmatrix} -\frac{k_1 u_{\max}}{m_1^2 \omega^4}\cos(\omega t) + \frac{u_{\max}}{\omega^2 m_1}(\frac{k_1}{\omega^2 m_1} + \frac{k_1}{2m_2}t^2) \\ \frac{k_1 u_{\max}}{m_1 m_2 \omega^4}\cos(\omega t) + \frac{u_{\max}}{\omega^2 m_1}(\frac{k_1}{\omega^2 m_1} + \frac{k_1}{2m_2}t^2 - 1) \\ \frac{u_{\max}}{\omega m_1(1+\frac{m_1}{m_2})}\sin(\omega t) + \frac{u_{\max}}{m_1+m_2}t \\ -\frac{u_{\max}}{\omega(m_1+m_2)}\sin(\omega t) + \frac{u_{\max}}{m_1+m_2}t \end{pmatrix}$$

$$\lambda^* = \begin{pmatrix} \frac{k_1}{m_2\omega}\sin(\omega(t-t_f)) \\ -\frac{k_1}{m_2\omega}\sin(\omega(t-t_f)) \\ \frac{m_1}{m_1+m_2}(\cos(\omega(t-t_f)) - 1) \\ -\frac{m_2+m_1\cos(\omega(t-t_f))}{m_1+m_2} \end{pmatrix}$$

A.2 Transformationmatrix for the Modal Analysis

The transformation matrix arising in the course of modal analysis for the 3 DoF mass spring system with constant stiffness in Chapter 4.1 reads as follows

$$Q = \begin{bmatrix} q_{11} & q_{12} & 1 \\ q_{21} & q_{22} & 1 \\ 1 & 1 & 1 \end{bmatrix}$$

where the entries of the matrix are

$$
\begin{aligned}
q_{11} =& \frac{-4k_1(-m_1k_2 + k_1m_3)m_3^2m_2}{(C_2 + C_1 - 2m_3m_1k_2 - 2m_3m_1k_1 - 2m_3k_1m_2)(C_2 + C_1 - 2m_3k_1m_2)} \\
q_{12} =& \frac{-4k_1(-m_1k_2 + k_1m_3)m_3^2m_2}{(-C_2 + C_1 + 2m_3m_1k_2 + 2m_3m_1k_1 + 2m_3k_1m_2)(-C_2 + C_1 + 2m_3k_1m_2)} \\
q_{21} =& \frac{2m_3(-m_1k_2 + k_1m_3)}{C_2 + C_1 - 2m_3m_1k_2 - 2m_3m_1k_1 - 2m_3k_1m_2} \\
q_{22} =& \frac{-2m_3(-m_1k_2 + k_1m_3)}{-C_2 + C_1 + 2m_3m_1k_2 + 2m_3m_1k_1 + 2m_3k_1m_2}
\end{aligned}
$$

with constants C_1, C_2

$$
\begin{aligned}
C_1 :=& (k_2^2m_2^2m_1^2 - 2k_2m_2m_1^2m_3k_1 + 2k_2^2m_2m_1^2m_3 - 2k_2m_2^2m_1k_1m_3 + m_3^2m_1^2k_1^2 \cdots \\
&+ 2m_3^2m_1^2k_1k_2 + 2m_3^2m_1k_1^2m_2 + m_3^2m_1^2k_2^2 - 2m_3^2m_1k_2k_1m_2 + k_1^2m_2^2m_3^2)^{\frac{1}{2}} \\
C_2 :=& m_3k_1m_2 + k_2m_1m_2 + m_3m_1k_2 + m_3m_1k_1
\end{aligned}
$$

A.3 Inductive Proof for the Special Structure of the Controllability Matrix

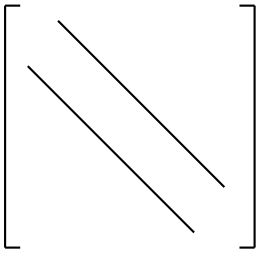

Figure A.1: Structure of the matrix A

For

$$
\begin{aligned}
C &= [b, Ab, A^2b, A^3b, \ldots, A^{m-1}b] \in \mathbb{R}^{m \times m} \\
A &= \text{Tridi}[\underbrace{a_{21}, a_{32}, \ldots}_{\in \mathbb{R}^{m+1}}; \underbrace{0, \ldots, 0}_{\in \mathbb{R}^{m}}; \underbrace{a_{12}, a_{23}, \ldots}_{\in \mathbb{R}^{m+1}}] \\
b &= (b_1, 0, \ldots, 0) \in \mathbb{R}^m
\end{aligned}
$$

the matrix C takes an upper triangular form and the values are displayed in equation (4.33). In order to show that, first the upper triangular form needs to be proven and then the series that describes the diagonal entries.

Proof

(i) Upper triangular
The first column of C is b and therefore zero except the first entry and it is trivial to

see that the second column Ab is zero after the second entry due to the tridiagonal structure of A, the third column $A^2b = A(Ab)$ is zero after the third entry etc.

(*ii*) Proof by induction for diagonal elements:

(a) Initial steps:

The first diagonal element of C is b_1, the second $b_1 \cdot a_{21}$. The first column of A^2 ($i \in \{1, ..., m\}$) can be described by

$$(a^2)_{i1} = \sum_{k=1}^{n} a_{ik} \cdot a_{k1} = a_{i1} \cdot \underbrace{a_{11}}_{=0} + a_{i2} \cdot a_{21} + \underbrace{\sum_{k=3}^{n} a_{ik} \cdot \underbrace{a_{k1}}_{=0}}_{=0} = a_{i2} \cdot a_{21}$$

The third diagonal element of C for $i = 2$ is $(a^2)_{31} = a_{32} \cdot a_{21}$ and therefore, the first column of A^3 ($i \in \{1, ..., m\}$) equals

$$\begin{aligned}(a^3)_{i1} &= \sum_{k=1}^{n} a_{ik} \cdot (a^2)_{k1} = \sum_{k=1}^{n} a_{ik} \cdot (a^2)_{k1} = \sum_{k=1}^{n} a_{ik} \cdot a_{k2} \cdot a_{21} \\ &= \sum_{k=1}^{3} a_{ik} \cdot a_{k2} \cdot a_{21} + \sum_{k=4}^{n} a_{ik} \cdot \underbrace{a_{k2}}_{=0} \cdot a_{21} \\ &= a_{i1} \cdot a_{12} \cdot a_{21} + a_{i2} \cdot \underbrace{a_{22}}_{=0} \cdot a_{21} + a_{i3} \cdot a_{32} \cdot a_{21}\end{aligned}$$

Fourth diagonal element of C for $i = 3$:

$$b_1(a^3)_{41} = b_1 \cdot \underbrace{a_{41}}_{=0} \cdot a_{12} \cdot a_{21} + b_1 \cdot a_{43} \cdot a_{32} \cdot a_{21} = b_1 \cdot a_{43} \cdot a_{32} \cdot a_{21}$$

(b) Inductive assumption:

$$b_1 \cdot (a^i)_{i+1,1} = b_1 \cdot \prod_{k=1}^{i} a_{k+1,k} \qquad \text{for } i \in \{1, ..., m-1\}$$

(c) Inductive step:

$$\begin{aligned}
b_1 \cdot (a^{i+1})_{i+2,1} &= b_1 \sum_{k=1}^{n} a_{l+2,k} \cdot (a^i)_{k1} \\
&= b_1 \sum_{k=1}^{i} \underbrace{a_{i+2,k}}_{=0} \cdot (a^i)_{k1} + b_1 \cdot a_{i+2,i+1} \cdot (a^i)_{i+1,1} \\
&\quad + b_1 \cdot \underbrace{a_{i+2,i+2}}_{=0} \cdot (a^i)_{i+2,1} + b_1 \cdot a_{i+2,i+3} \cdot (a^i)_{i+3,1} \\
&\quad + b_1 \sum_{k=i+4}^{n} \underbrace{a_{l+2,k}}_{=0} \cdot (a^i)_{k1} \\
&= a_{i+2,i+1} \cdot \underbrace{b_1 \cdot (a^i)_{i+1,1}}_{\text{I.A.}} + b_1 \cdot a_{i+2,i+3} \cdot (a^i)_{i+3,1} \\
&= a_{i+2,i+1} \cdot b_1 \cdot \prod_{k=1}^{i} a_{k+1,k} + b_1 \cdot a_{i+2,i+3} \cdot (a^i)_{i+3,1} \\
&= b_1 \cdot \prod_{k=1}^{i+1} a_{k+1,k} + b_1 \cdot a_{i+2,i+3} \cdot \underbrace{(a^i)_{i+3,1}}_{=0} \\
&= b_1 \cdot \prod_{k=1}^{i+1} a_{k+1,k}
\end{aligned}$$

□

⇒ Controllability Matrix upper triangular and diagonal elements are

$$\text{diag}(C) = \{b_1, b_1 \cdot a_{21}, b_1 \cdot a_{21} \cdot a_{32}, \ldots, b_1 \cdot \prod_{k=1}^{m-1} a_{k+1,k}\}$$

	m_1 [kg]	m_2 [kg]	m_3 [kg]	k_1 [N/m]	k_2 [N/m]	$u_{\max}$[N]	t_f [s]
Figure 4.3	2	1.5	0.5	80	25	4	1.5
Figure 4.4	2	2	8	40	10	4	10
Figure 4.6	2	2	-	25	-	4	3
Figure 4.11	2	2	-	[25,80]	-	4	1.2
Figure 4.14	2	2	-	25,80,[25,80]	-	4	2.5133
Figure 4.15	2	2	-	γ, [25,80]	-	4	2.5133
Figure 4.16	2	2	-	80	-	4	2.5133

Table A.1: Numerical values with $u_{\max} = -u_{\min}$

Chapter B

Double Pendulum Dynamics

$$M\ddot{q} + c(q,\dot{q}) + g(q) - \tau_J(q,\theta) = 0$$
$$B\ddot{\theta} + \tau_J(q,\theta) = u$$

$$M(q) = \begin{bmatrix} \frac{1}{4}m_1 l_1^2 + \frac{1}{4}m_2 l_2^2 + J_{zz1} + m_2 l_1^2 + m_2 l_1 l_2 \cos(q_2) + J_{zz2} & \frac{1}{4}m_2 l_2^2 + \frac{1}{2}m_2 l_1 l_2 \cos(q_2) + J_{zz2} \\ \frac{1}{4}m_2 l_2^2 + \frac{1}{2}m_2 l_1 l_2 \cos(q_2) + J_{zz2} & \frac{1}{4}m_2 l_2^2 + J_{zz2} \end{bmatrix}$$

$$c(q,\dot{q}) = \begin{pmatrix} -\frac{1}{2}m_2 l_1 l_2 \sin(q_2)(2\dot{q}_1\dot{q}_2 + \dot{q}_2^2) \\ \frac{1}{2}m_2 l_1 l_2 \dot{q}_1 \sin(q_2) \end{pmatrix}$$

$$g(q) = \begin{pmatrix} \frac{1}{2}m_1 g \sin(q_1) l_1 + m_2 g(\sin(q_1) l_1 + \frac{1}{2}\sin(q_1+q_2) l_2) \\ \frac{1}{2}m_2 g \sin(q_1+q_2) l_2 \end{pmatrix}$$

$$B = \begin{bmatrix} b_1 & 0 \\ 0 & b_2 \end{bmatrix}$$

$$\tau_J = K(\theta - q) = \begin{bmatrix} k_1 & 0 \\ 0 & k_2 \end{bmatrix} (\theta - q)$$

where q are joint angles, $\dot{q}$ angular velocities, θ motor angles and $\dot{\theta}$ motor velocities. The moments of inertia for the links $J_{zzi} = \frac{1}{3}m_i l_i^2$, $i \in \{1,2\}$ and the motors $b_1 = b_2 = \frac{1}{12}m_m l_m^2 i_g^2$ result from the consideration of a thin rod model for both.

Name	Symbol	Value	Unit
Motor mass	m_m	0.24	kg
Link mass	m_1, m_2	7.4,4.1	kg
Rotor length	l_m	0.0204	m
Link length	l_1, l_2	0.45,0.46	m
Gear ratio	i_g	80	-
Gravity constant	g	9.81	m/s^2
Stiffness constant	k_1,k_2	600	Nm/rad

Table B.1: Numerical values for the elastic double pendulum (Properties also used for the elastic single pendulum). Link masses and link lengths chosen according to the human leg [10], which are in the same order of magnitude as the DLR HASy. The motor properties are taken from DLR HASy.

Bibliography

[1] Human anatomy. `http://www.mananatomy.com/`.

[2] Variable Impedance ACTuation systems embodying advanced interaction behaviORS. `http://www.viactors.eu/`.

[3] A. Albu-Schäffer, O. Eiberger, M. Fuchs, M. Grebenstein, S. Haddadin, C. Ott, A. Stemmer, T. Wimböck, S. Wolf, C. Borst, et al. Anthropomorphic soft robotics–from torque control to variable intrinsic compliance. *Robotics Research*, pages 185–207, 2011.

[4] A. Albu-Schäffer, C. Ott, and G. Hirzinger. A unified passivity-based control framework for position, torque and impedance control of flexible joint robots. In *International Journal of Robotics Research, Vol. 26, No. 2*, pages 23–39, 2007.

[5] R. Alexander. Optimum timing of muscle activation for simple models of throwing. *Journal of theoretical biology*, 150(3):349–372, 1991.

[6] B. Andresen, K. H. Hoffmann, J. Nulton, A. Tsirlin, and P. Salamon. Optimal control of the parametric oscillator. In *European Journal of Physics, 32*, 2011.

[7] M. Aronna, J. F. Bonnans, and P. Lotito. Continous time optimal hydrothermal scheduling. In *International Conference on Engineering Optimization*, 2008.

[8] U. Ascher, R. Mattheij, and R. D. Russell. Numerical solution of boundary value problems for differential equations. In *SIAM*, 1988.

[9] J. C. Baez. Lectures on classical mechanics. University of California, 2005.

[10] S.K. Banala and S.K. Agrawal. Gait rehabilitation with an active leg orthosis. ASME, 2005.

[11] V.M. Becerra. Solving complex optimal control problems at no cost with psopt. In *IEEE Multi-conference on Systems and Control*, pages 1391–1396, 2010.

[12] R. Bellman. *Dynamic Programming and Modern Control Theory.* Academic Press, New York, NY, 1965.

[13] D. Benson. *A Gauss Pseudospectral Transcription for Optimal Control.* PhD thesis, Massachusetts Institute of Technology, 2005.

[14] P. Berkmann and H. J. Pesch. Abort landing in windshear: Optimal control problem with third-order state constraint and varied switching structure. In *Journal of Optimization Theory and Applications, 85*, pages 21–57, 1995.

[15] D. Bertsekas. *Dynamic programming and Optimal Control*. Vol. 1, Edition 3, Athena Scientific, Belmont, 2005.

[16] D. Bestle. *Analyse und Optimierung von Mehrkörpersystemen: Grundlagen und rechnergestützte Methoden*. Springer Berlin Heidelberg, 1994.

[17] A. Bicchi and G. Tonietti. Fast and soft-arm tactics [robot arm design]. *Robotics & Automation Magazine, IEEE*, 11(2):22–33, 2004.

[18] D.J. Braun, M. Howard, and S. Vijayakumar. Exploiting variable stiffness in explosive movement tasks. RSS, 2011.

[19] H. Bremer. Höhere Kinetik - Mehrkörpersysteme. Vorlesungsskript Universität Linz, 2007.

[20] S. Breun. *Optimale Steuerung redundanter Roboter auf Mannigfaltigkeiten: Strukturanalyse und numerische Realisierung*. PhD thesis, Technische Universität München, 2007.

[21] A. E. Bryson, W. Denham, and S. E. Dreyfus. Optimal programming problems with inequality constraints I: Necessary conditions for extremal solutions. In *AIAA Journal Vol.1*, pages 2544–2550, 1963.

[22] A. E. Bryson and Y.-C. Ho. *Applied Optimal Control*. Hemisphere Publishing New York, 1975.

[23] R. Bulirsch. Die Mehrzielmethode zur numerischen Lösung von nichtlinearen Randwertproblemen und Aufgaben der optimalen Steuerung. Technical report, Carl-Cranz-Gesellschaft, 1971.

[24] R. Bulirsch, F. Montrone, and H. J. Pesch. Abort landing in the presence of windshear as a minimax optimal control problem part 2: Multiple shooting and homotopy. In *Journal of Optimization Theory and Applications, 70*, pages 223–254, 1991.

[25] R. Callies and R. Rentrop. Optimal control of rigid-link manipulators by indirect methods. In *GAMM-Mitt. 31, No.1*, pages 27–58, 2008.

[26] C. Canuto, M.Y. Hussaini, A. Quarteroni, and T.A. Zang. *Spectral Methods in Fluid Dynamics*. Springer-Verlag, New York, 1988.

[27] F. Carpi, R. Kornbluh, P. Sommer-Larsen, and G. Alici. Electroactive polymer actuators as artificial muscles: are they ready for bioinspired applications? In *Bioinspiration and Biomimetics*, 2011.

[28] H. Chaudhary and S. K. Saha. *Dynamics and Balacing of Multibody Systems*. Lecture Notes in Applied and Computational Mechanics. Springer Berlin Heidelberg, 2008.

[29] C. Chou and B. Hannaford. Measurement and modeling of mckibben pneumatic artificial muscles. In *IEEE Transactions on Robotics and Automation, no. 12*, pages 90–102, 1996.

[30] J. J. Craig. *Introduction to Robotics: Mechanics and Control*. Third Edition. Pearson Prentice Hall, 2005.

[31] C. L. Darby, D. Garg, and A. V. Rao. Costate estimation using multiple-interval pseudospectral methods. In *AIAA: Journal of Spacecraft and Rockets, Vol. 48, No. 5*, pages 856–866, 2011.

[32] C. L. Darby, W. H. Hager, and A. V. Rao. An hp-adaptive pseudospectral method for solving optimal control problems. In *AIAA: Journal of Spacecraft and Rockets*, 2010.

[33] C. L. Darby, W. H. Hager, and A. V. Rao. A variable-order hp-adaptive pseudospectral method for solving optimal control problems. In *AIAA: Journal of Spacecraft and Rockets*, 2010.

[34] W. Denham and A. E. Bryson. Optimal programming problems with inequality constraints II: Solution by steepest-ascent. In *AIAA Journal Vol.2*, pages 25–34, 1964.

[35] P. Deuflhard. A modified newton method for the solution of ill-conditioned systems nonlinear equations with application to multiple shooting. In *Numer. Math. 22*, pages 289–315, 1974.

[36] P. Deuflhard, H.J. Pesch, and P. Rentrop. A modified continuation method for the numerical solution of nonlinear two-point boundary value problems by shooting techniques. *Numerische Mathematik*, 26(3):327–343, 1976.

[37] E. D. Dickmanns and K. H. Well. Approximate solution of optimal control problems using third order hermite polynomial functions. In *Lecture Notes in Computer Science, 27*, pages 158–166, 1975.

[38] H. Dresig and F. Holzweissig. *Maschinendynamik*. Springer Berlin Heidelberg, 2009.

[39] O. Eiberger, S. Haddadin, M. Weis, A. Albu-Schaffer, and G. Hirzinger. On joint design with intrinsic variable compliance: Derivation of the dlr qa-joint. In *Robotics and Automation (ICRA), 2010 IEEE International Conference on*, pages 1687–1694. IEEE, 2010.

[40] D. L. Elliott. *Bilinear Control Systems: Matrices in Action*. Springer (Applied Mathematical Sciences), 2009.

[41] G. Fraser-Andrews. Finding candidate singular optimal controls: A state of the art survey. In *Journal of Optimization Theory and Applications Vol. 60, No. 2*, pages 173–190, 1989.

[42] M. Garabini, A. Passaglia, F. Belo, P. Salaris, and A. Bicchi. Optimality principles in variable stiffness control: The vsa hammer. In *Intelligent Robots and Systems (IROS), 2011 IEEE/RSJ International Conference on*, pages 3770–3775. IEEE, 2011.

[43] D. Garg, M. Patterson, W. H. Hager, A. V. Rao, D. A. Benson, and G. T. Huntington. A unified framework for the numerical solution of optimal control problems using pseudospectral methods. In *Automatica*, 2009.

[44] J. Garner. *Kinematic and kinetic comparison of overhand and underhand pitching: Implications to proximal-to-distal sequencing*. PhD thesis, Auburn University, 2007.

[45] H. Gattringer. *Starr-elastische Robotersysteme: Theorie und Anwendungen.* Springer-Verlag Berlin Heidelberg, 2011.

[46] M. Ghallab, D. Nau, and P. Traverso. *Automated Planning: theory and practice.* Elsevier, 2004.

[47] P. E. Gill. User's guide for SNOPT Version 7: Software for large-scale nonlinear programming. Technical report, University of California, 2008.

[48] B. S. Goh. Necessary conditions for singular extremals involving multiple control variables. In *Siam Journal on Control and Optimization, Vol. 4*, pages 716–731, 1966.

[49] H. H. Goldstine. *A history of the calculus of variations from the 17th through the 19th century.* Springer New York/Heidelberg/Berlin, New York, 1980.

[50] M. Grebenstein, A. Albu-Schaffer, T. Bahls, M. Chalon, O. Eiberger, W. Friedl, R. Gruber, S. Haddadin, U. Hagn, R. Haslinger, et al. The dlr hand arm system. In *IEEE International Conference on Robotics and Automation (ICRA)*, pages 3175–3182. IEEE, 2011.

[51] S. Haddadin, A. Albu-Schäffer, O. Eiberger, and G. Hirzinger. New insights concerning intrinsic joint elasticity for safety. In *Proc. IEEE/RSJ International Conf. on Intelligent Robots and Systems (IROS), Taipeh, Taiwan*, pages 2181–2187, 2010.

[52] S. Haddadin, F. Huber, and A. Albu-Schäffer. Optimal control for exploiting the natural dynamics of variable stiffness robots. In *IEEE International Conference on Robotics and Automation*, pages 3347–3354, 2012.

[53] R. Ham, T. Sugar, B. Vanderborght, K. Hollander, and D. Lefeber. Compliant actuator designs. *Robotics & Automation Magazine, IEEE*, 16(3):81–94, 2009.

[54] R. Hannemann and W. Marquardt. Combining direct and indirect methods for optimal control - a case study. In *Proceedings of the 9th International Symposium on Dynamics and Control of Process Systems*, 2010.

[55] R. F. Hartl, S.P. Sethi, and R. Vickson. A survey of the maximum principle for optimal control problems with state constraints. In *Society for Industrial and Applied Mathematics Review Vol.37 Issue 2*, pages 181–218, 1995.

[56] I. P. Herman. *Physics of the Human Body.* Springer (Biological and Medical Physics, Biomedical Engineering), 2007.

[57] A. Hermant. Homotopy algorithm for optimal control problems with a second-order state constraint. *Applied Mathematics & Optimization*, 61(1):85–127, 2010.

[58] R. A. Horn and C. R. Johnson. *Matrix Analysis.* Cambridge University Press, 1985.

[59] F. Huber. Optimal control concepts for intrinsic elastic joint robots. Master's thesis, Universität Linz, 2012.

[60] G. T. Huntington. *Advancements and Analysis of a Gauss Pseudospectral Transcription for Optimal Control Problems.* PhD thesis, Massachusetts Institute of Technology, 2007.

[61] J.W. Hurst, J.E. Chestnutt, and A.A. Rizzi. An actuator with physically variable stiffness for highly dynamic legged locomotion. In *Proceedings International Conference on Robotics and Automation*, volume 5, pages 4662–4667. IEEE, 2004.

[62] H. J. Kelley. Gradient theory of optimal flight paths. In *Journal of the American Rocket Society Vol.30*, pages 947–953, 1960.

[63] H.J. Kelley, R.E. Kopp, and H.G. Moyer. Singular extremals. In *Topics in Optimization G. Leitmann (ed.) Vol. II Chapter 2 New York, Academic Press*, 1966.

[64] H. K. Khalil. *Nonlinear Systems*. Second Edition. Prentice Hall, New York, 1996.

[65] W. Khalil and E. Dombre. *Modeling, Identification and Control of Robots*. Kogan Page Science, 2004.

[66] M. Kimmel and A. Swierniak. Control theory approach to cancer chemotherapy. In *Tutorials in Mathematical Biosciences III, Vol. 1872 of Lecture Notes in Mathematics*, pages 185–221. Springer Berlin / Heidelberg, 2006.

[67] D. E. Kirk. *Optimal Control Theory: An Introduction*. Prentice-Hall, Englewood New Jersey, 1970.

[68] H. Kreim, B. Kugelmann, H. J. Pesch, and M. H. Breitner. Minimizing the maximum heating of a re-entering space shuttle: An optimal control problem with multiple control constraints. In *Optimal Control Applications and Methods, 17*, pages 45–69, 1996.

[69] E. Kreindler. Additional necessary conditions for optimal control with state-variable inequality constraints. In *Journal of Optimization and Applications, Vol. 38, No.2*, pages 241–250, 1982.

[70] A.J. Krener. The high order maximal principle and its application to singular extremals. In *Siam Journal on Control and Optimization, Vol. 15, No.2*, 1977.

[71] D. Liberzon. *Calculus of Variations and Optimal Control Theory: A Concise Introduction*. Princeton University Press, 2011.

[72] L. Meirovitch. *Principles and Techniques of Vibration*. Prentice-Hall Inc., Englewood Cliffs, 1997.

[73] U. Mettin and A.S. Shiriaev. Ball-pitching challenge with an underactuated two-link robot arm. *Power (Nm/s)*, 1:270, 2011.

[74] R. R. Mohler. *Bilinear Control Processes*. Academic Press (New York), 1973.

[75] T. Morita and S. Sugano. Development of one-dof robot arm equipped with mechanical impedance adjuster. In *Intelligent Robots and Systems 95.'Human Robot Interaction and Cooperative Robots', Proceedings. 1995 IEEE/RSJ International Conference on*, volume 1, pages 407–412. IEEE, 1995.

[76] R. M. Murray, Z. Li, and S. S. Sastry. *A Mathematical Introduction to Robotic Manipulation*. CRC Press, 1994.

[77] C. Navasca and A. Krener. Solution of Hamilton Jacobi Bellman equations. In *39th Proceedings of the IEEE Conference on Decision and Control*, pages 570–574, 2000.

[78] D. Negrut, R. Serban, and F. A. Potra. A topology based approach for exploiting sparsity in multibody dynamics joint formulation. Reports on computational mathematics, no. 94, Department of Mathematics, the University of Iowa, 1996.

[79] S. Ober-Blöbaum, O. Junge, and J. E. Marsden. Discrete mechanics and optimal control: An analysis. In *ESAIM: Control, Optimisation and Calculus of Variations*, pages 322–352, 2011.

[80] H.J. Oberle. Vorlesungsskript Variationsrechnung und Optimale Steuerung. Universität Hamburg, 2008.

[81] H.J. Oberle and W. Grimm. Bndsco a program for the numerical solution of optimal control problems. *Hamburger Beitraege zur Angewandten Mathematik*, B(36), 2001.

[82] M. C. Özparpucu. Optimal control concepts for robots with varying stiffness joints. Master's thesis, Technische Universität Darmstadt, 2012.

[83] H. J. Pesch. A practical guide to the solution of real-life optimal control problems, 1994.

[84] H. J. Pesch and R. Bulirsch. The maximum principle, bellman's equation, and carathodory's work. In *Journal of optimization theory and applications, Vol. 80, No. 2*, pages 199–225, 1994.

[85] L. S. Pontryagin, V. G. Boltyanskii, R. V. Gamkrelidze, and E. F. Mishchenko. *The mathematical theory of optimal processes.* Interscience Publishers, New York, 1962.

[86] B.I. Prilutsky and V.M. Zatsiorsky. Tendon action of two-joint muscles: transfer of mechanical energy between joints during jumping, landing, and running. *Journal of biomechanics*, 27(1):25–34, 1994.

[87] C.A. Putnam. Sequential motions of body segments in striking and throwing skills: descriptions and explanations. *Journal of biomechanics*, 26:125–135, 1993.

[88] A. V. Rao. A primer on pseudospectral methods for solving optimal control problems. 2011.

[89] I. M. Ross and F. Fahroo. Users manual for dido 2001 : A matlab application for solving optimal control problems. Technical Report AAS-01-03, Department of Aeronautics and Astronautics, Naval Postgraduate School, Monterey, CA., 2001.

[90] P. Rutquist and M. Edvall. Propt: Matlab optimal control software. Technical report, Tomlab Optimization, Inc. Pullman, WA., 2008.

[91] D. Saez and A. Cipriano. Economic optimal control with environmental constraints for combined cycle power plants. In *Industrial Electronics Society, 1998. IECON '98. Proceedings of the 24th Annual Conference of the IEEE*, pages 640–645, 1998.

[92] K. Sasaki and R.R. Neptune. Muscle mechanical work and elastic energy utilization during walking and running near the preferred gait transition speed. *Gait & posture*, 23(3):383–390, 2006.

[93] G. F. Schanzer. *Optimale Steuerung eines Mehrfinger-Greifers mit konkurrierenden Steuerungen unter Berücksichtigung von Elastizitäten.* PhD thesis, Technische Universität München, 2007.

[94] R. Schiavi, G. Grioli, S. Sen, and A. Bicchi. Vsa-ii: A novel prototype of variable stiffness actuator for safe and performing robots interacting with humans. In *IEEE International Conference on Robotics and Automation*, pages 2171–2176. IEEE, 2008.

[95] W. Schiehlen. *Technische Dynamik*. Mechanik. Teubner Studienbücher Mathematik, 1986.

[96] R. Serban, D. Negrut, E. J. Haug, and F. A. Potra. A topology-based approach for exploiting sparsity in multibody dynamics in cartesian formulation. In *Mechanics of Structures and Machines, Vol. 25, No. 3*, 1997.

[97] A. A. Shabana. *Dynamics of Multibody Systems*. Third Edition. Cambridge University Press, 2005.

[98] D. Shin, I. Sardellitti, and O. Khatib. A hybrid actuation approach for human-friendly robot design. In *Robotics and Automation, 2008. ICRA 2008. IEEE International Conference on*, pages 1747–1752. IEEE, 2008.

[99] B. Siciliano and O. Khatib. Springer handbook of robotics. chapter Robots with Flexible Elements, pages 287–306. Springer Berlin Heidelberg, 2008.

[100] I. Y. Smets, J. E. Claesm, E. J. November, G. P. Bastin, and J. F. Van Impe. Optimal adaptive control of (bio)chemical reactors: past, present and future. In *Journal of Process Control, Vol. 14, No. 7*, pages 795–805, 2004.

[101] M. W. Spong, S. Hutchinson, and M. Vidyasagar. *Robot Modeling and Control*. First Edition. John Wiley and sons, Inc., 2005.

[102] J. Stoer and R. Bulirsch. *Numerische Mathematik II*. Berlin - Heidelberg - New York: Springer, Heidelberger Taschenbuch, Band 114, 1973.

[103] S. Sugano, S. Tsuto, and I. Kato. Force control of the robot finger joint equipped with mechanical compliance adjuster. In *Proceedings of the IEEE/RSJ International Conference on Intelligent Robots and Systems*, volume 3, pages 2005–2013. IEEE, 1992.

[104] B. Tondu and P. Lopez. Modeling and control of mckibben artificial muscle robot actuators. *Control Systems, IEEE*, 20(2):15–38, 2000.

[105] G. Tonietti, R. Schiavi, and A. Bicchi. Design and control of a variable stiffness actuator for safe and fast physical human/robot interaction. In *Proceedings of the IEEE International Conference on Robotics and Automation*, pages 526–531. Ieee, 2005.

[106] J. Denavit und R. S. Hartenberg. A kinematic notation for lower-pair mechanisms based on matrices. In *ASME J. Applied Mechanics*, pages 215–221, 1955.

[107] S. Wolf, O. Eiberger, and G. Hirzinger. The dlr fsj: Energy based design of a variable stiffness joint. In *IEEE Int. Conf. on Robotics and Automation*, pages 5082–5089, 2011.

[108] S. Wolf and G. Hirzinger. A new variable stiffness design: Matching requirements of the next robot generation. In *IEEE International Conference on Robotics and Automation*, pages 1741–1746. IEEE, 2008.

[109] J. Yamaguchi, S. Inoue, D. Nishino, and A. Takanishi. Development of a bipedal humanoid robot having antagonistic driven joints and three dof trunk. In *Intelligent*

Robots and Systems, 1998. Proceedings., 1998 IEEE/RSJ International Conference on, volume 1, pages 96–101. IEEE, 1998.

[110] J. Yamaguchi, D. Nishino, and A. Takanishi. Realization of dynamic biped walking varying joint stiffness using antagonistic driven joints. In *Robotics and Automation, 1998. Proceedings. 1998 IEEE International Conference on*, volume 3, pages 2022–2029. IEEE, 1998.

[111] J.-M. Yang and J.-H. Kim. Sliding mode control for trajectory tracking of nonholonomic wheeled mobile robots. In *IEEE Transactions on robotics and automation, Vol. 15, No. 3*, 1999.

[112] M. Zinn, B. Roth, O. Khatib, and J.K. Salisbury. A new actuation approach for human friendly robot design. *The international journal of robotics research*, 23(4-5):379–398, 2004.